NASA TECHNICAL MEMORANDUM

NASA TM X-62,319

ACOUSTIC CHARACTERISTICS OF A LARGE-SCALE WIND-TUNNEL MODEL OF AN UPPER-SURFACE BLOWN FLAP TRANSPORT HAVING TWO ENGINES

Michael D. Falarski, Kiyoshi Aoyagi and David G. Koenig

Ames Research Center
and
U. S. Army Air Mobility R&D Laboratory
Moffett Field, Calif. 94035

September 1973

ACOUSTIC CHARACTERISTICS OF A LARGE–SCALE WIND–TUNNEL MODEL OF AN UPPER–SURFACE BLOWN FLAP TRANSPORT HAVING TWO ENGINES

Michael D. Falarski and Kiyoshi Aoyagi

Ames Research Center
and
U. S. Army Air Mobility R&D Laboratory
Moffett Field, California 94035

ABSTRACT

The upper-surface blown (USB) flap as a powered-lift concept has evolved because of the potential acoustic shielding provided when turbofan engines are installed on a wing upper surface. This report presents the results from a wind tunnel investigation of a large-scale USB model powered by two JT15D-1 turbofan engines. The effects of coanda flap extent and deflection, forward speed, and exhaust nozzle configuration were investigated. To determine the wing shielding the acoustics of a single engine nacelle removed from the model were also measured.

Effective shielding occurred in the aft underwing quadrant. In the forward quadrant the shielding of the high frequency noise was counteracted by an increase in the lower frequency wing-exhaust interaction noise. The fuselage provided shielding of the opposite engine noise such that the difference between single and double engine operation was 1.5 PNdB under the wing. The effects of coanda flap deflection and extent, angle of attack, and forward speed were small. Forward speed reduced the perceived noise level (*PNL*) by reducing the wing-exhaust interaction noise. A forward speed of 40 m/s (130 fps) decreased the *PNL* by 2 PNdB.

NOTATION

b	wing span, m (ft)
$OASPL$	overall sound pressure level, dB ref. 2×10^{-5} N/m^2 (0.0002 microbar)
PNL	perceived noise level, PNdB
q	free-stream dynamic pressure, N/m^2 (psf)
$\frac{S}{L}$	sideline
SPL	sound pressure level, dB ref. 2×10^{-5} N/m^2 (0.0002 microbar)
$\frac{U}{W}$	underwing
V_J	average exhaust velocity at nozzle exit, m/s (fps)
V_∞	free-stream velocity, m/s (fps)
y	spanwise distance perpendicular to the plane of symmetry, m (ft)
α	angle of attack with respect to wing chord, deg
δ_f	deflection of coanda plate trailing-edge measured parallel to plane of symmetry, deg (see fig. 2(b))
η_{co}	spanwise extent of coanda plate surface, $\frac{y}{b/2} \times 100$, percent

ACOUSTIC CHARACTERISTICS OF A LARGE–SCALE WIND–TUNNEL MODEL OF AN UPPER–SURFACE BLOWN FLAP TRANSPORT HAVING TWO ENGINES

Michael D. Falarski and Kiyoshi Aoyagi

Ames Research Center
and
U. S. Army Air Mobility R&D Laboratory
Moffett Field, California 94035

SUMMARY

The upper-surface blown (USB) flap as a powered-lift concept has evolved because of the potential acoustic shielding provided when turbofan engines are installed on a wing upper surface. This report presents the results from a wind tunnel investigation of a large-scale USB model powered by two JT15D-1 turbofan engines. The effects of coanda flap extent and deflection, forward speed, and exhaust nozzle configuration were investigated. To determine the wing shielding the acoustics of a single engine nacelle removed from the model were also measured.

Effective shielding occurred in the aft underwing quadrant. In the forward quadrant the shielding of the high frequency noise was counteracted by an increase in the lower frequency wing-exhaust interaction noise. The fuselage provided shielding of the opposite engine noise such that the difference between single and double engine operation was 1.5 PNdB under the wing. The effects of coanda flap deflection and extent, angle of attack, and forward speed were small. Forward speed reduced the perceived noise level (*PNL*) by reducing the wing-exhaust interaction noise. A forward speed of 40 m/s (130 fps) decreased the *PNL* by 2 PNdB.

INTRODUCTION

Several powered-lift concepts are being applied to transport aircraft in an effort to produce an aircraft which can land and takeoff in short distances. Commercial aircraft will be required to be significantly quieter than today's conventional aircraft because of their operation out of airports in densely populated areas. For this reason, research in powered-lift technology is on-going in acoustics as well as aerodynamics. Many acoustic investigations have already been carried out using small-scale model under static conditions ($V_\infty = 0$). Some of these results are reported in references 1 and 2.

The upper-surface blown flap (USB) concept has evolved because of its ability to produce powered-lift while shielding observers under the aircraft from the engine exhaust noise. The USB concept has turbofan engines mounted on the wing upper surface with the exhaust flowing over a curved coanda plate inducing high lift from supercirculation in the manner that a jet flap produces lift. The results of two acoustic investigations of small-scale USB models have been reported in references 3 and 4.

This report presents the results from a wind tunnel acoustic investigation of a large-scale upper-surface blown flap transport model. The model was equipped with two JT15D-1 turbofan engines. The investigation was performed in the Ames 40- by 80-Foot Wind Tunnel. The aerodynamic characteristics were also investigated and have been reported in reference 5.

MODEL AND APPARATUS

The model was a swept, high-wing configuration powered by two JT15D-1 engines. It is shown installed in the wind tunnel in figures 1(a) and 1(b). For acoustic research outside the wind tunnel the model was installed in the static test facility as shown in figure 1(c). To determine the acoustic shielding, a single nacelle was mounted in the static facility as shown in figure 1(d). The geometric details of the various configurations are presented in figures 2(a)-2(e).

Wing

The wing-nacelle details are shown in figure 2(b). The wing had a quarter-chord sweep of 25°, an aspect ratio of 7.28, and an incidence of 0°. The airfoil section had an NACA 63_2A214 airfoil shape at the root tapering linearly to an NACA 63_2A211 distribution at the tip. The upper surface was modified from $\eta_{CO} = 11$ to 48 to provide an improved fairing between the nacelle nozzle and coanda surface. Full-span, leading-edge slats were installed as detailed in figure 2(c).

Trailing-Edge Flap System

The basic flap system had two segments with fixed pivot points (see fig. 2(d)). A detachable coanda surface was installed over the flaps from $\eta_{CO} = 11$ to 48 with breaks at $\eta_{CO} = 15$ and 39. Separate coanda plates were used for each jet flap deflection investigated. A 0.254 m (0.834 ft) chord extension was attached to the trailing edge of the flap at 75° to provide $\delta_f = 90°$.

Propulsion

The two JT15D-1 engines were housed in the nacelles sketched in figure 2(b). The engines had a bypass ratio of 3 and a nominal maximum thrust of 9800N (2200 lb). The nacelle centerline was coincident with the engine centerline but pitched up 1° with respect to the wing chord plane. The nacelle spanwise location was $\eta_{CO} = 25.6$. The three nozzle configurations which were investigated are detailed in figure 2(d). They were designated "B," "B" with deflector, and "D."

For the nacelle static investigation a small nozzle extension plate was attached to the nozzle lower surface as shown in figure 2(e). The plate was required to mount the deflector and maintain nozzle exit areas.

TESTS

Wind Tunnel

Wind tunnel tests were performed to document the underwing acoustic characteristics at forward speed and angle of attack. The microphone arrangement for these acoustic measurements is presented in figure 3(a). The measurements were made using 1.27 cm (1/2 in.) Bruel and Kjaer (B&K) condenser microphones equipped with aerodynamic-shaped nose cones to reduce wind noise and give omnidirectional response. The signal was recorded on an Ampex F1300A multichannel tape recorder at 30 ips and 108 kHz centerband frequency.

The noise of the model was measured for each of the nozzle configurations from $V_\infty = 0$ to 77 m/s (0 to 130 fps) and angle of attack from 0° to 20°. To determine the effect of exhaust velocity, V_J was varied from 0 to 246 m/s (0 to 810 fps). Flap deflections of 30° and 75° were investigated. Unless otherwise specified the flap deflection was 75°.

Model Static

To determine the sideline acoustic characteristics and the wind tunnel reverberation, the USB model was mounted outside the tunnel as shown in figure 1(c). The underwing microphone arrangement duplicated that used in the tunnel. The sideline noise was measured using nine 1.27 cm (1/2 in.) microphones on 4.88 m (16 ft) stands (see fig. 3(b)). The first seven microphones were equipped with porous, polyurethane, sponge wind screens while the last two were equipped with the nose cones used during the tunnel tests to reduce any effect of the model slipstream impingement. The static tests were performed for each of the nozzles at a flap deflection of 75° and at the same thrust settings recorded during the tunnel tests. Tests were also performed with the left engine out to measure the shielding of the wing and fuselage.

Nacelle Static

A single nacelle was tested statically to determine the wing acoustic shielding. The left nacelle and nozzle were removed from the model and installed on the static test facility as shown in figure 1(d). The nozzle extension plate was installed as described in figure 2(e). Measurements were made during the investigation of nozzle "B" with and without this plate. The microphone arrangement was a duplication of that used for the model static tests (see fig. 3).

DATA REDUCTION

Reverberation Corrections

The acoustic environment of the wind has been investigated with several acoustic sources. From these studies various techniques have been derived to allow prediction of free-field noise levels from wind tunnel acoustic measurements. These techniques and comparison of wind tunnel and flight data are reported in references 6 and 7.

The analog noise data were reduced to one-third octave band frequency spectrum using a B&K Real Time Spectra Analyzer. The wind tunnel spectra were corrected for test section reverberation. The corrections were derived from the difference between the spectra of the static and wind tunnel results for nozzle "B" with deflector at several exhaust velocities. This technique assumes the difference is created by reverberation only. Typical corrections for several microphones are presented in figure 4(a). They are independent of exhaust velocity and when applied to wind tunnel results for other configurations produced the comparisons with static results shown in figures 4(b)-4(e).

As would be expected, comparison of the wind tunnel and static results for the nozzle "B" with deflector agree within the accuracy of the correction data. When the reverberation corrections were applied to other configurations the comparison is within ±1.5 PNdB except for underwing

microphone #3 (U/W angle = 88°). The wind tunnel *PNL* for this microphone is consistently lower than that of the static with the difference increasing with exhaust velocity. The frequency spectra in figure 4(e) show the tunnel data to be lower over the complete spectra.

Background Noise

The operation of the wind tunnel and flow of air over the microphones creates a background noise floor. To study the acoustics of a source in this environment, the *SPL* of the source must be of sufficient magnitude to be distinguishable from the background. A comparison of the USB model and wind tunnel background frequency spectra is presented in figure 5. Above a frequency of 80 Hz the model *SPL* is at least 10 dB above the background, eliminating any need for concern. Below 80 Hz the background levels approach and in some cases exceed the model levels. Caution should be exhibited when interpreting the forward speed data at low exhaust velocities.

Immersion of a microphone in the model slipstream also created a low-frequency noise floor by producing high *SPL* distortion. This occurred at times with the most aft underwing and sideline microphones (see fig. 2(d)).

Data Projection

The frequency spectra of each microphone was projected to 152.5 m (500 ft) along a ray from the assumed model acoustic center. The projection was accomplished using Society of Automotive Engineers (SAE) procedures outlined in reference 8. These consist of corrections for spherical divergence and atmospheric absorption. No correction was made for extra ground attenuation (EGA) because of the close proximity of the microphone to the model. The data was also not corrected for ground reflection because close examination of the results showed no consistent trends that could be related to these reflections.

Nacelle Nozzle Extension Plate

To determine the effect of the extension plate on the nacelle acoustics, tests were made with nozzle "B" without the plate. These results are outlined in figures 6 and 7. The plate reduced the underwing *PNL* at low exhaust velocities. The effect decreased with increasing exhaust velocity until at $V_J = 230$ m/s (755 fps) the *PNL* directivity with and without the plate were essentially equal. The lower *PNL* with the plate were created by reduction in the mid and high frequencies of the nacelle spectra, indicating the plate was providing some shielding of the exhaust noise. The plate provided no shielding of the sideline noise as shown in figure 7 where the directivity patterns for the two configurations are coincident.

When comparisons are made between the nacelle and model acoustics to determine the shielding, the nacelle data should be adjusted for the extension plate effect.

RESULTS AND DISCUSSION

Exhaust Velocity

Some insight into the primary noise mechanism of a source can be achieved by determining the variation of the source noise with exhaust velocity. These results for the USB model are presented in figure 8. The overall sound pressure level (*OASPL*) of the nacelle varies as the eighth power of the average velocity both under the wing and at the sideline. This indicates the nacelle dominant acoustic generation mechanism is the turbulent mixing of the exhaust jet and surrounding air.

When the nacelle is mounted over the wing and its exhaust blown over the coanda surface, the *OASPL* becomes a sixth power function of the exhaust velocity. The dominant generation mechanism has become the interaction of the turbulent exhaust with the wing coanda surface. It can also

be seen that the noise levels were little affected by the variations in nozzle configuration. These characteristics were exhibited both underwing and at sideline although the sideline levels were approximately 2 dB lower.

Coanda Deflection and Extent

Deflecting or varying the extent of the wing coanda surface had little effect on the USB acoustic characteristics. Changing the deflection from 30° to 75° causes an increase of 1 PNdB under the wing as shown in figure 9(a). The primary consequence of deflection can be seen in the USB frequency spectra as a large increase in the low-frequency *SPL* (see fig. 9(b)). The effect of coanda extent is presented in figure 10. The *PNL* directly under the wing decreased slightly.

Forward Speed and Angle of Attack

The variation of acoustics with forward speed (V_∞) is described in figures 11 and 12. The underwing *PNL* was reduced by 1-2 PNdB at $V_\infty = 40$ m/s (130 fps) for the nozzle "B" arrangement. Installing the deflector decreased this effect. The lower *PNL* was created by lower spectra *SPL* where the peak wing-exhaust interaction noise occurs (frequency = 63-500 Hz). These results are similar to those experienced in other powered-lift concepts as reported in reference 9.

Varying angle of attack from 0° to 20° produced no discernible change in either the underwing *PNL* directivity or one-third octave band frequency spectra. This can be seen in figures 13-15.

Fuselage Shielding

To assess the fuselage shielding of the noise from the opposite nacelle, the model acoustics were investigated with only the right engine operating (the microphones were located on the model right). These results are compared with the two engine noise in figures 16 and 17. In the absence of

shielding, doubling the power of an acoustic source will increase the sound pressure levels by 3 dB. Figure 16(a) shown the underwing *PNL* for the single engine was approximately 1.5 PNdB lower than that for 2 engine. The fuselage and wing have shielded the noise from the left engine. This is verified by the frequency spectra which show a difference of 3 dB at the low frequencies while at the high frequencies the difference is 1.5 dB.

The wing and fuselage provide less shielding to the sideline of the opposite engine as shown in figure 17(a). The increment is 2 to 3 PNdB between single and double engine operation. These trends can also be seen in the frequency spectra (see figs. 17(b)-17(c)).

Underwing Acoustic Shielding

The upper-surface blown flap is being developed because of its potential for wing-flap shielding of the engine exhaust high frequency noise. To evaluate this shielding the characteristics of the model and nacelle are compared in figures 18 to 21. The underwing *PNL* directivity patterns indicate effective shielding has occurred in the aft underwing quadrant but not directly under the model. The peak shielding was 5 PNdB. The frequency spectra show that the wing did shield the high frequency noise at all stations under the wing. In all but the aft quadrant, shielding was overcome by the addition of the wing-exhaust interaction noise. This can be seen in the spectra of figures 19(b) to 19(d) as the increase in *SPL* at frequencies of 12.5 Hz to 1000 Hz.

As was the case with fuselage shielding, the wing provided little effective shielding to the sideline. Figures 20 and 21(a) show that in most cases the sideline *PNL* is greater for the model than the nacelle alone. This is especially true for the very forward and aft regions. Any high frequency shielding which does occur is overcome by the interaction noise at lower frequencies (see figs. 21(b)-21(d)).

REFERENCES

1. Gibson, Fredrick W.: Noise Measurements of Model Jet-Augmented Lift System. NASA TN D-6710, April, 1972.

2. Dorsch, R. G.; Kreim, W. J.; and Olsen, W. A.: Externally-Blown-Flap Noise. AIAA Paper 72-129, 1972.

3. Phelps, A. E.: Aerodynamics of Upper-Surface Blown Flap. STOL Technology Conference, NASA SP-320, 1972.

4. Von Glahn, U.; Reshotko, M.; and Dorsch, R.: Acoustic Results Obtained With Upper-Surface Blowing Lift-Augmentation System. NASA TM X-68,159, Dec., 1972.

5. Aoyagi, Kiyoshi; Falarski, M. D.; and Koenig, D. G.: Wind Tunnel Investigation of a Large-Scale Upper-Surface Blown-Flap Transport Model Having Two Engines. NASA TM X-62,296. 1973.

6. Atencio, Adolph and Soderman, Paul T.: Comparison of Aircraft Noise Characteristics Measured in Flight Tests and in the NASA Ames 40- by 80-Foot Wind Tunnel. AIAA Paper 73-1047, 1973.

7. Falarski, M. D.; Koenig, D. G.; and Soderman, P. T.: Aspects of Investigating STOL Noise Using Large-Scale Wind Tunnel Models. NASA TM X-62,164, June, 1972.

8. Anon.: Standard Valves of Atmospheric Absorption as a Function of Temperature and Humidity for Use in Evaluating Aircraft Flyover Noise. SAE ARP-866, August, 1964.

9. Falarski, Michael D.; Aoyagi, Kiyoshi; and Koenig, David G.: Acoustic Characteristics of Large-Scale STOL Models at Forward Speed. NASA TM X-62,251, 1972.

TABLE I.– INDEX TO DATA FIGURES.

Figure	Variable	Plot Type	Mic. Angle, deg.	Nozzle	Config.	η_{CO}, %	δ_f, deg.	No. Engine	V_J, m/s(fps)	V_∞, m/s(fps)	α, deg.	
6-a	Noz. Ext. Plate	U/W direct.	~	"B"	Nacelle	–	–	1	~	0	0	
-b	↓	U/W Spectra	110	↓	↓	↓	↓	↓	230(755)	↓	↓	
-c		U/W Spectra	110						157(513)			
7-a		S/L direct.	~						~			
-b		S/L Spectra	50						216(710)			
-c		S/L Spectra	90						216(710)			
8-a	V_J	$OASPV$ vs. V_J	88	~					~			Noz. Ext. Plate On
-b	↓	↓	90	↓	↓	↓	↓	↓	↓			Noz. Ext. Plate On
-c			88		Model	11-42	75	2				
-d			90		↓	11-42	75	↓				
9-a	δ_f	U/W direct.	~	"B" $\bar{w}$ defl.		11-39	~					
-b	δ_f	U/W Spectra	110	↓		11-39	~		↓			
10-a	η_{CO}	U/W direct.	~			~	75		203(667)			
-b	η_{CO}	U/W Spectra	88	↓		~	↓		203(667)	↓		
11-a	V_∞	U/W direct.	~	"B"		11-48			216(710)	~		
-b	↓	U/W direct.	~	"B" $\bar{w}$ defl.		↓			246(805)	↓		
12-a		U/W Spectra	64	"B"					216(710)			
-b		↓	88	"B"					216(710)			
-c			110	"B"					216(710)			
-d			64	"B" $\bar{w}$ defl.					246(805)			
-e			110	↓					246(805)			
-f	↓	↓	140		↓				246(805)	↓	↓	
13-a	α	U/W direct.	~						144(475)	19.8 (65)	~	
-b	↓	↓	↓	↓		↓	↓		246(805)	19.8 (65)	↓	
-c						11-39	30		238(781)	19.7 (64.5)		
-d				"D"		11-43	75	↓	254(835)	17.2 (56.5)		

TABLE I.– INDEX TO DATA FIGURES – Concluded.

Figure	Variable	Plot Type	Mic. Angle. deg.	Nozzle	Config.	η_{CO}, %	δ_f, deg.	No. Engine	V_J, m/s(fps)	V_∞, m/s(fps)	α, deg.	
14-a	α	*U/W* Spectra	64	"B" $\overline{w}$ defl.	Model	11-39	30	2	238(781)	19.7 (64.5)	~	
-b	↓	↓	110	"B" $\overline{w}$ defl.	↓	11-39	30	↓	238(781)	19.7 (64.5)	↓	
-c	↓	↓	140	"B" $\overline{w}$ defl.	↓	11-39	30	↓	238(781)	19.7 (64.5)	↓	
15	↓	↓	110	"D"	↓	11-43	75	↓	254(835)	17.2 (56.5)	↓	
16-a	No. Engines	*U/W* direct.	~	"B" $\overline{w}$ defl.	↓	11-42	↓	~	~	0	0	
-b	↓	*U/W* Spectra	64	↓	↓	↓	↓	↓	247(810)	↓	↓	
-c	↓	*U/W* Spectra	110	↓	↓	↓	↓	↓	247(810)	↓	↓	
-d	↓	*U/W* Spectra	140	↓	↓	↓	↓	↓	247(810)	↓	↓	
17-a	↓	*S/L* direct.	~	↓	↓	↓	↓	↓	~	↓	↓	
-b	↓	*S/L* Spectra	50	↓	↓	↓	↓	↓	247(810)	↓	↓	
-c	↓	*S/L* Spectra	90	↓	↓	↓	↓	↓	247(810)	↓	↓	
-d	↓	*S/L* Spectra	130	↓	↓	↓	↓	↓	247(810)	↓	↓	
18	Shielding	*U/W* direct.	~	"B"	~	↓	↓	2	~	↓	↓	Noz. Ext. Plate Off
19-a	↓	*U/W* direct.	~	"B" $\overline{w}$ defl.	↓	↓	↓	1	~	↓	↓	
-b	↓	*U/W* Spectra	64	↓	↓	↓	↓	↓	250(820)	↓	↓	
-c	↓	*U/W* Spectra	110	↓	↓	↓	↓	↓	250(820)	↓	↓	
-d	↓	*U/W* Spectra	140	↓	↓	↓	↓	↓	250(820)	↓	↓	
20	↓	*S/L* direct.	~	"B"	↓	↓	↓	2	~	↓	↓	Noz. Ext. Plate Off
21-a	↓	*S/L* direct.	~	"B" $\overline{w}$ defl.	↓	↓	↓	1	~	↓	↓	
-b	↓	*S/L* Spectra	30	↓	↓	↓	↓	↓	250(820)	↓	↓	
-c	↓	*S/L* Spectra	90	↓	↓	↓	↓	↓	250(820)	↓	↓	
-d	↓	*S/L* Spectra	150	↓	↓	↓	↓	↓	250(820)	↓	↓	

(a) Top view of model installed in wind tunnel.

Figure 1.– Installation of USB model in test facilities.

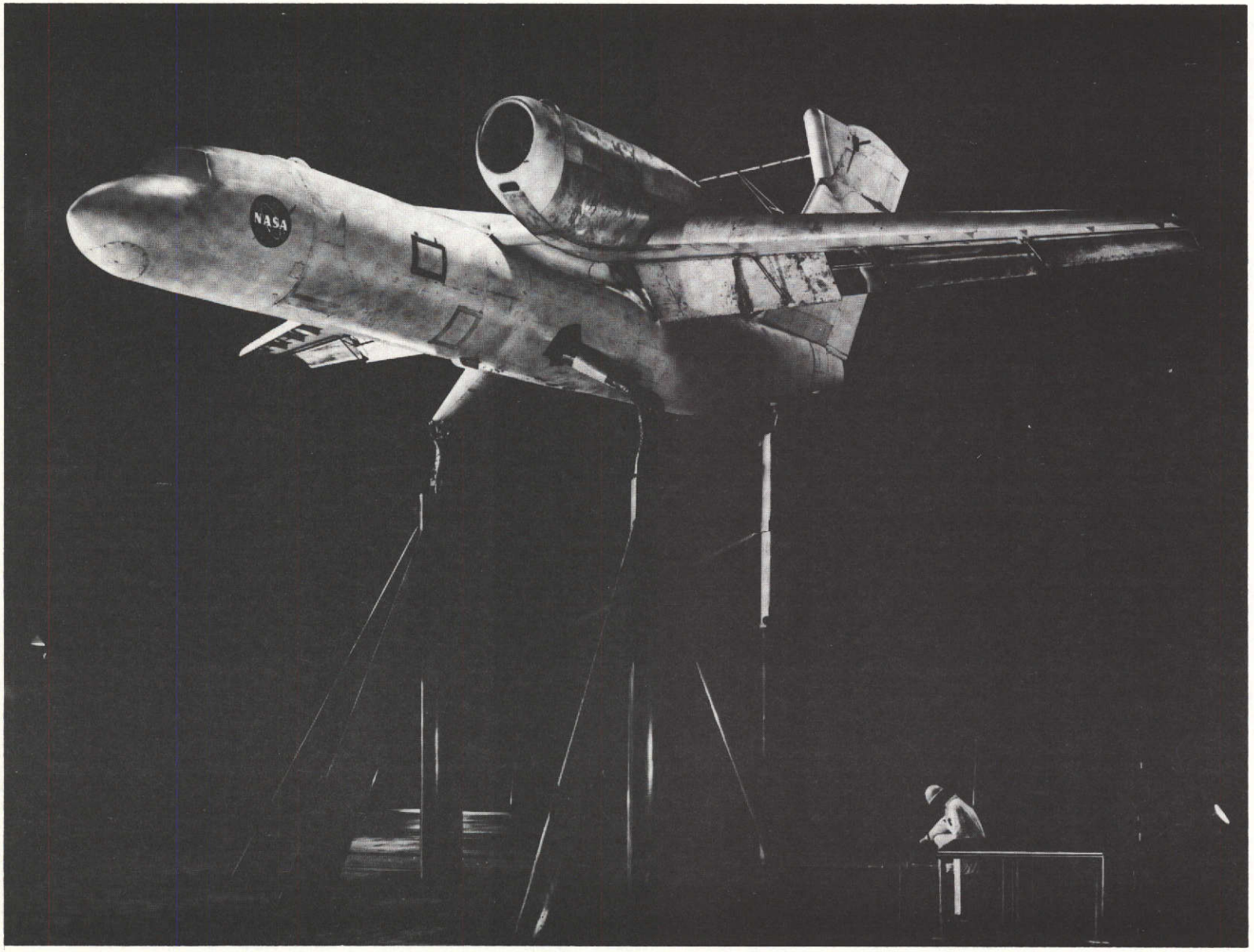

(b) Three-quarter front view of model in wind tunnel.

Figure 1.– Continued.

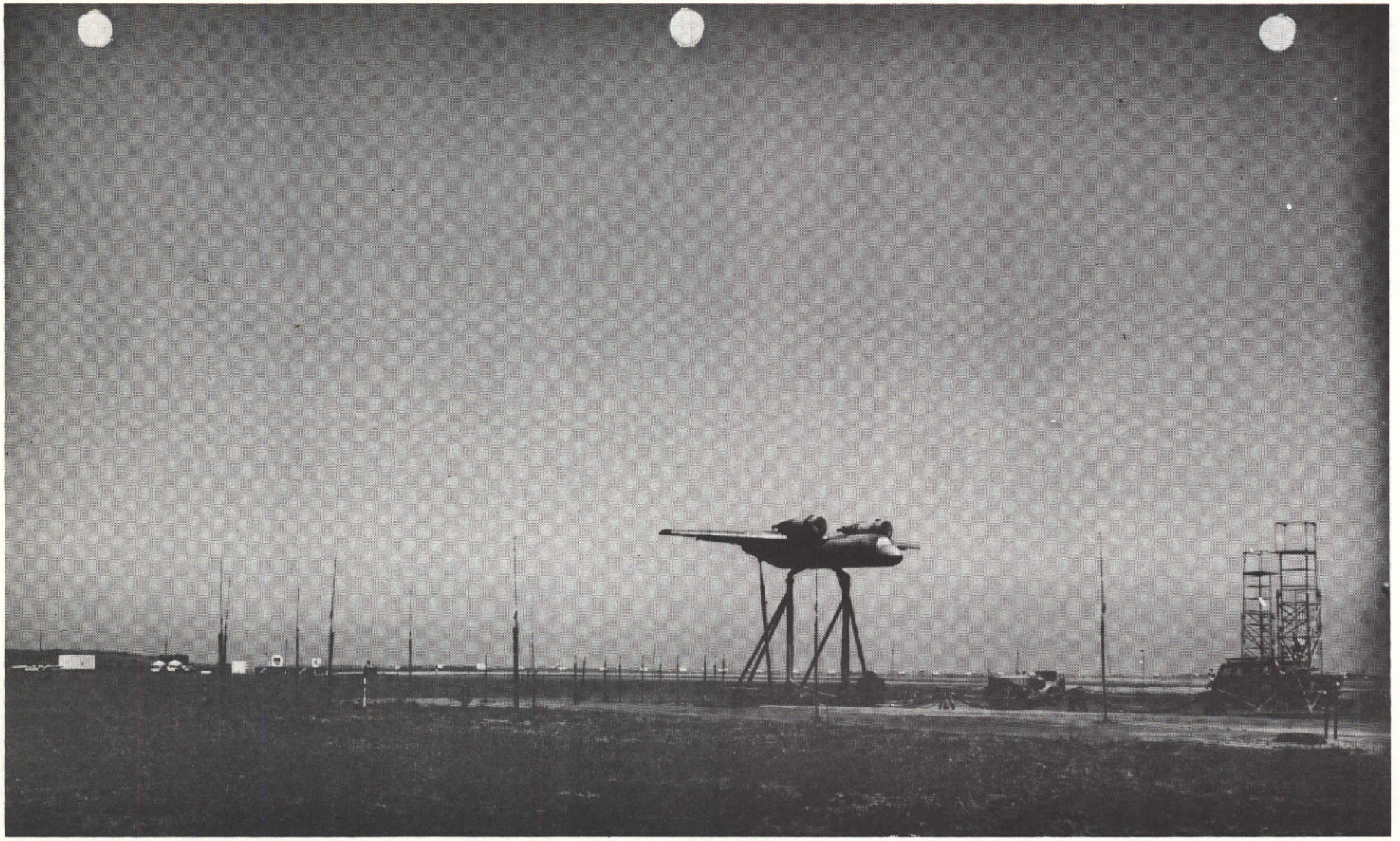

(c) Model installed in static test facility

Figure 1.– Continued.

(d) Nacelle installed in static test facility

Figure 1.– Concluded.

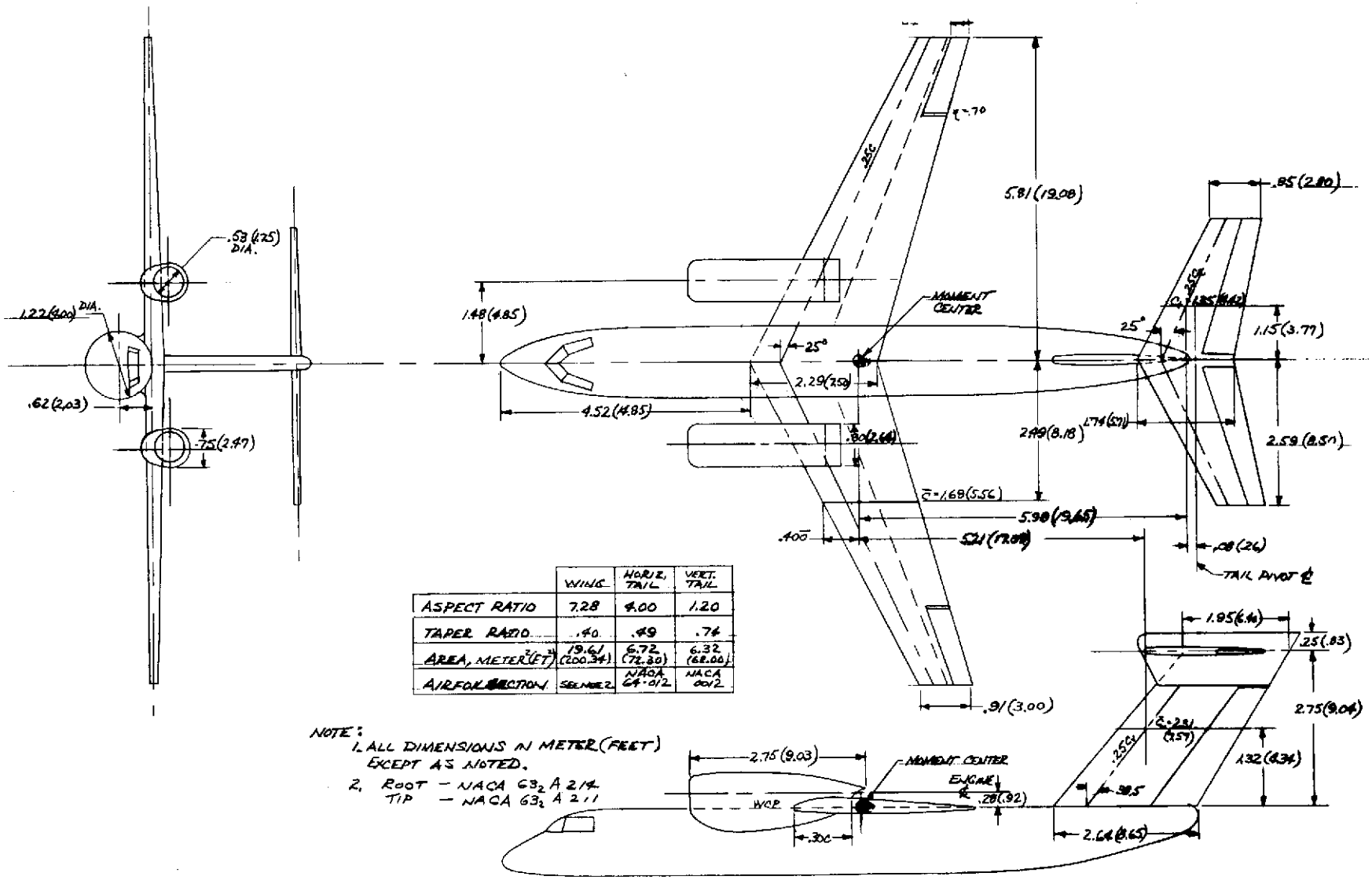

	WING	HORIZ. TAIL	VERT. TAIL
ASPECT RATIO	7.28	4.00	1.20
TAPER RATIO	.40	.49	.74
AREA, METER^2(FT^2)	19.61 (200.34)	6.72 (72.30)	6.32 (68.06)
AIRFOIL SECTION	SEE NOTE 2	NACA 64-012	NACA 0012

NOTE:
1. ALL DIMENSIONS IN METER (FEET) EXCEPT AS NOTED.
2. ROOT – NACA 63_2 A 2.14
   TIP – NACA 63_2 A 2.11

(a) General arrangement of USB model.

Figure 2.– Geometry of USB model.

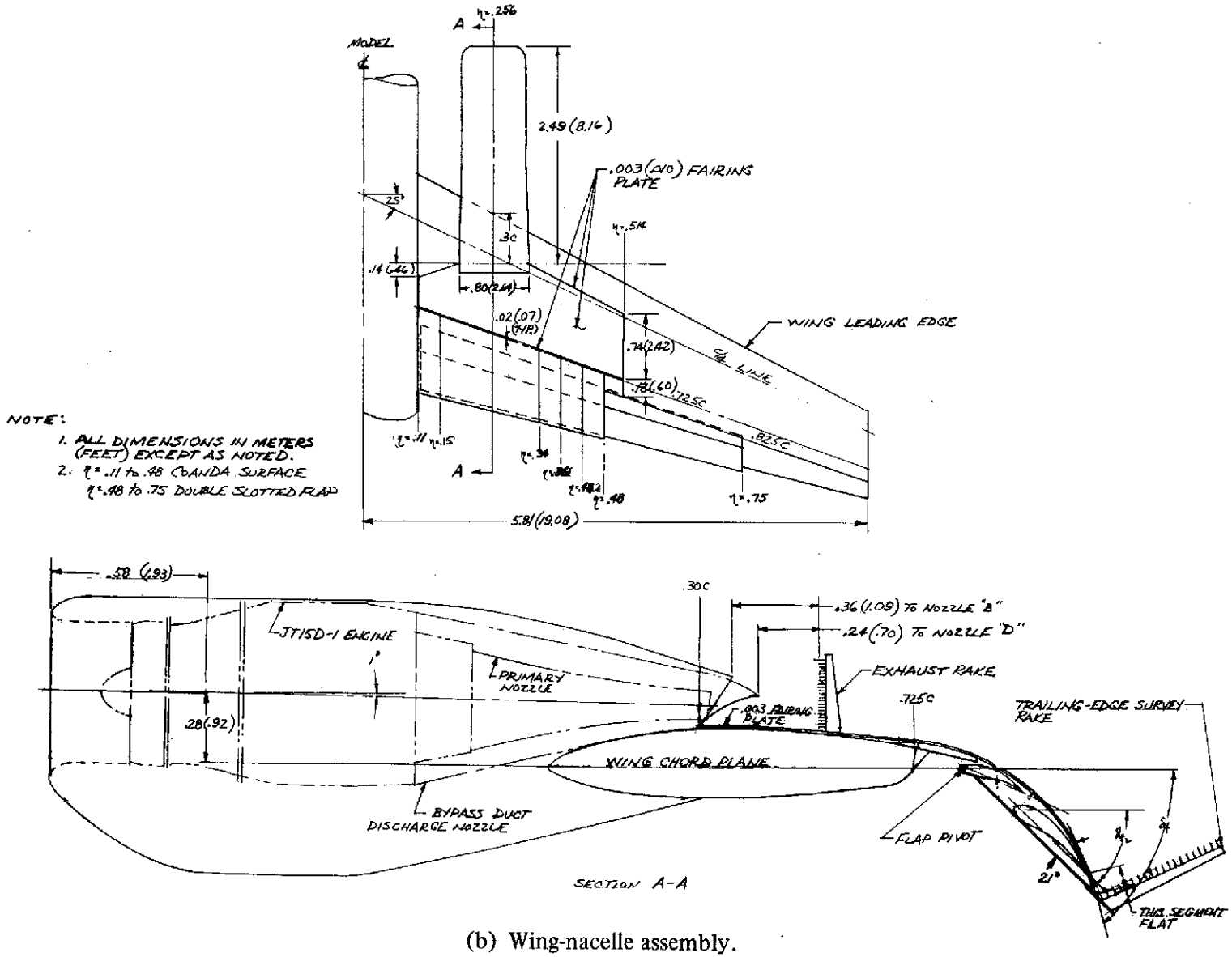

(b) Wing-nacelle assembly.

Figure 2.– Continued.

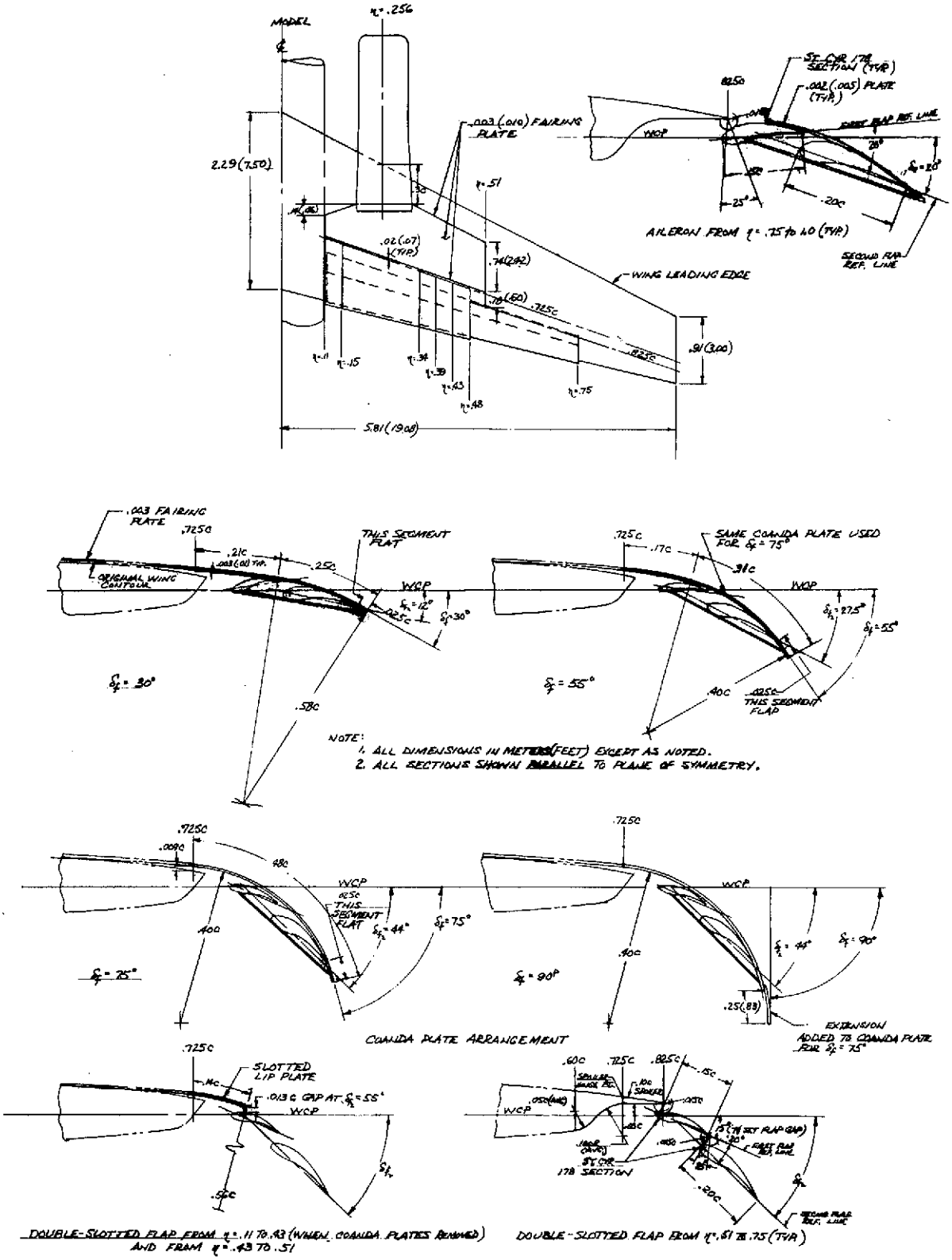

(c) Trailing-edge flap and aileron arrangement.

Figure 2.– Continued.

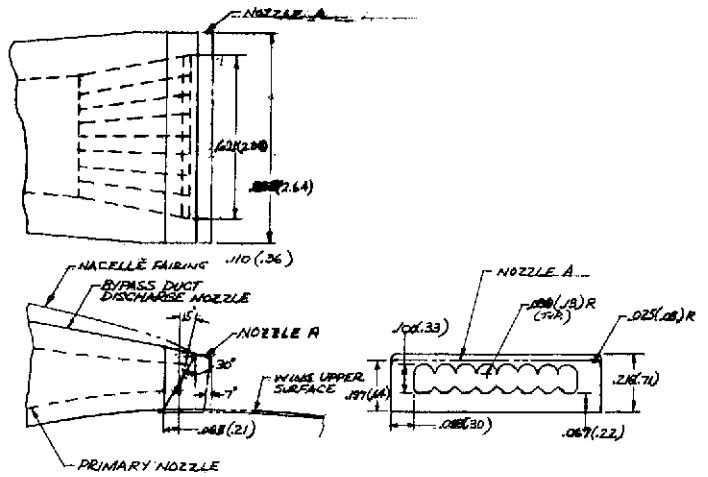

NOZZLE A & B

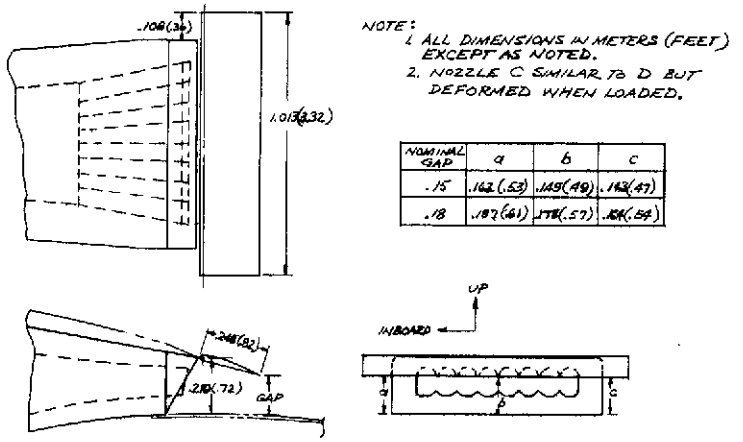

NOTE:
1. ALL DIMENSIONS IN METERS (FEET) EXCEPT AS NOTED.
2. NOZZLE C SIMILAR TO D BUT DEFORMED WHEN LOADED.

NOMINAL GAP	a	b	c
.15	.162 (.53)	.149(.49)	.162(.47)
.18	.187(.61)	.173(.57)	.156(.54)

NOZZLE B WITH DEFLECTOR

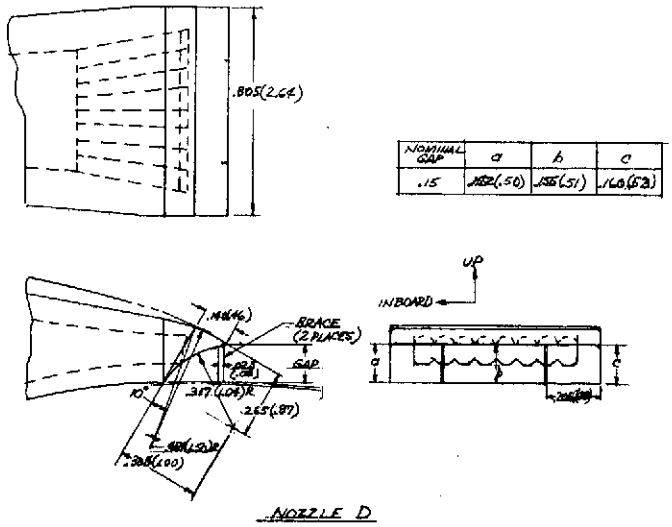

NOMINAL GAP	a	b	c
.15	.152(.50)	.155(.51)	.160(.53)

NOZZLE D

(d) Engine nozzle arrangement.

Figure 2.– Continued.

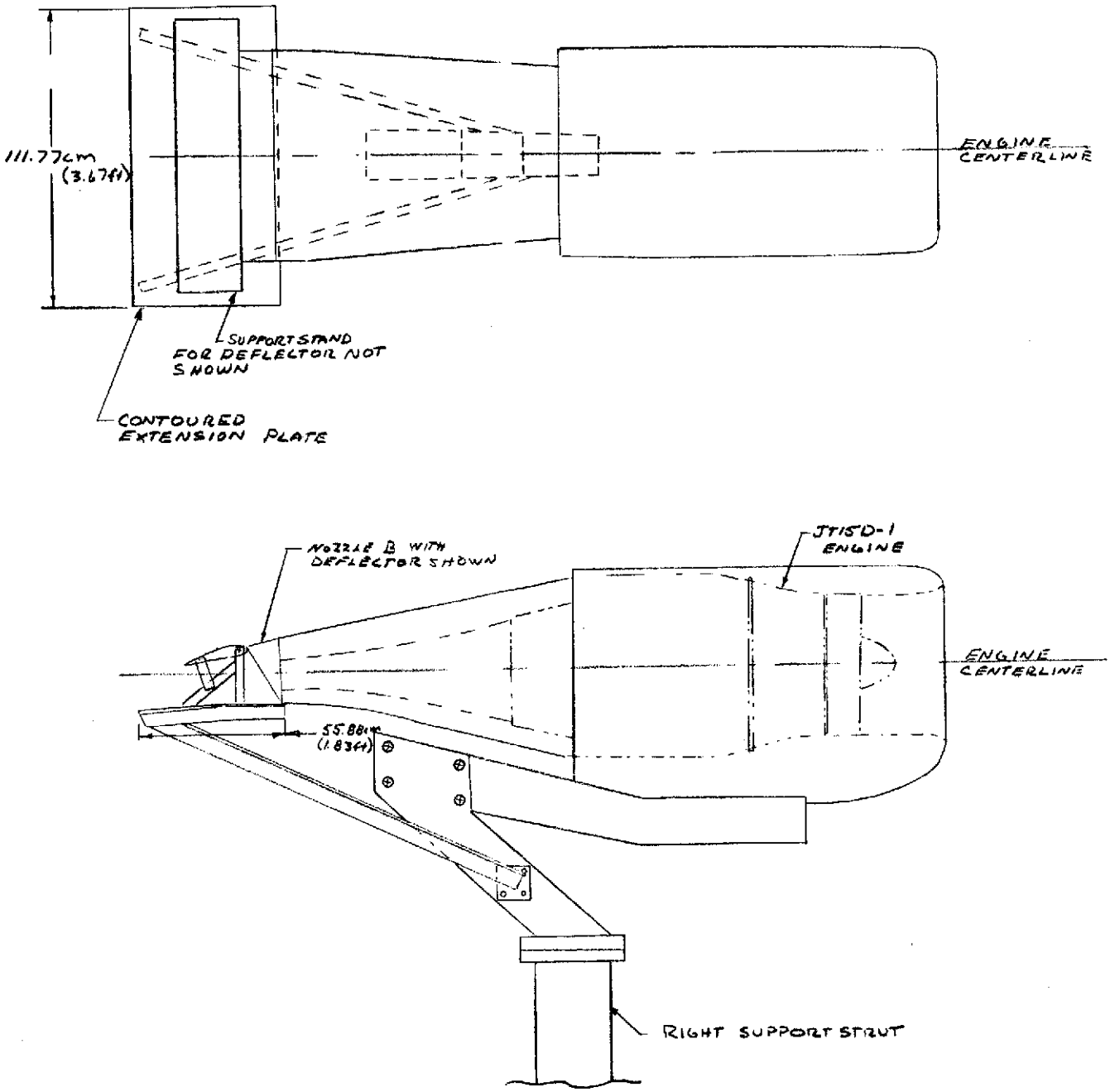

(e) Nacelle with nozzle static test extension plate.

Figure 2.– Concluded.

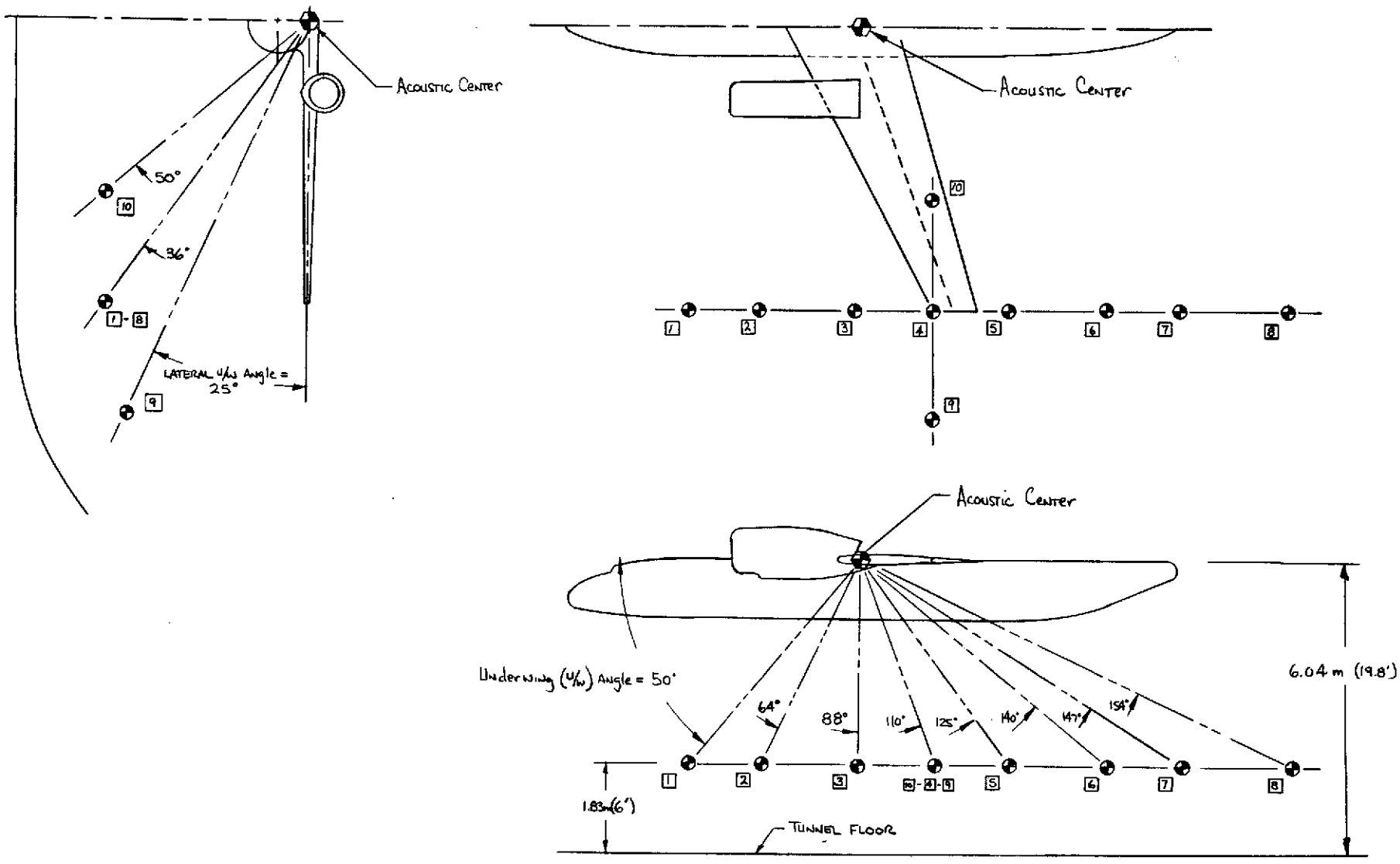

(a) Underwing and lateral underwing mics

Figure 3.– Microphone arrangements.

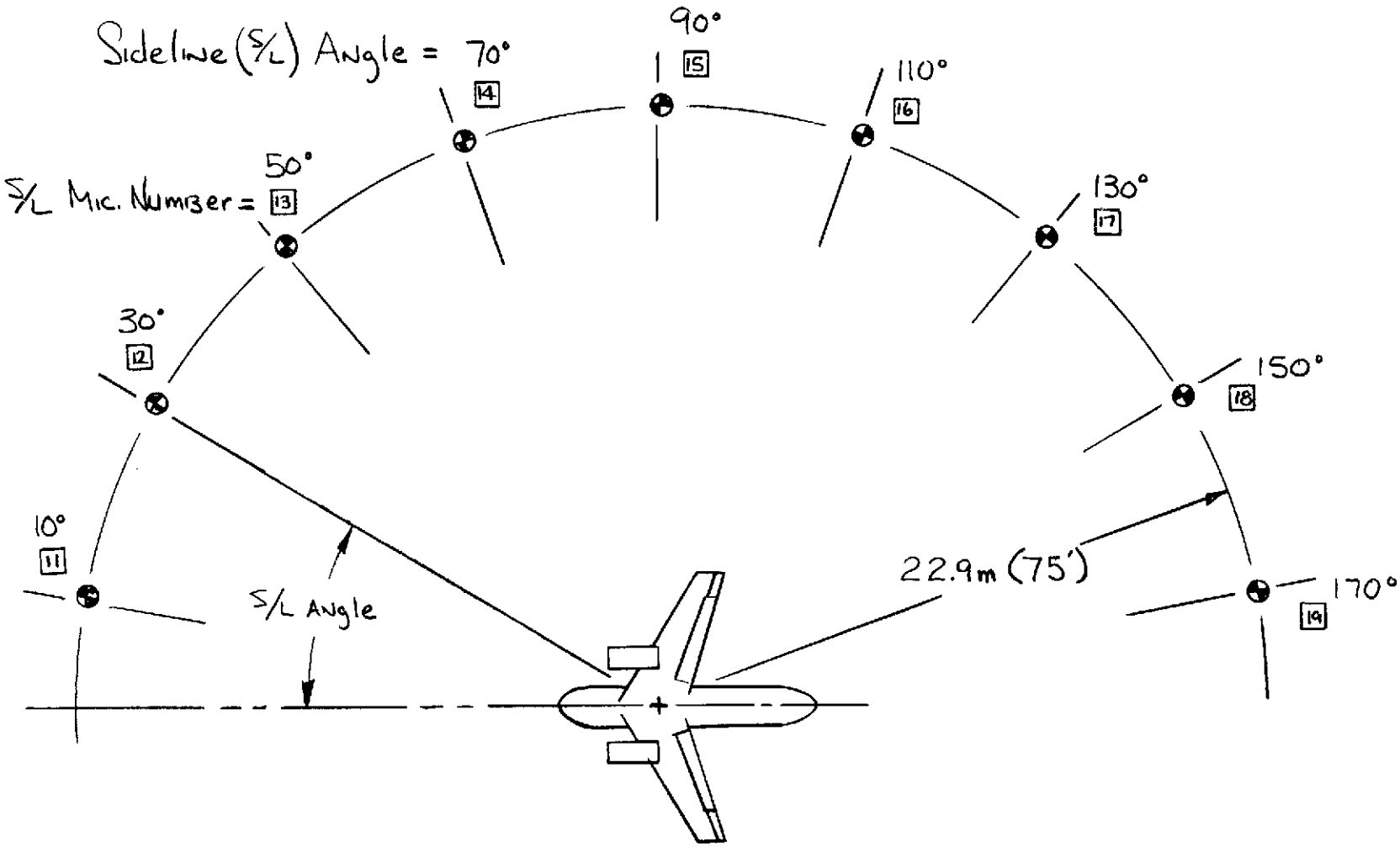

(b) Sideline microphone arrangement

Figure 3.– Concluded.

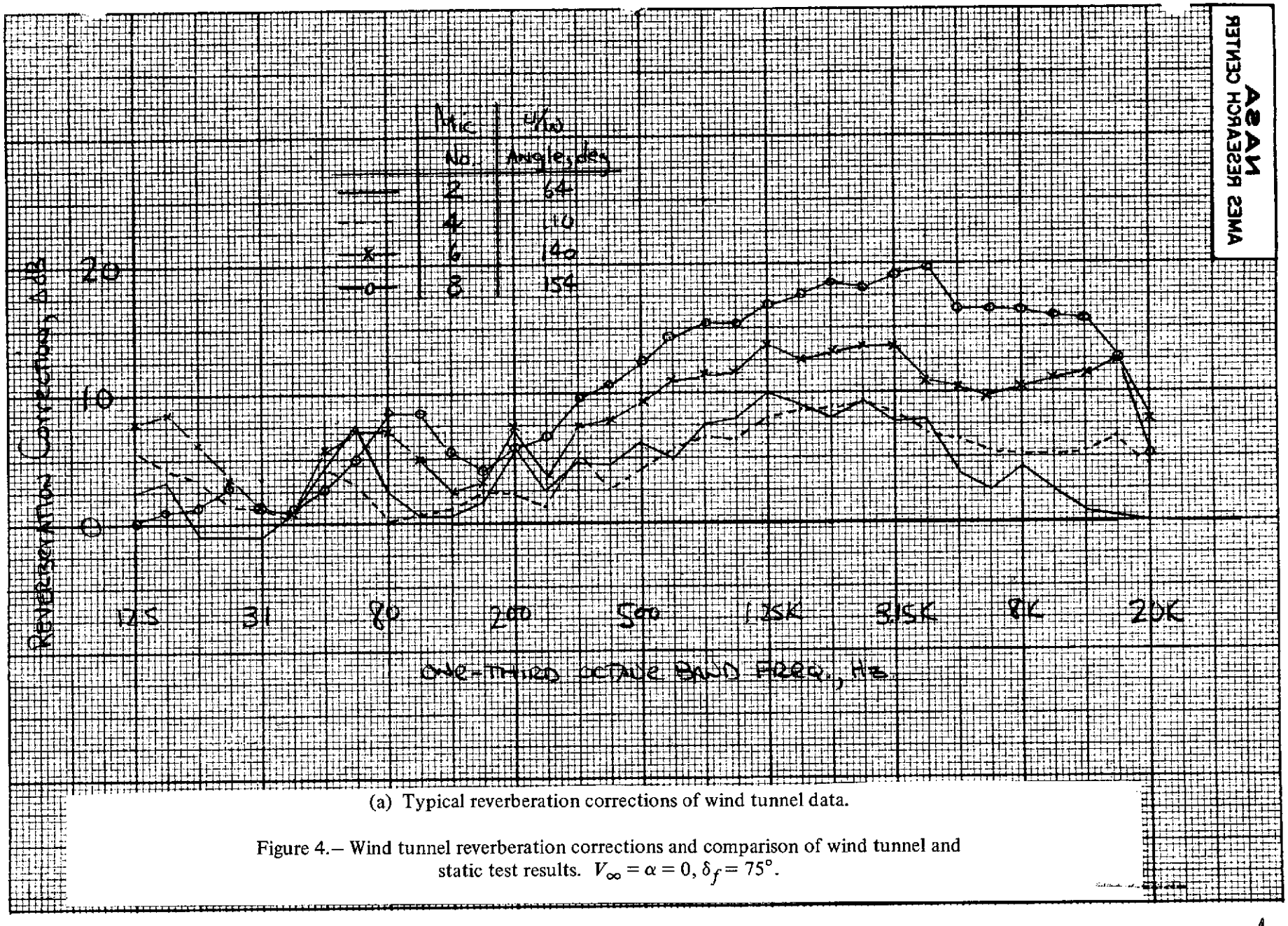

(a) Typical reverberation corrections of wind tunnel data.

Figure 4.– Wind tunnel reverberation corrections and comparison of wind tunnel and static test results. $V_\infty = \alpha = 0, \delta_f = 75°$.

4a

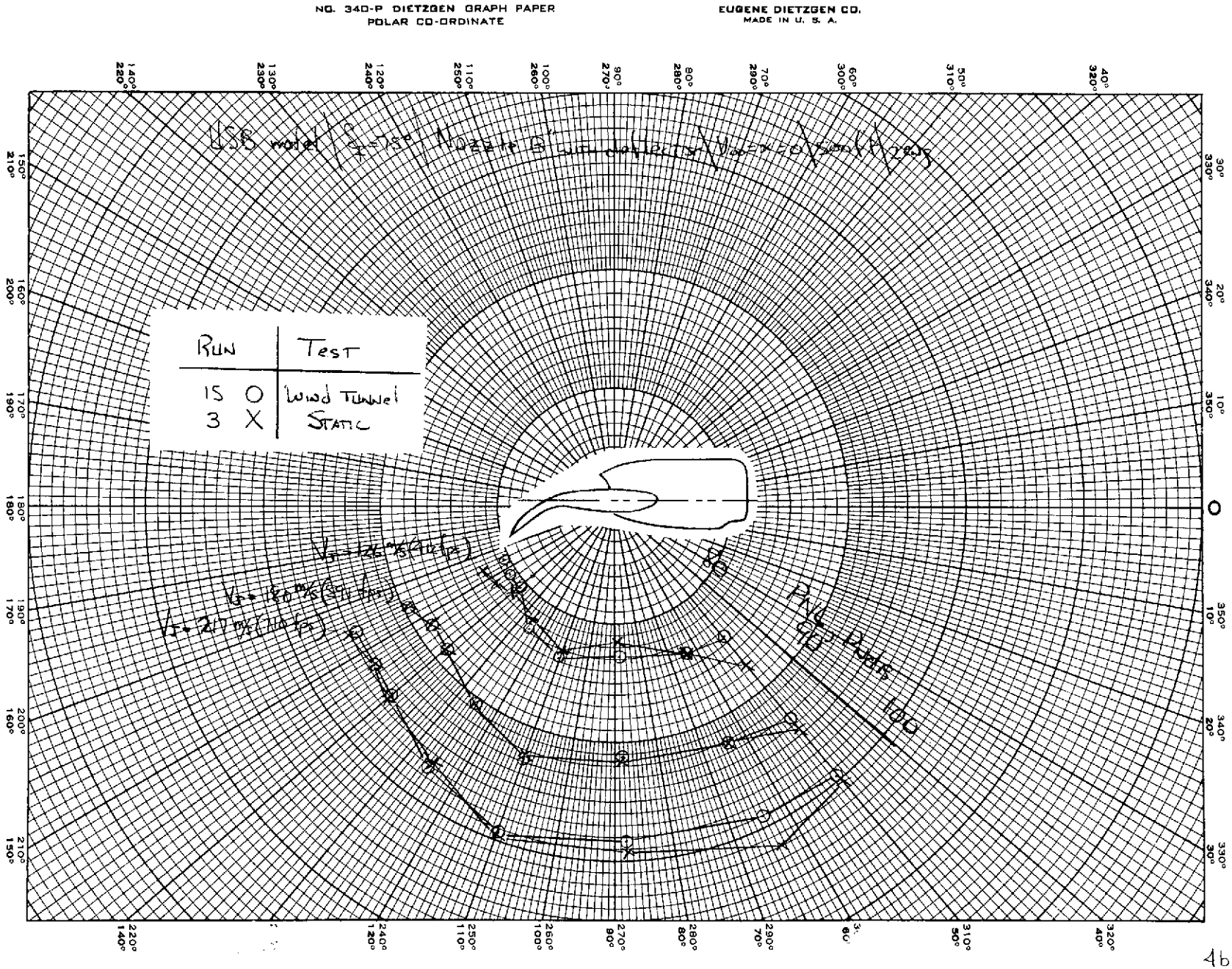

(b) *PNL* directivity; nozzle "B" with deflector.

Figure 4.– Continued.

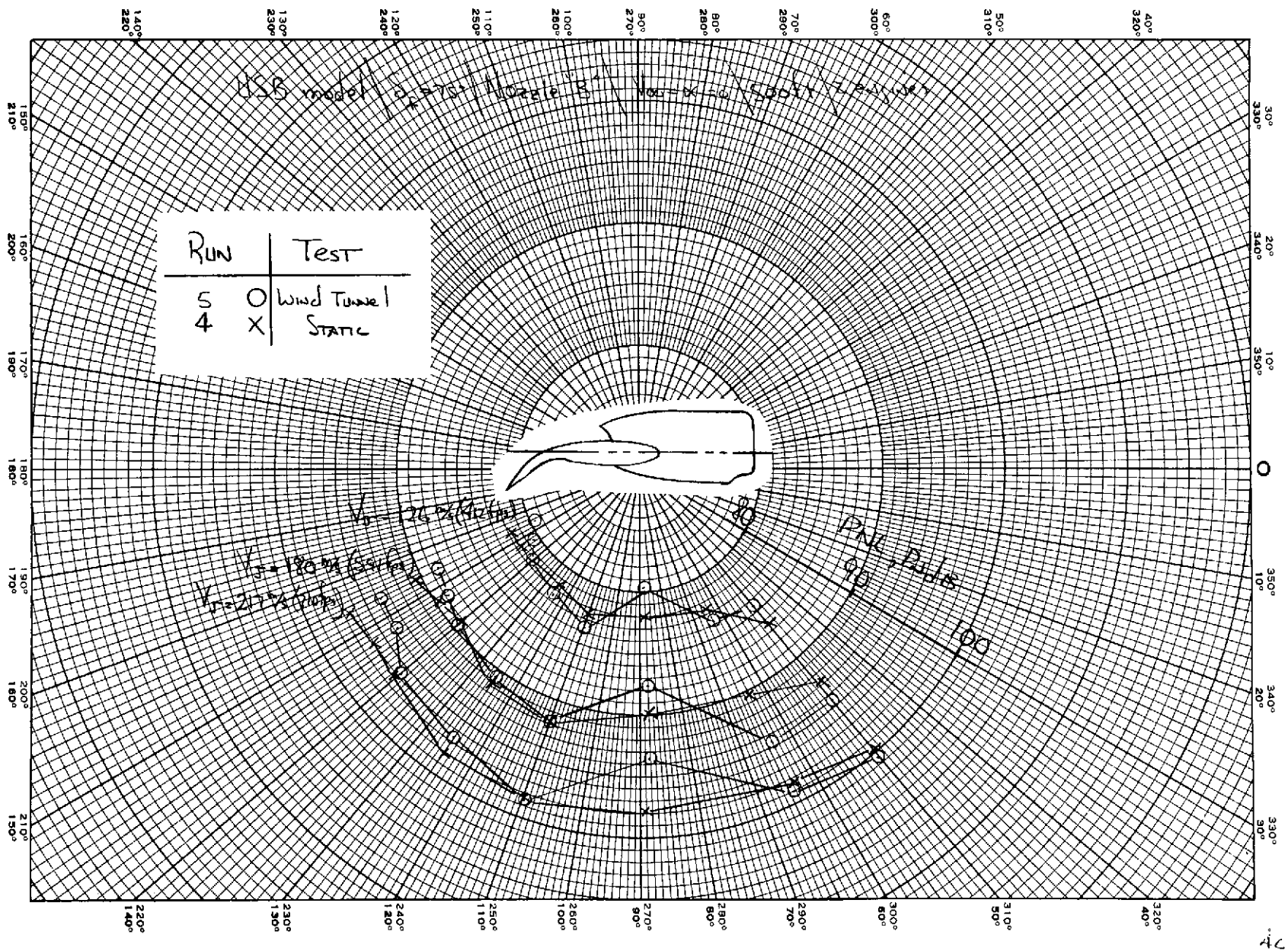

(c) *PNL* directivity; nozzle "B".

Figure 4.– Continued.

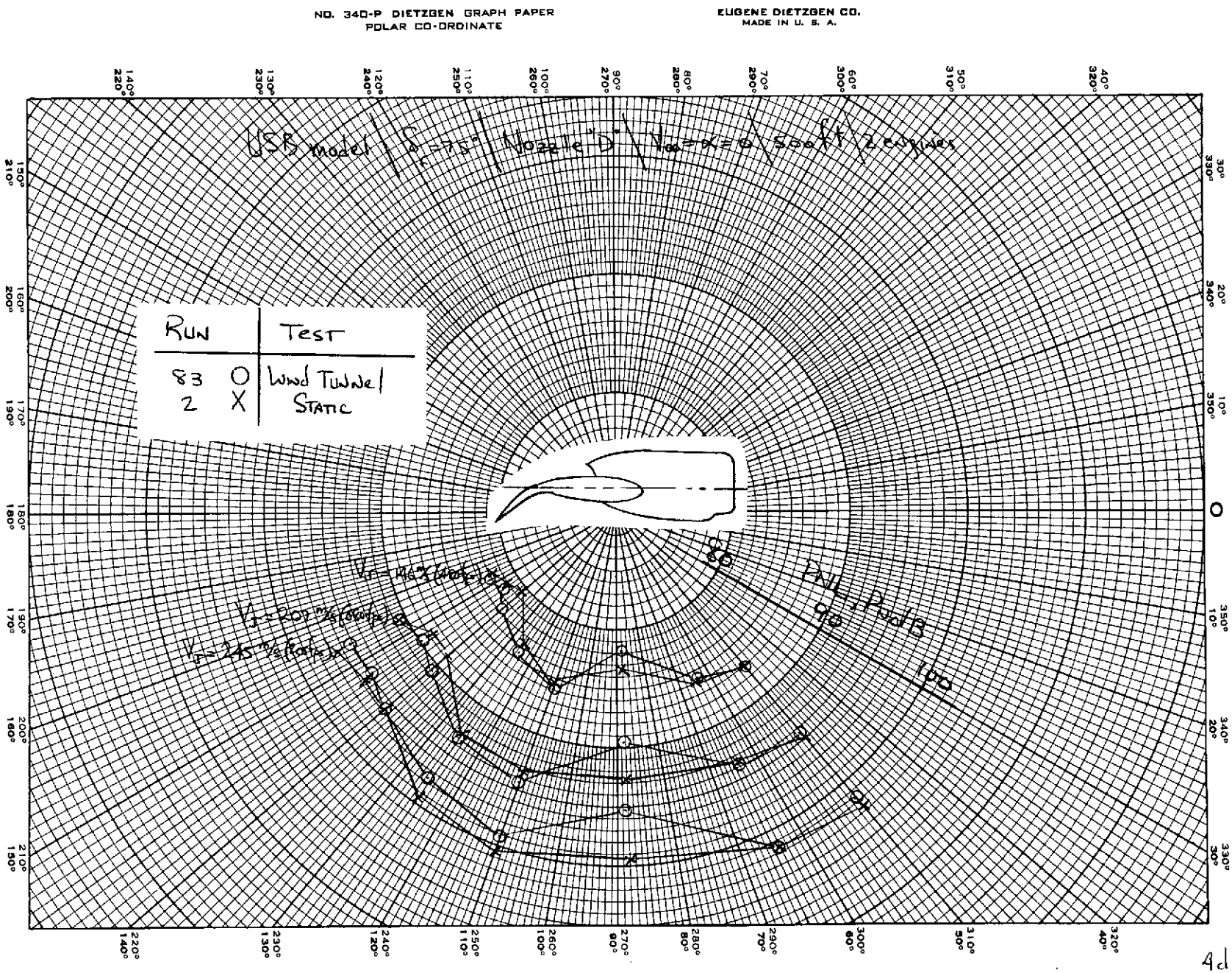

(d) *PNL* directivity; nozzle "D".

Figure 4.– Continued.

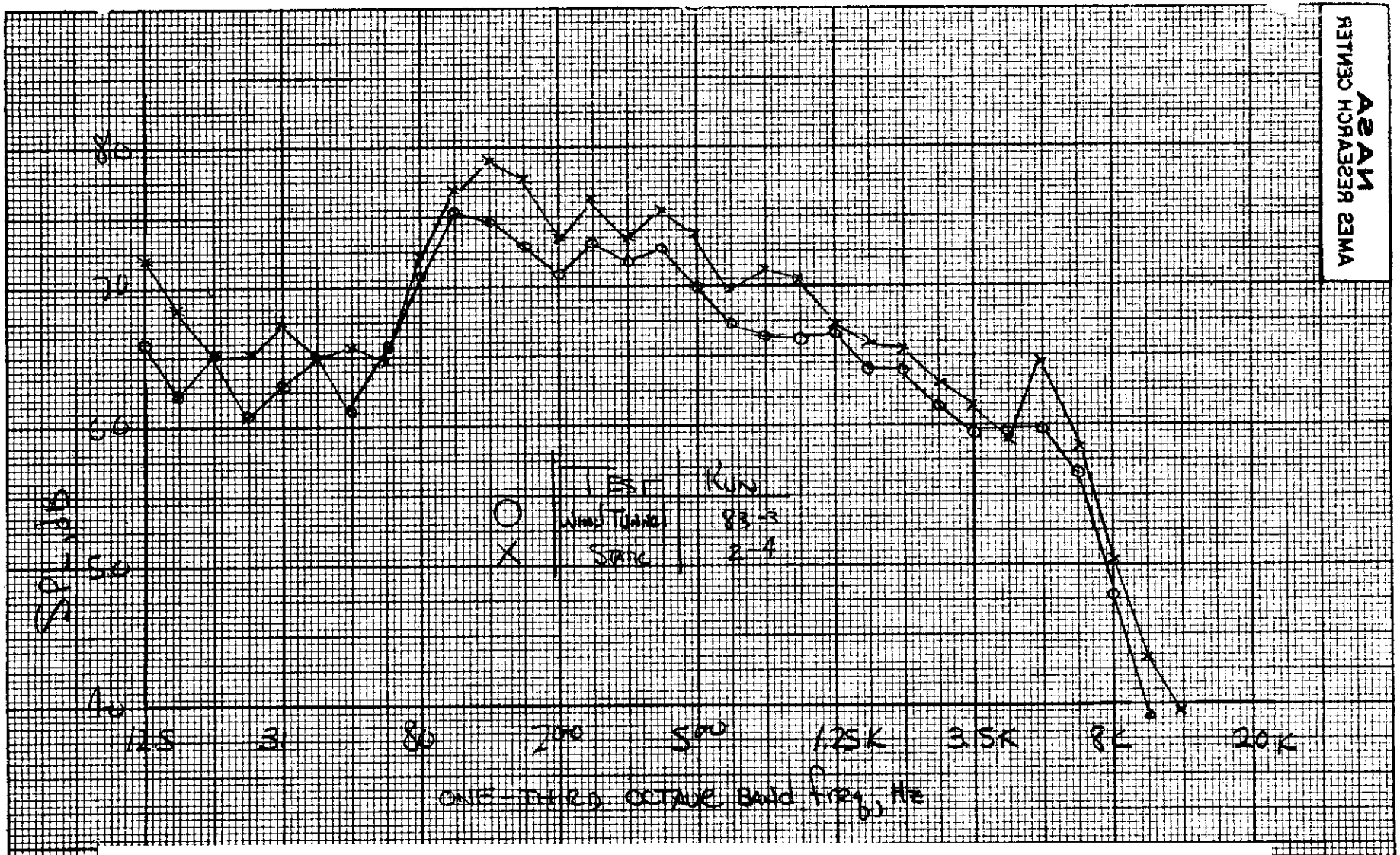

(e) Frequency spectra; nozzle "D", U/W angle = 88°, V_J = 207 m/s (680 fps).

Figure 4.– Concluded.

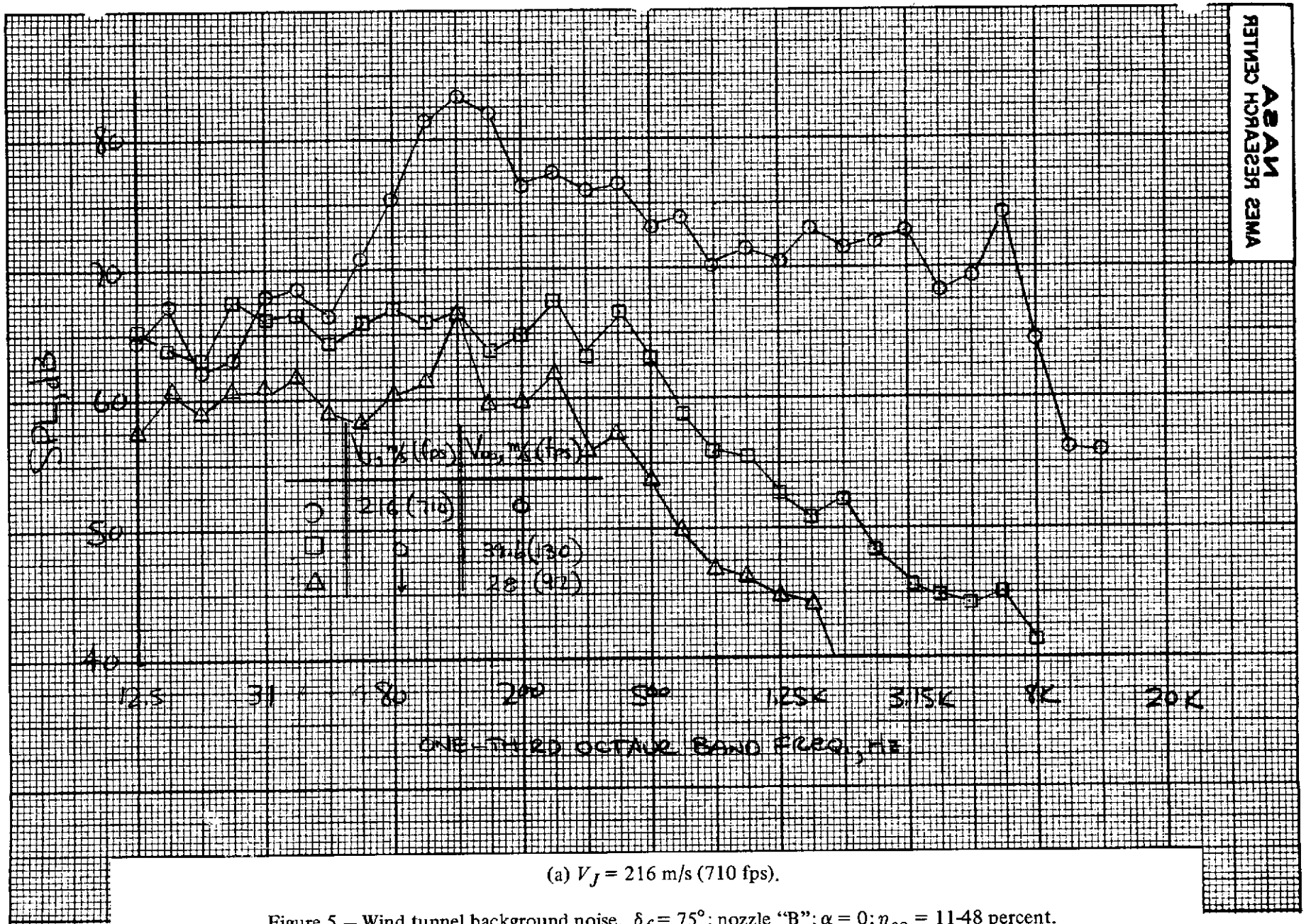

(a) V_J = 216 m/s (710 fps).

Figure 5.– Wind tunnel background noise. $\delta_f = 75°$; nozzle "B"; $\alpha = 0$; η_{CO} = 11-48 percent.

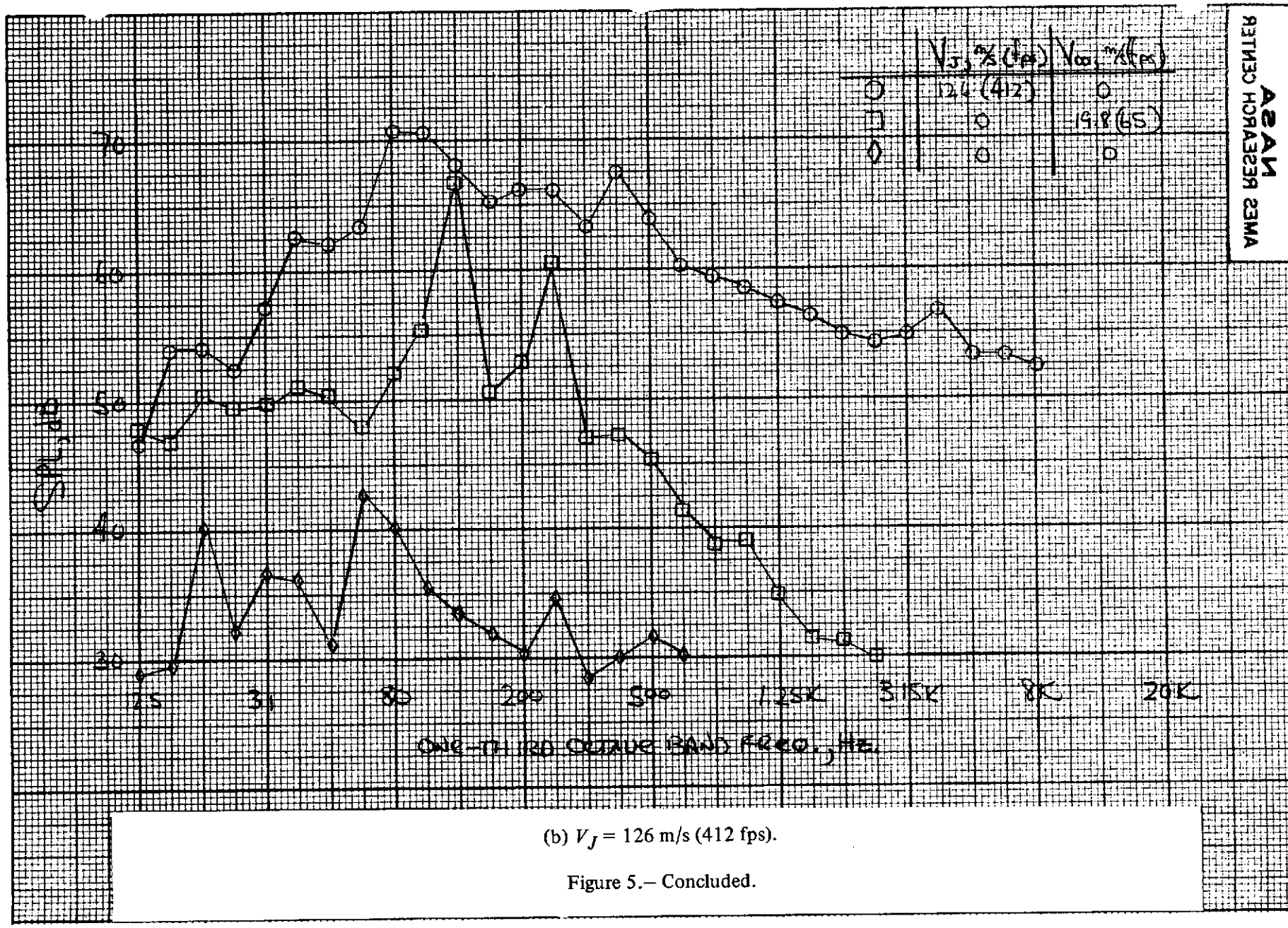

(b) V_J = 126 m/s (412 fps).

Figure 5.– Concluded.

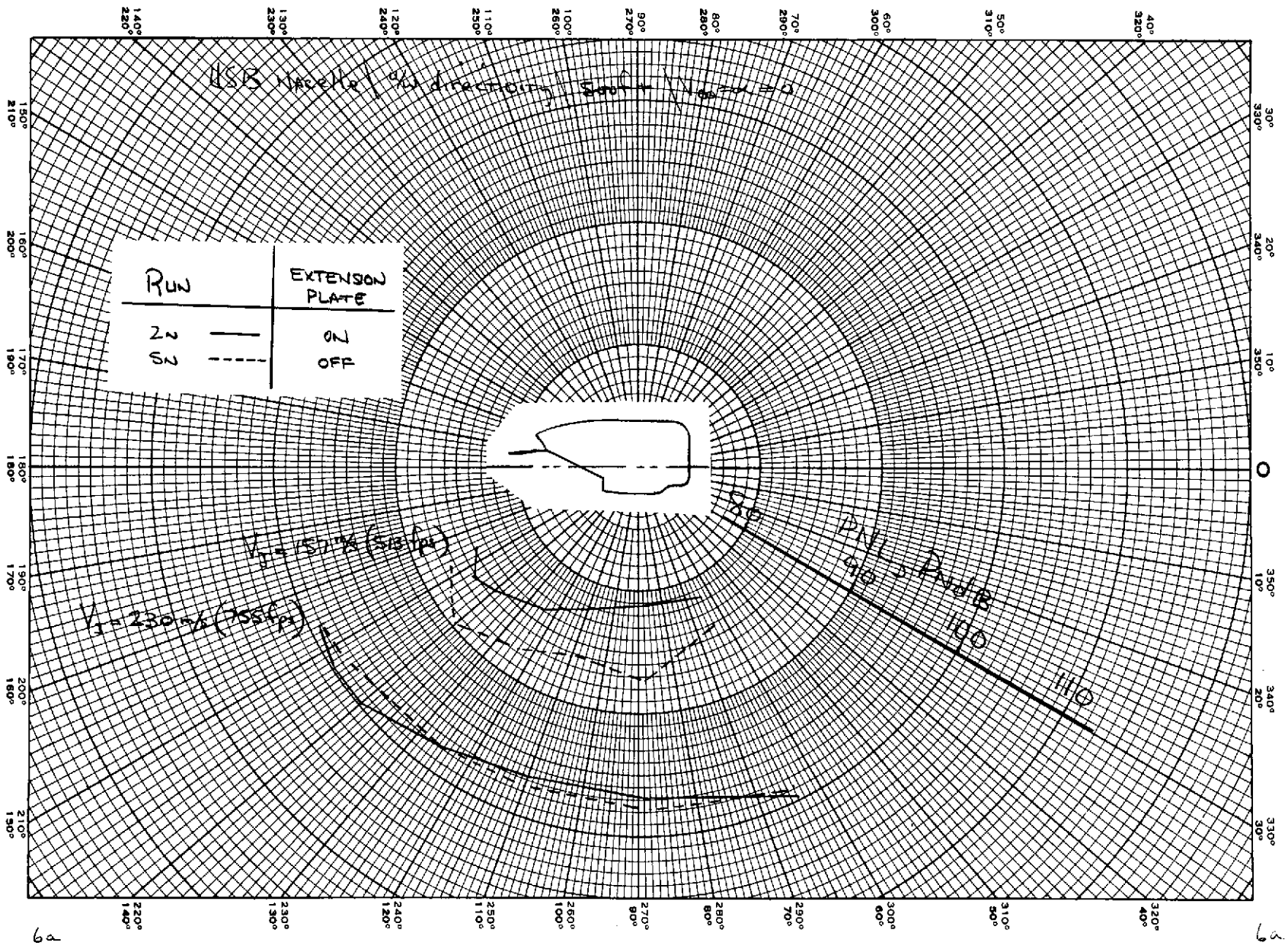

(a) Underwing *PNL* directivity.

Figure 6.– Effect of nozzle extension plate on nacelle underwing acoustic characteristics.
Nozzle "B", $V_\infty = \alpha = 0$.

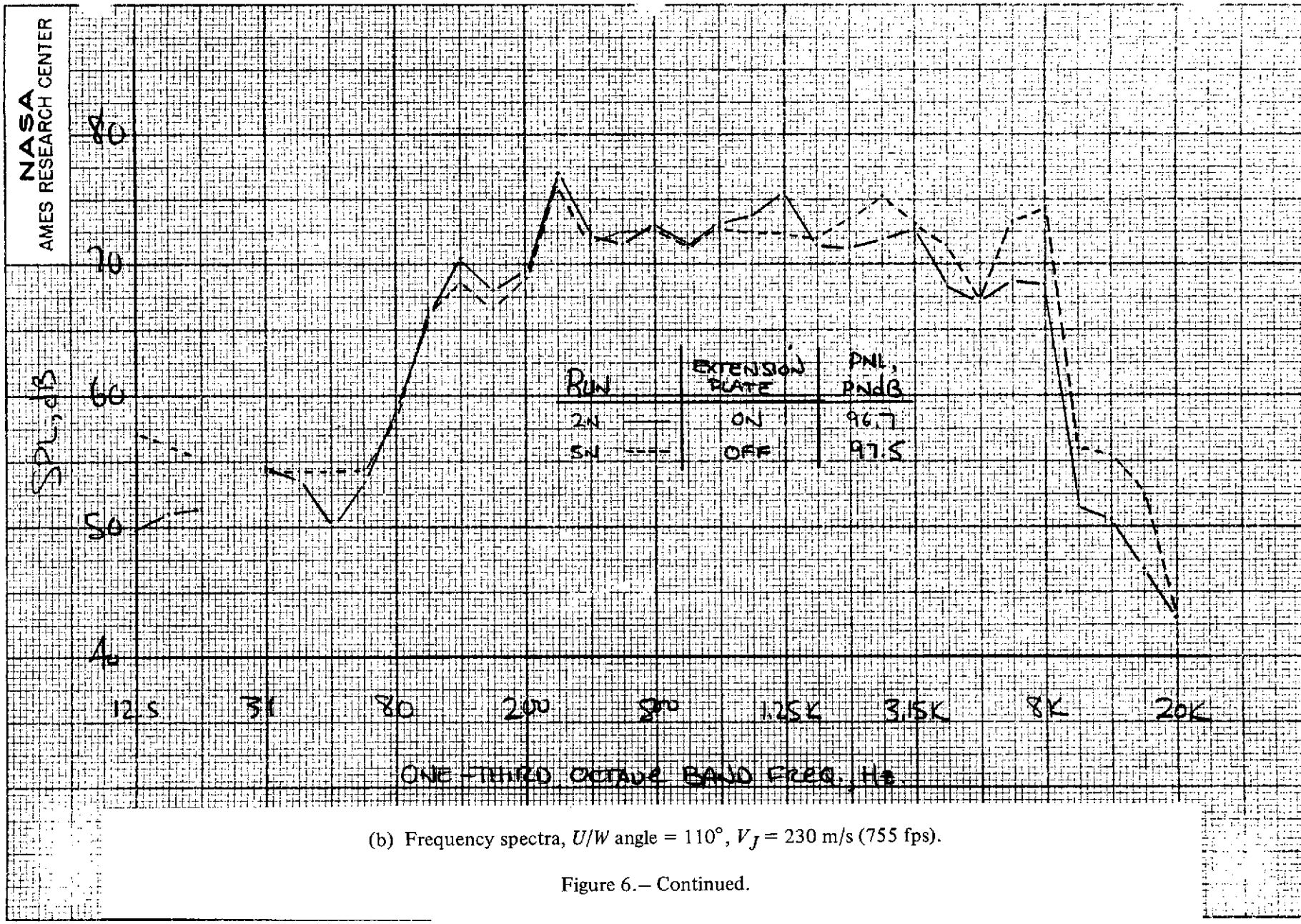

(b) Frequency spectra, U/W angle = 110°, V_J = 230 m/s (755 fps).

Figure 6.– Continued.

66

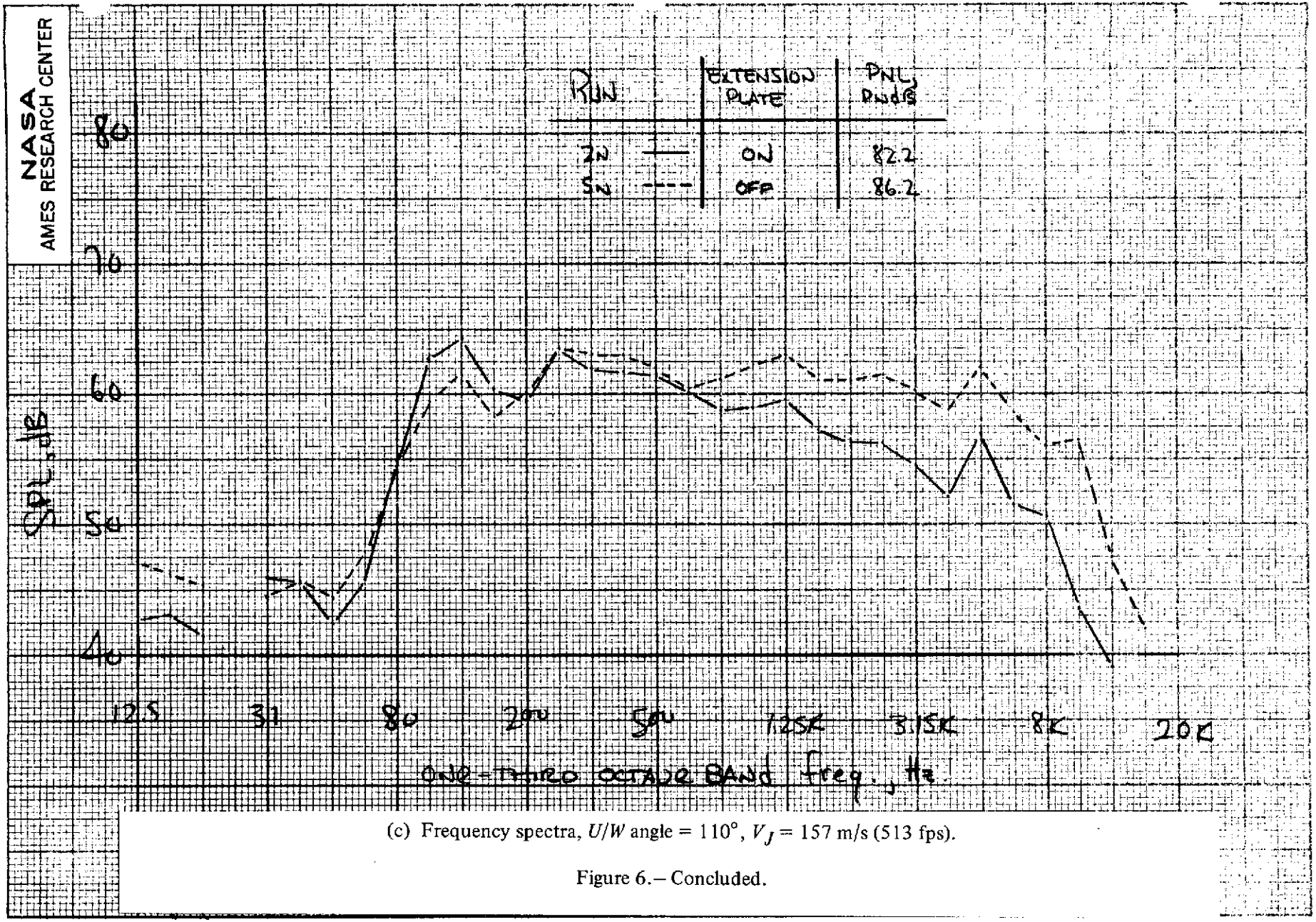

(c) Frequency spectra, U/W angle = 110°, V_J = 157 m/s (513 fps).

Figure 6.– Concluded.

6c

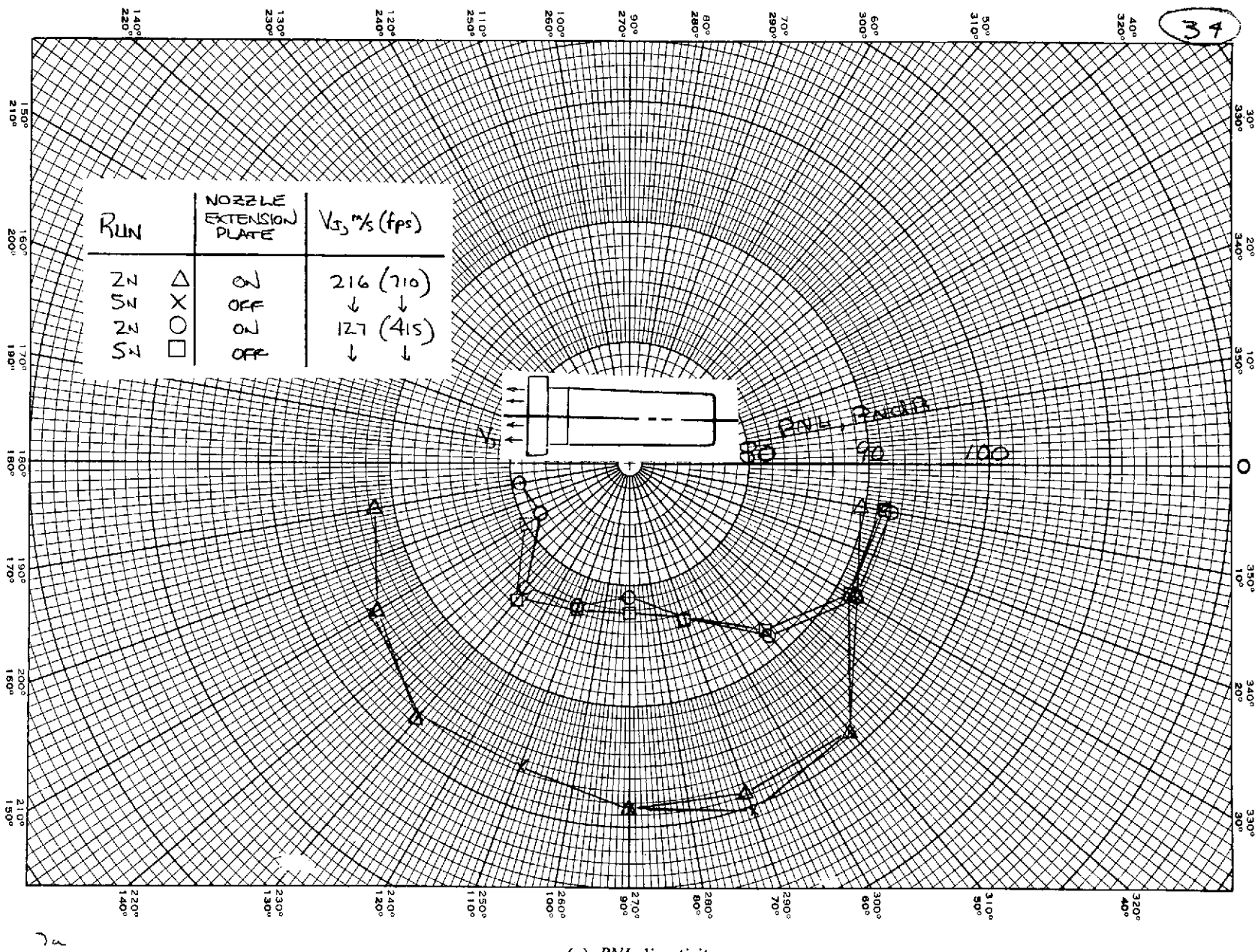

(a) *PNL* directivity.

Figure 7.– Effect of nozzle extension plate on nacelle sideline acoustic characteristics.
Nozzle "B", $V_\infty = \alpha = 0$.

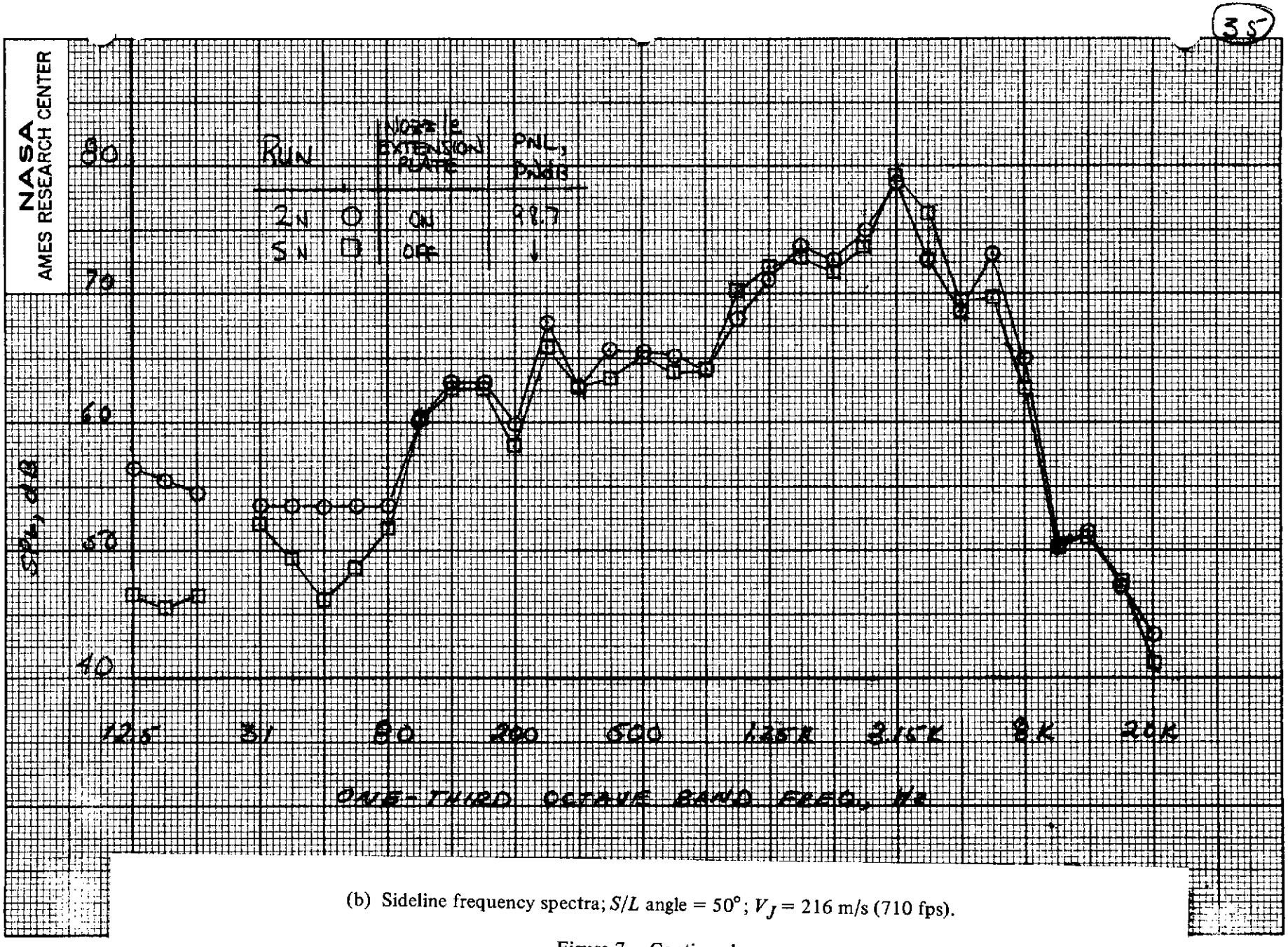

(b) Sideline frequency spectra; S/L angle = 50°; V_J = 216 m/s (710 fps).

Figure 7.– Continued.

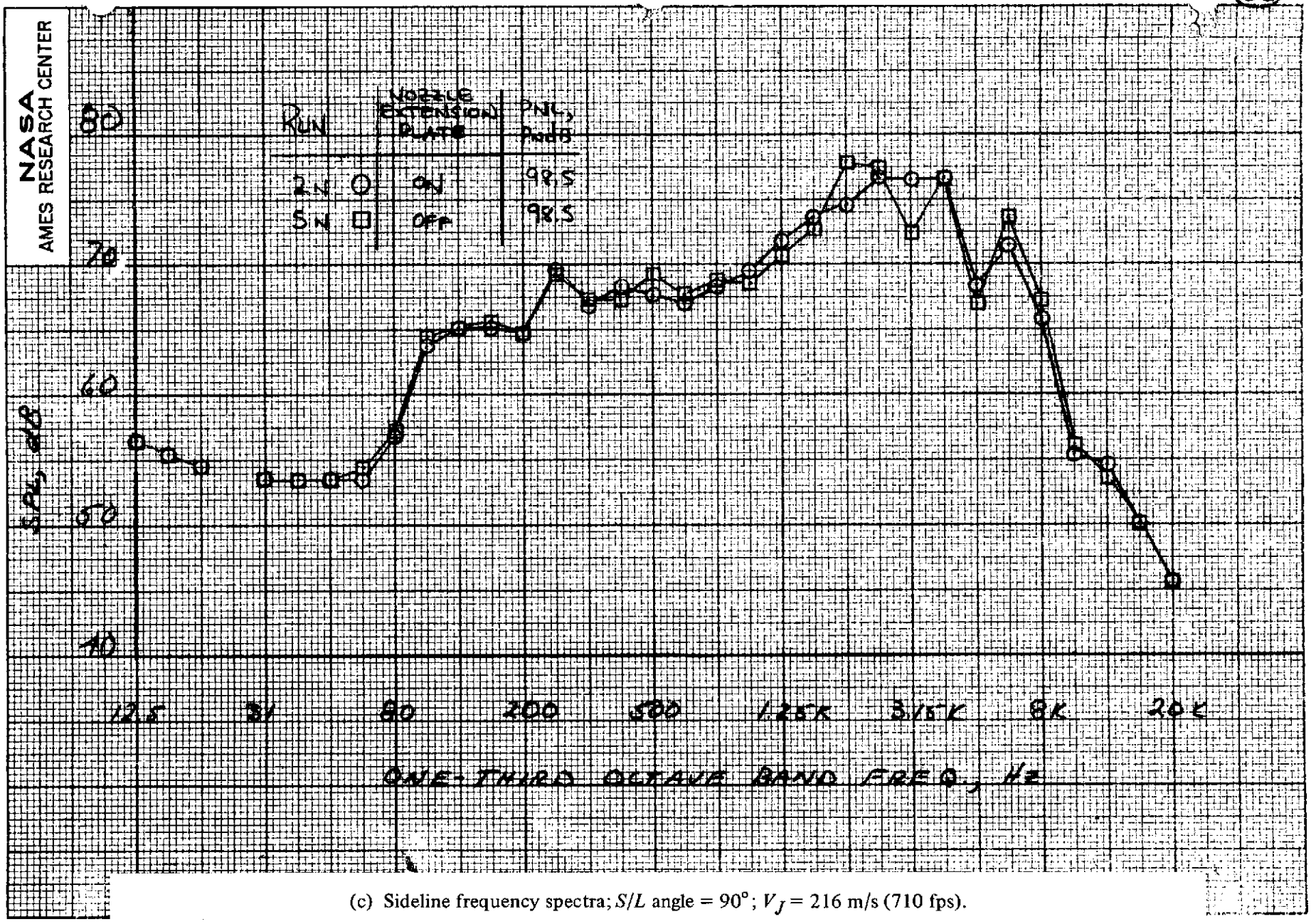

(c) Sideline frequency spectra; S/L angle = 90°; V_J = 216 m/s (710 fps).

Figure 7.– Concluded.

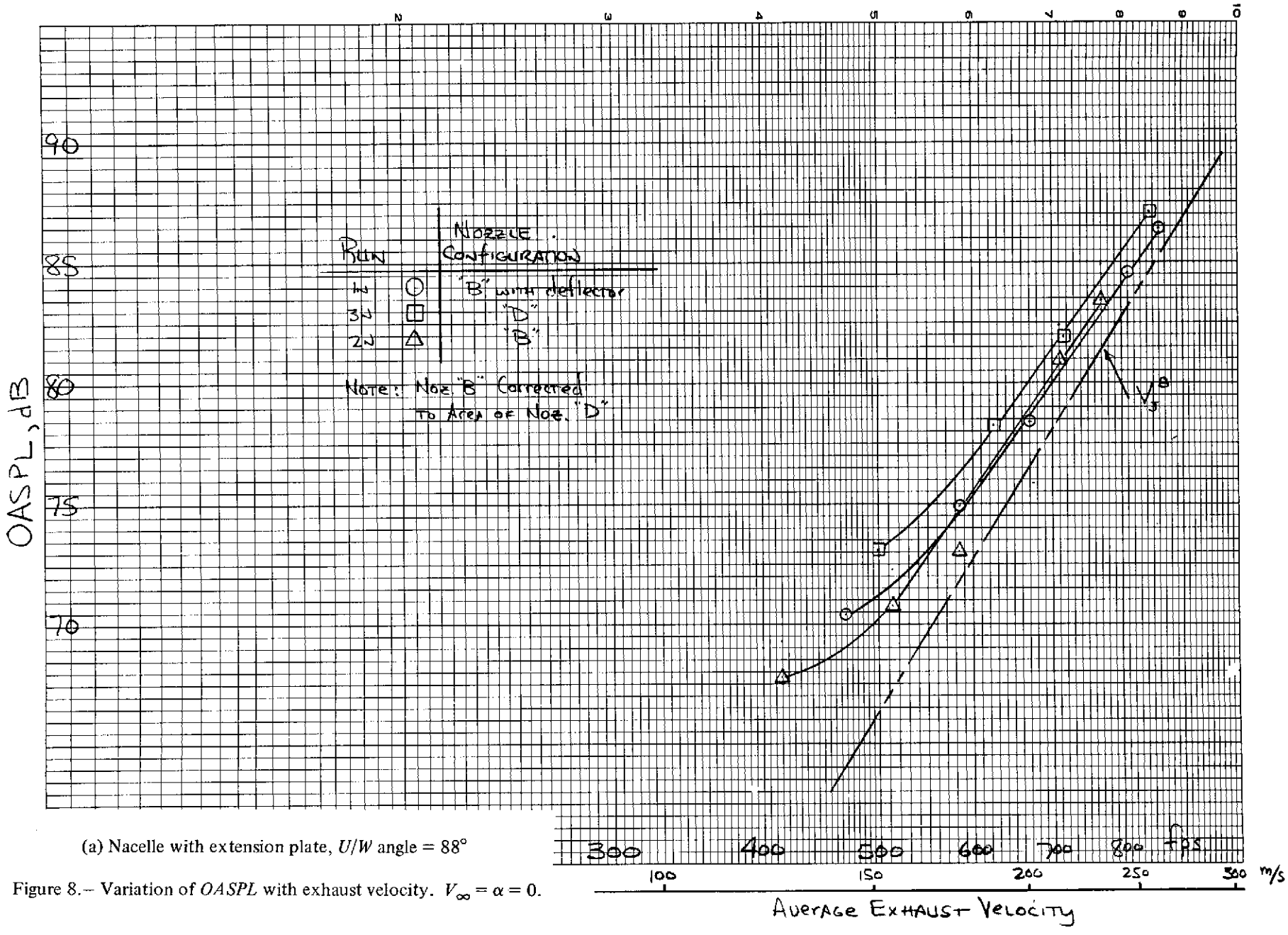

(a) Nacelle with extension plate, U/W angle = 88°

Figure 8.– Variation of *OASPL* with exhaust velocity. $V_\infty = \alpha = 0$.

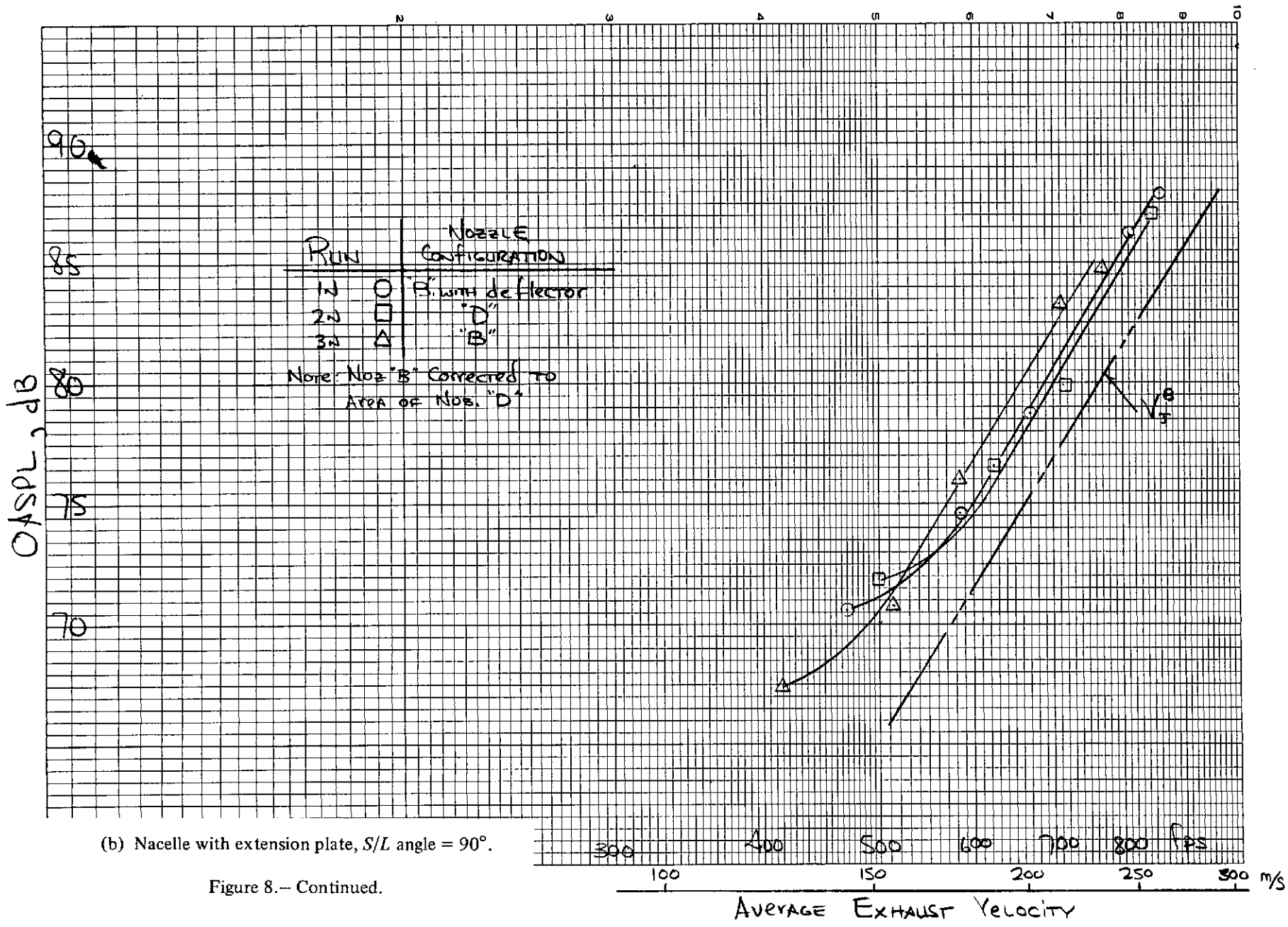

(b) Nacelle with extension plate, S/L angle = 90°.

Figure 8.– Continued.

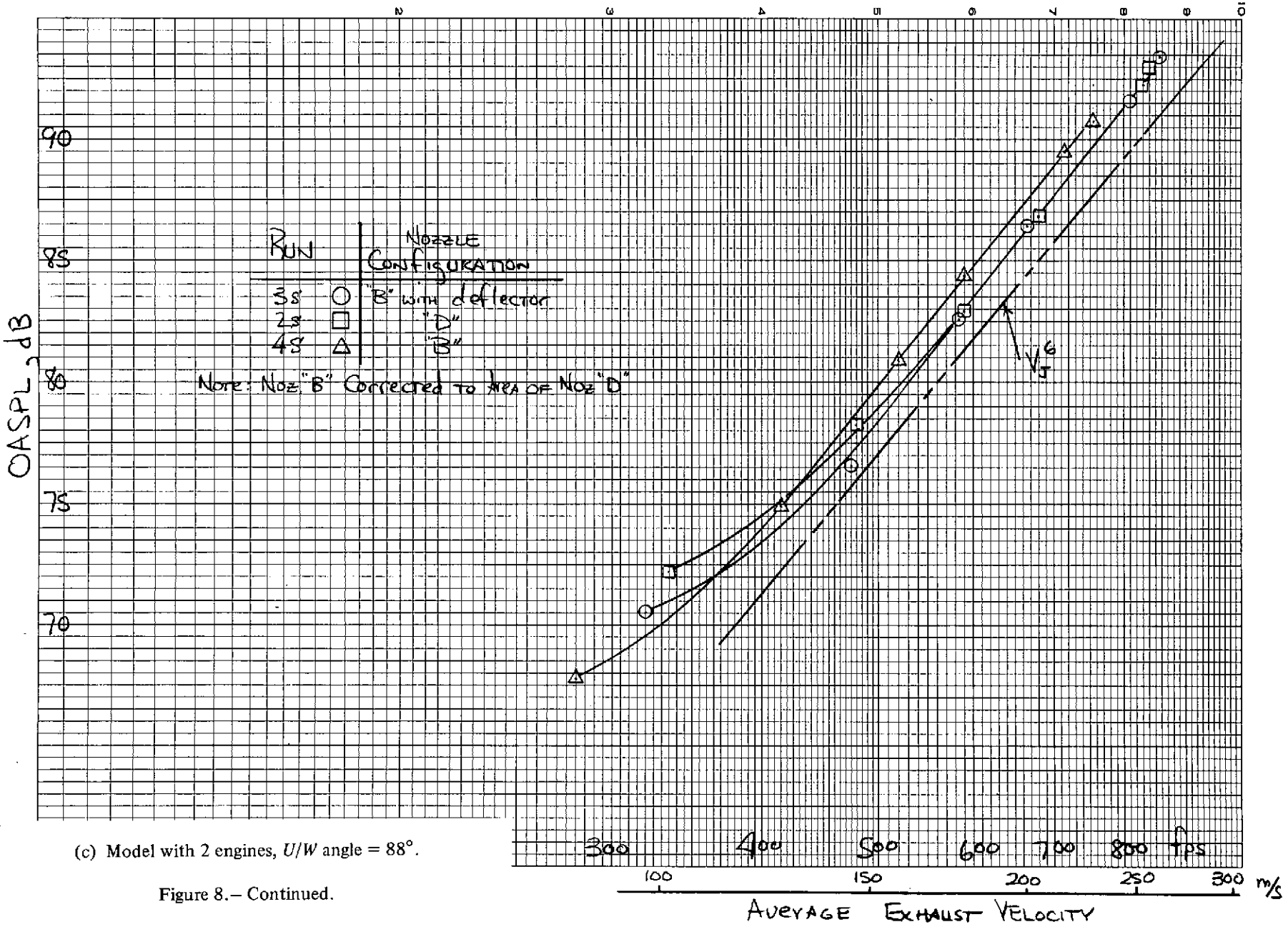

(c) Model with 2 engines, U/W angle = 88°.

Figure 8.– Continued.

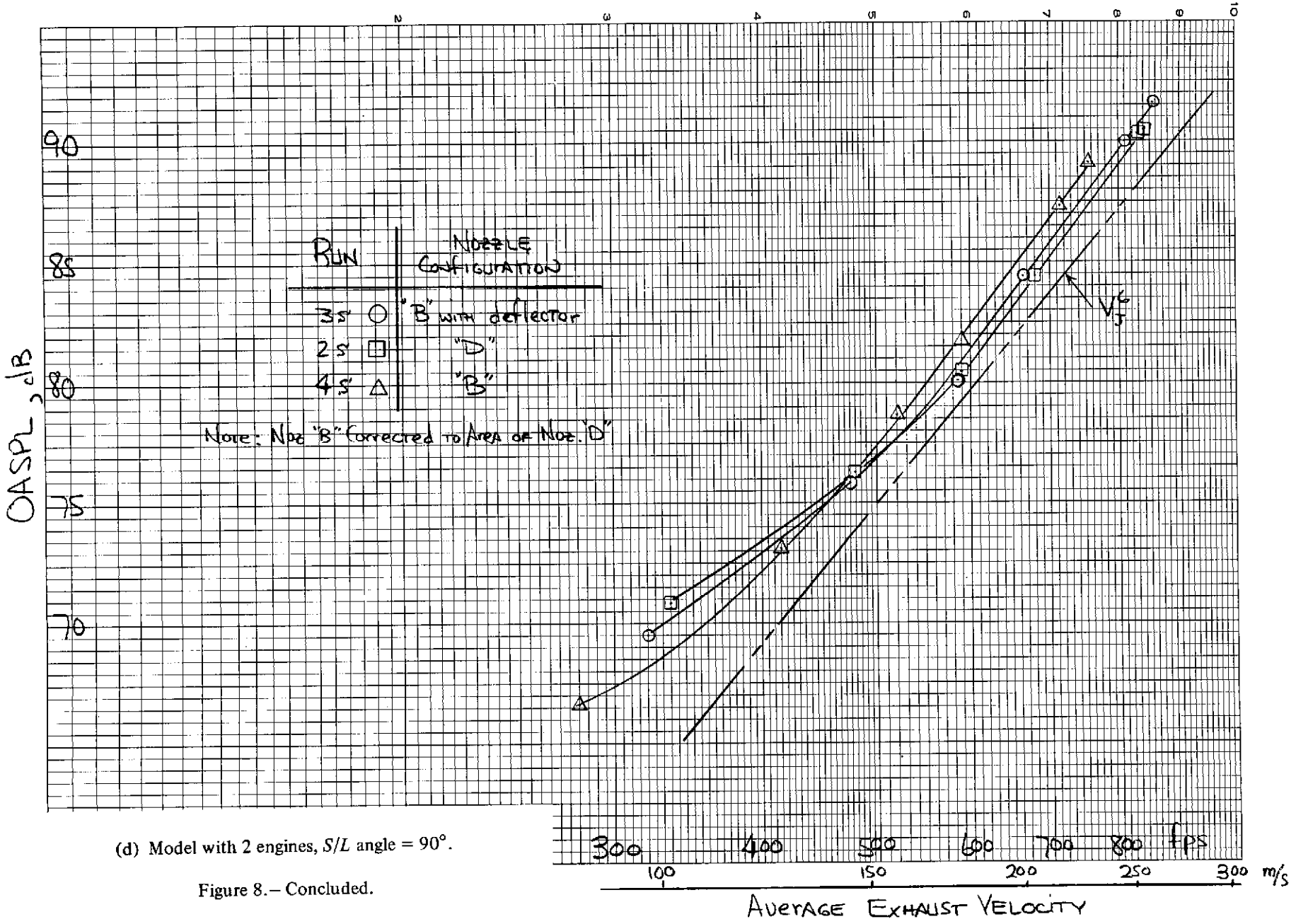

(d) Model with 2 engines, S/L angle = 90°.

Figure 8.– Concluded.

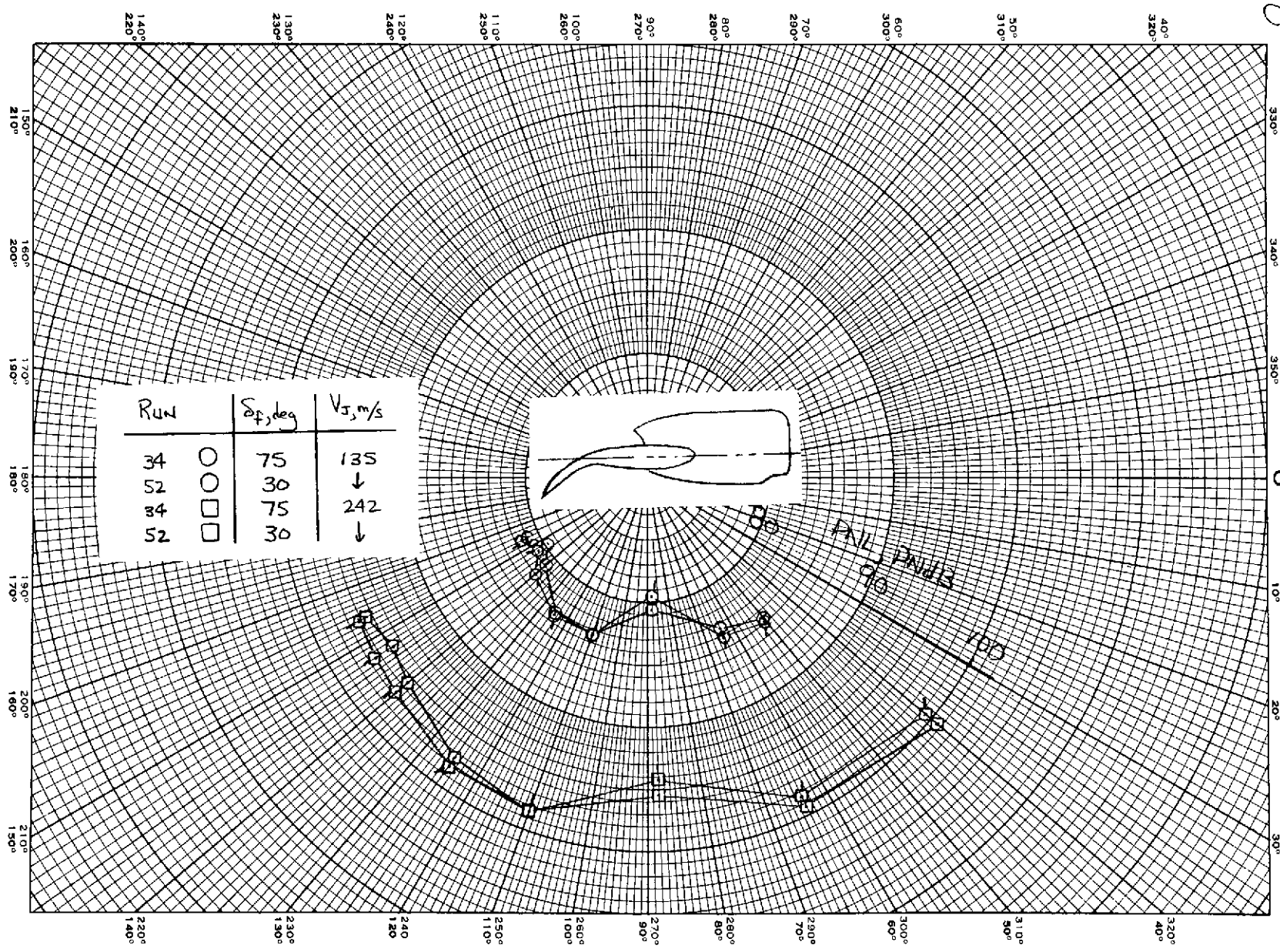

(a) Underwing *PNL* directivity pattern.

Figure 9.– Effect of δ_f on acoustic characteristics. Nozzle "B" with deflector; $V_\infty = \alpha = 0$; η_{CO} = 11-39 percent.

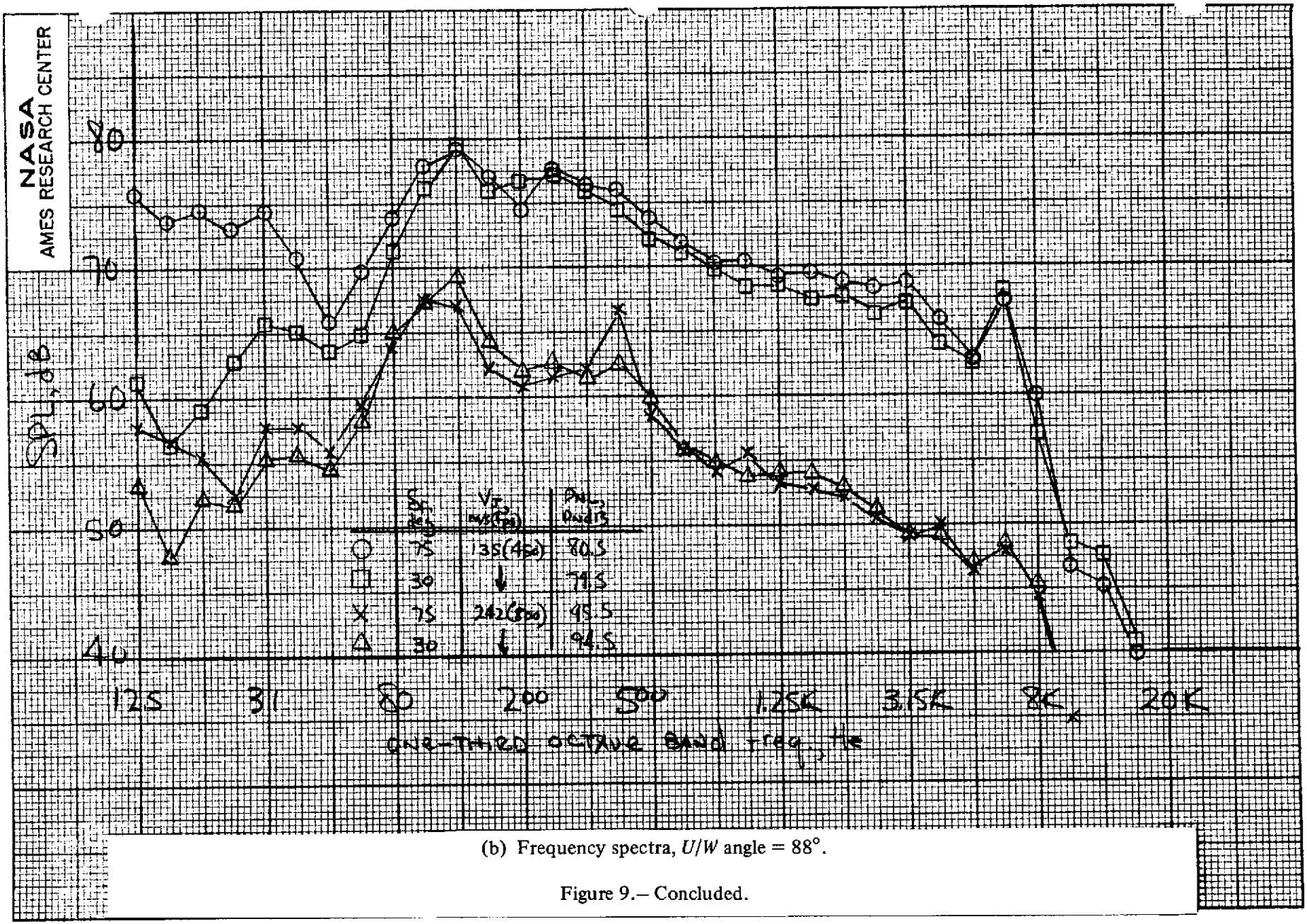

(b) Frequency spectra, U/W angle = 88°.

Figure 9.– Concluded.

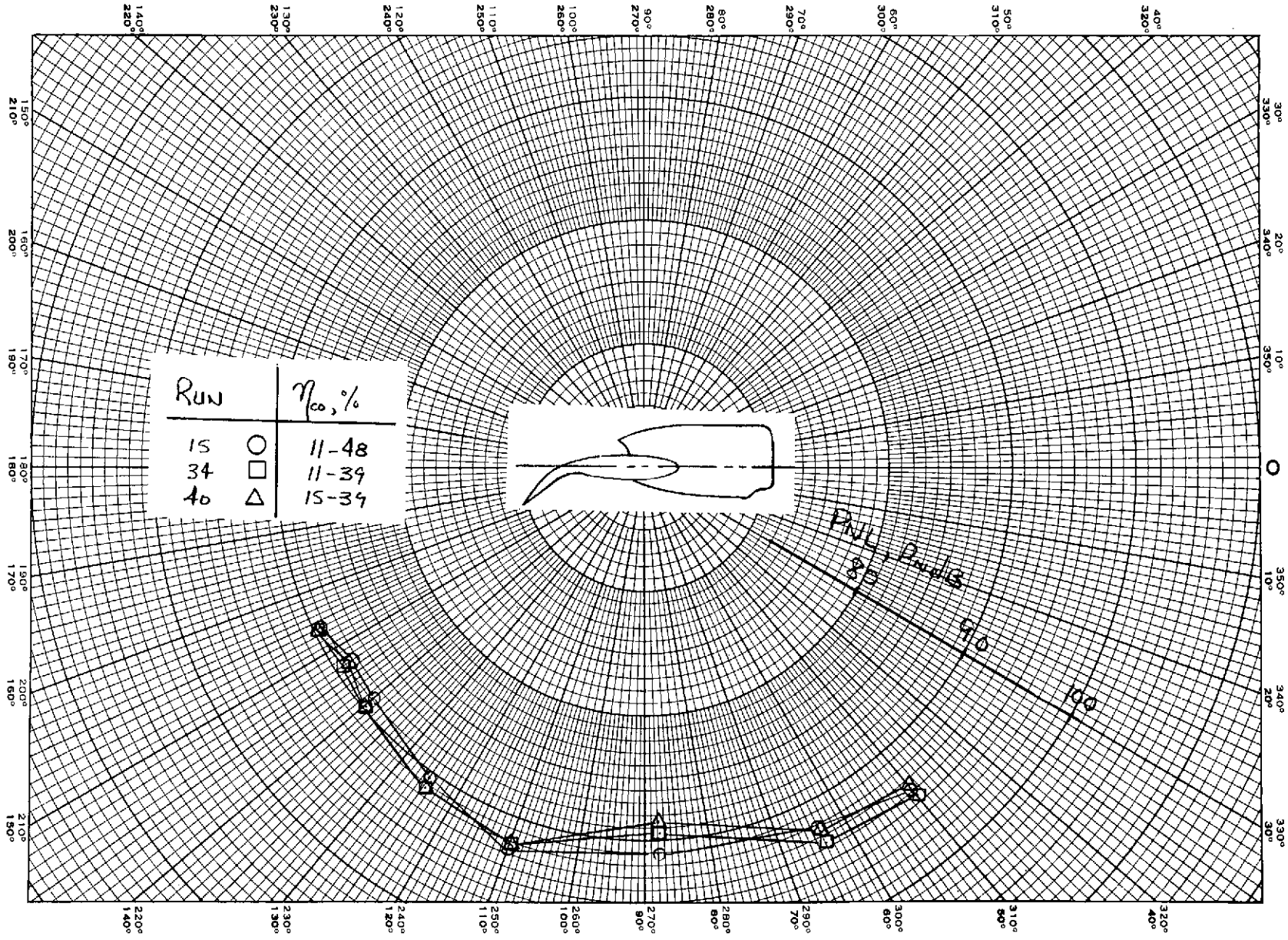

(a) Underwing *PNL* directivity pattern.

Figure 10.– Effect of η_{CO} on acoustic characteristics. Nozzle "B" with deflector; $V_\infty = \alpha = 0$; $\delta_f = 75°$; $V_J = 203$ m/s (667 fps).

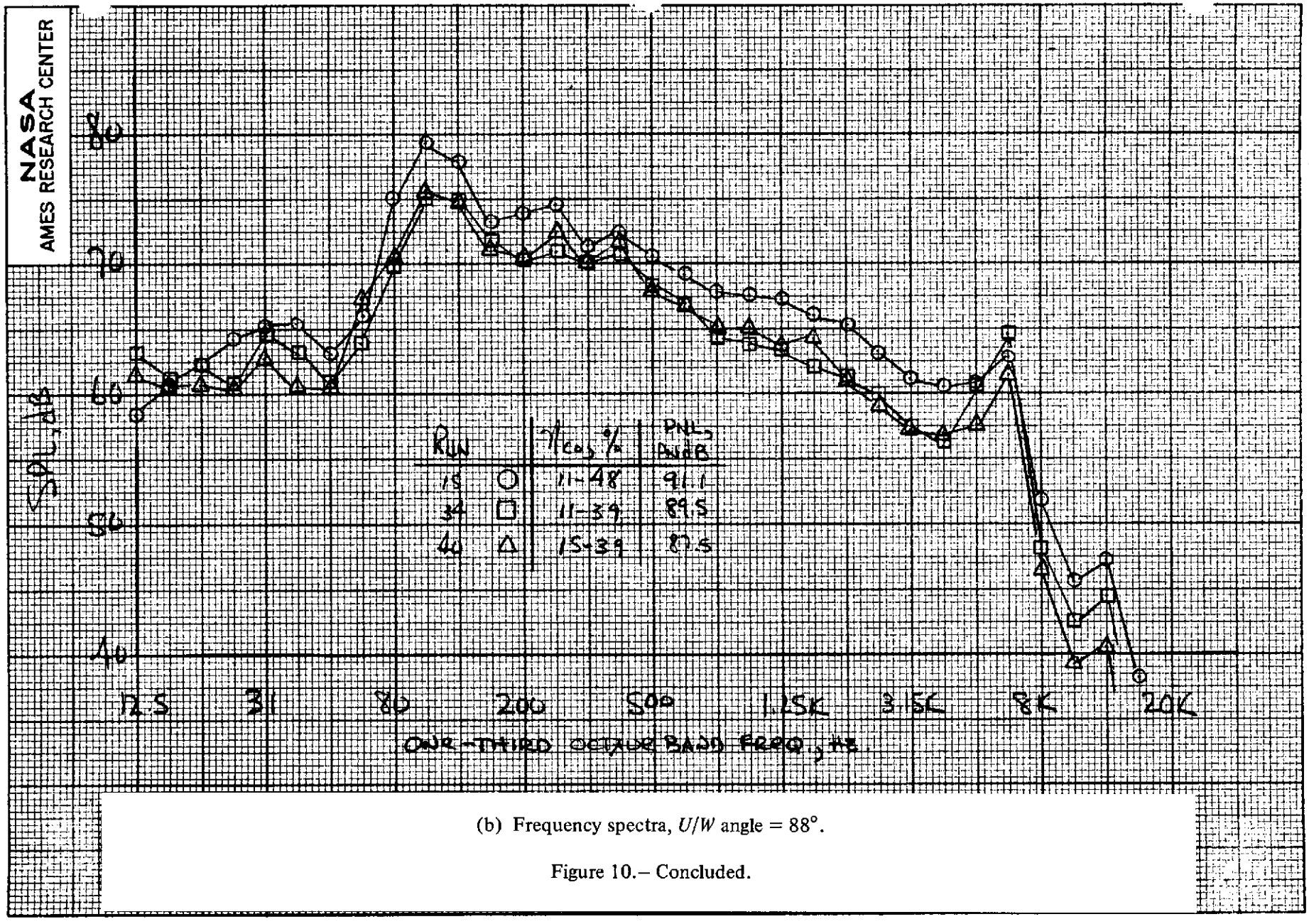

(b) Frequency spectra, U/W angle = 88°.

Figure 10.– Concluded.

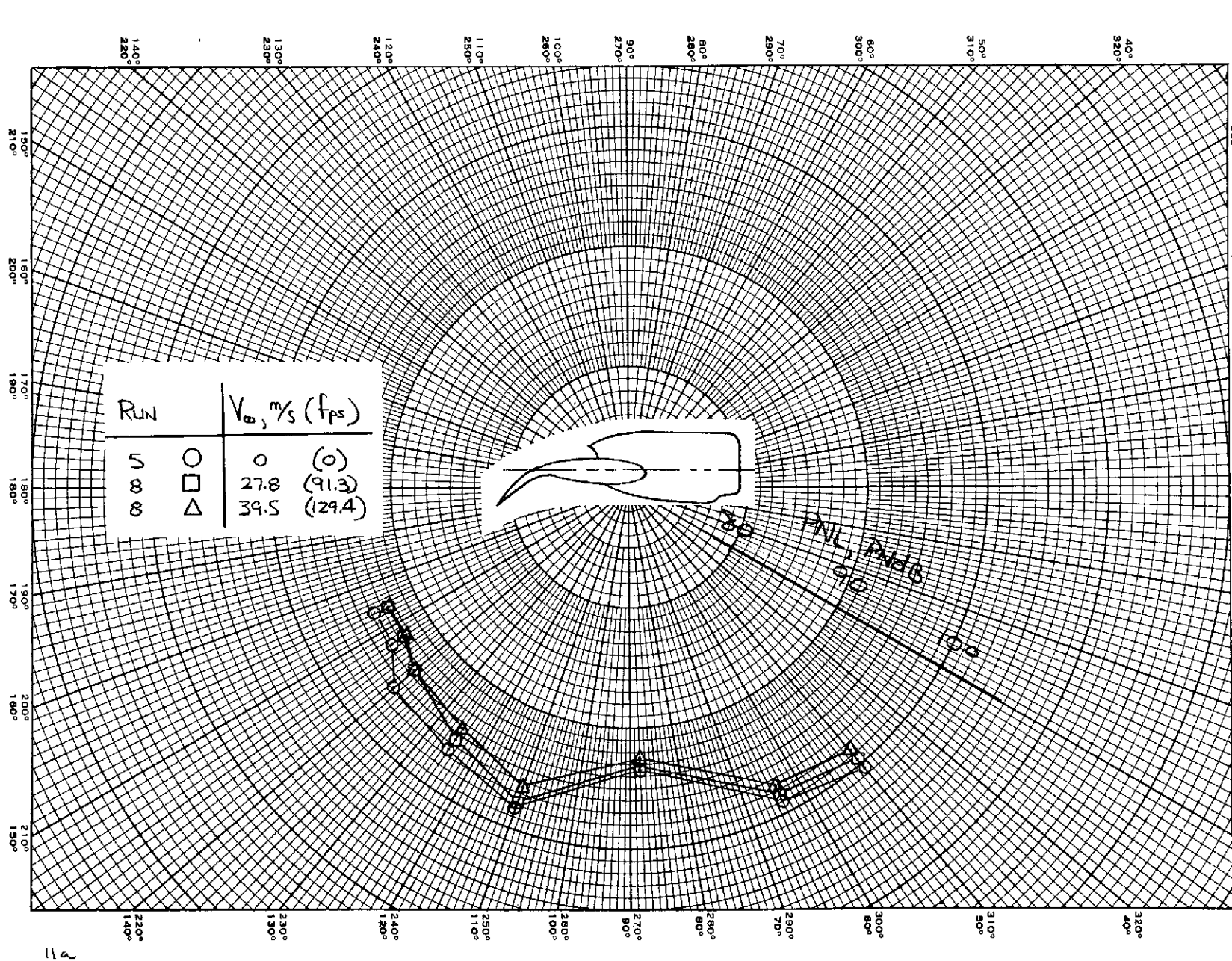

(a) Nozzle "B", $V_J = 216$ m/s (710 fps).

Figure 11.– Variation of underwing *PNL* directivity with forward speed. $\delta_f = 75°$; $\alpha = 0°$; $\eta_{CO} = 11$-48 percent.

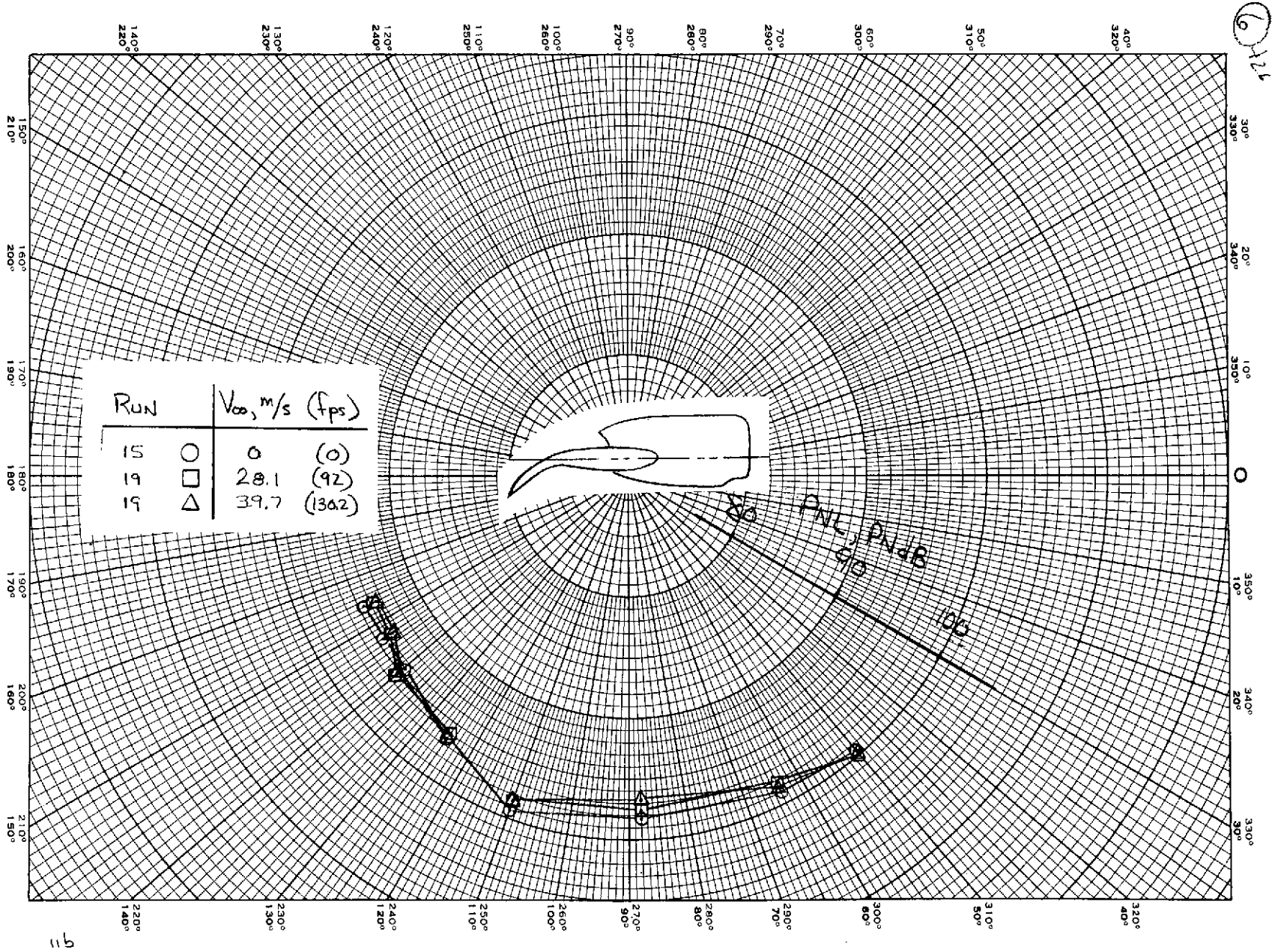

(b) Nozzle "B" with deflector; $V_j = 246$ m/s (805 fps).

Figure 11.– Concluded.

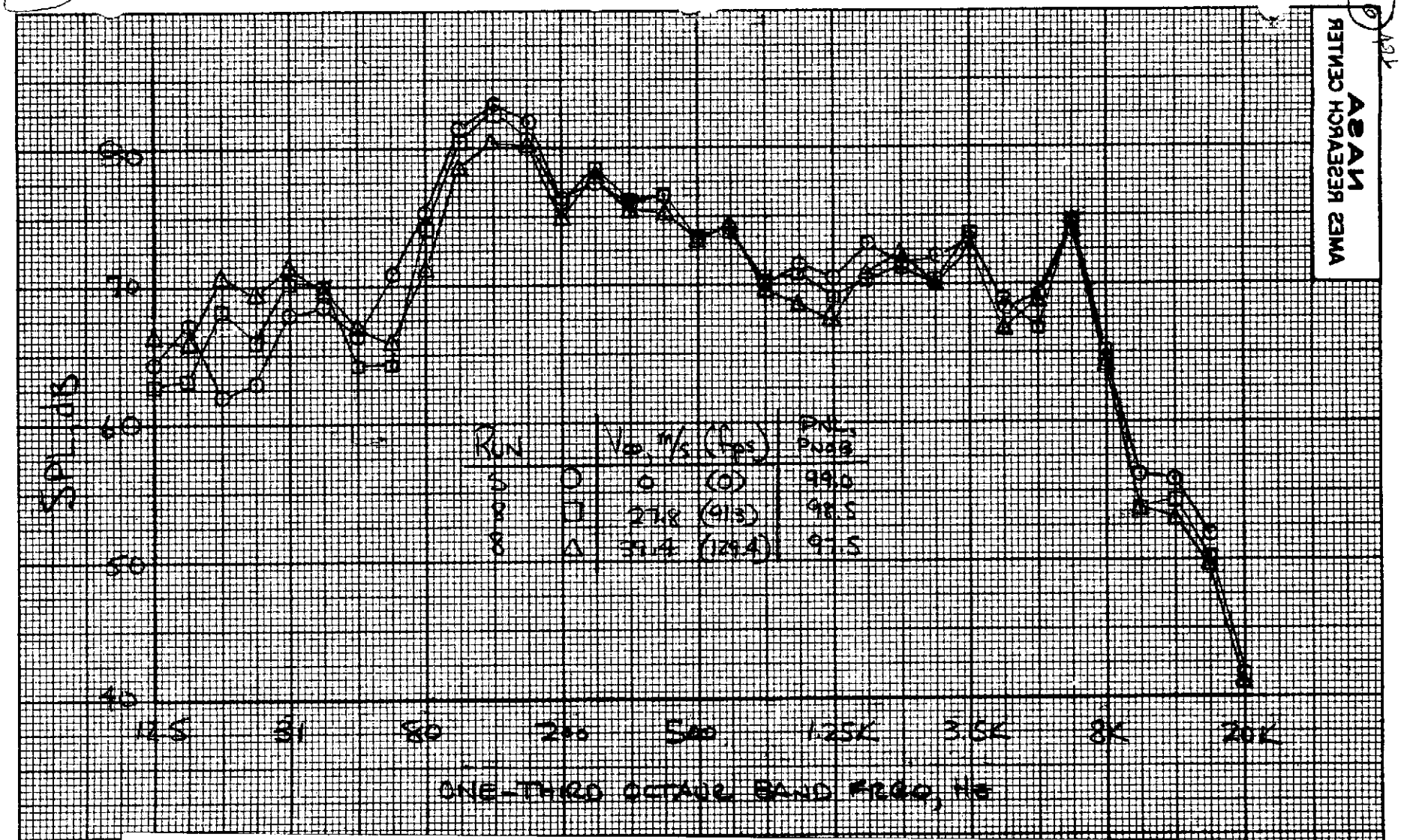

(a) Nozzle "B"; V_J = 216 m/s (710 fps); U/W angle = 64°.

Figure 12.– Variation of frequency spectra with forward speed. δ_f = 75°; α = 0°; η_{CO} = 11-48 percent.

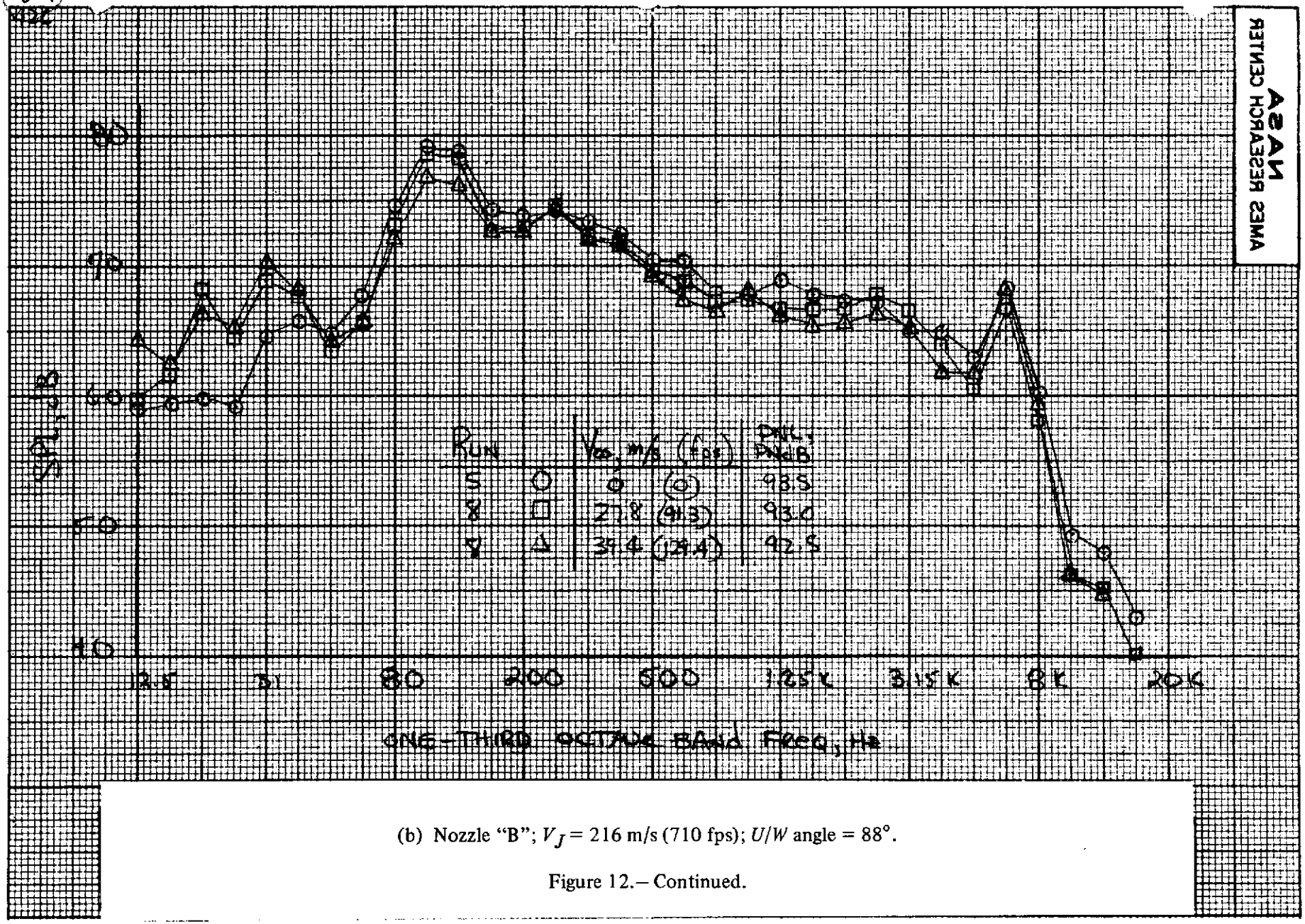

(b) Nozzle "B"; V_J = 216 m/s (710 fps); U/W angle = 88°.

Figure 12.– Continued.

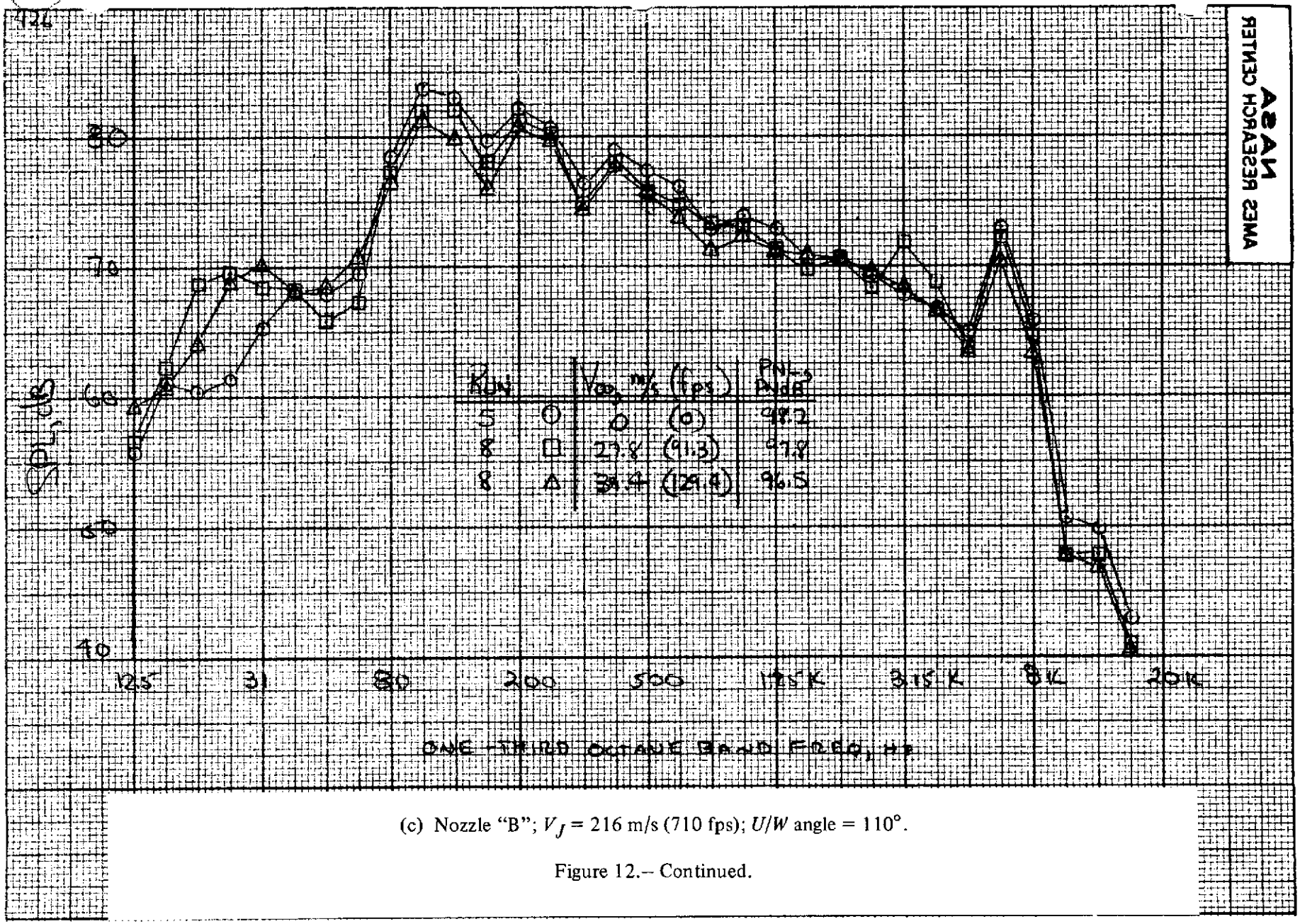

(c) Nozzle "B"; V_J = 216 m/s (710 fps); U/W angle = 110°.

Figure 12.– Continued.

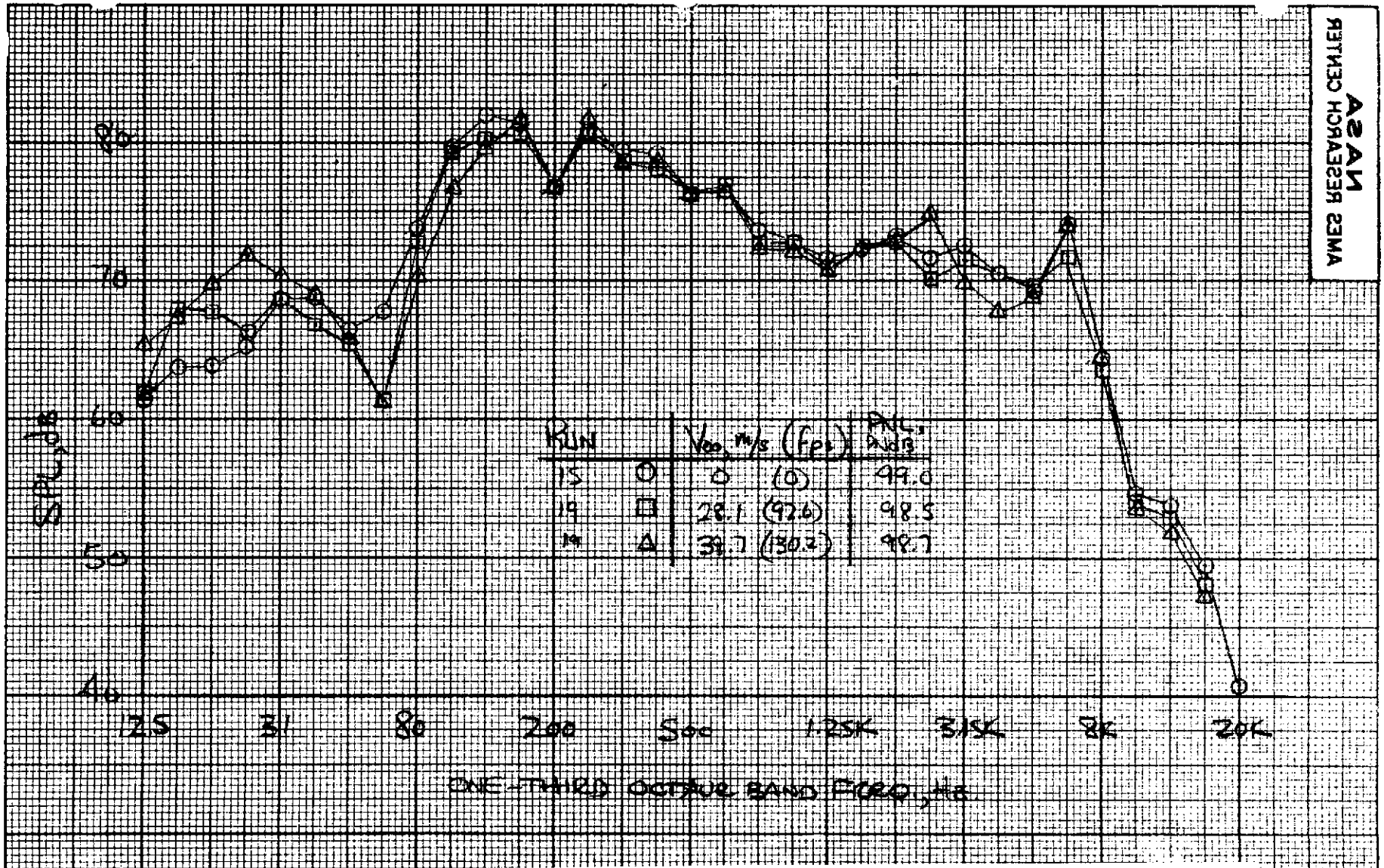

(d) Nozzle "B" with deflector; V_J = 246 m/s (805 fps); U/W angle = 64°.

Figure 12.– Continued.

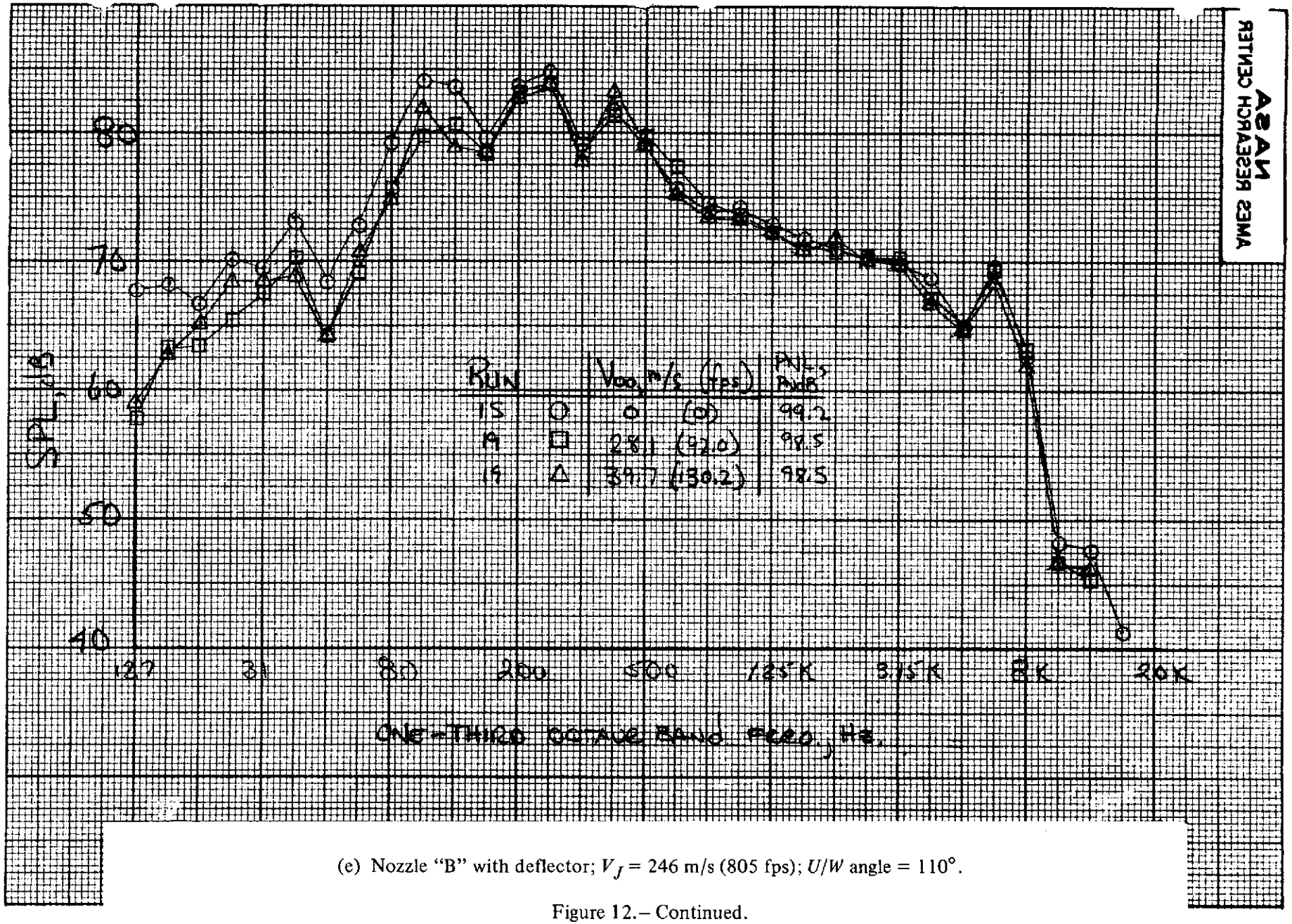

(e) Nozzle "B" with deflector; V_J = 246 m/s (805 fps); U/W angle = 110°.

Figure 12.– Continued.

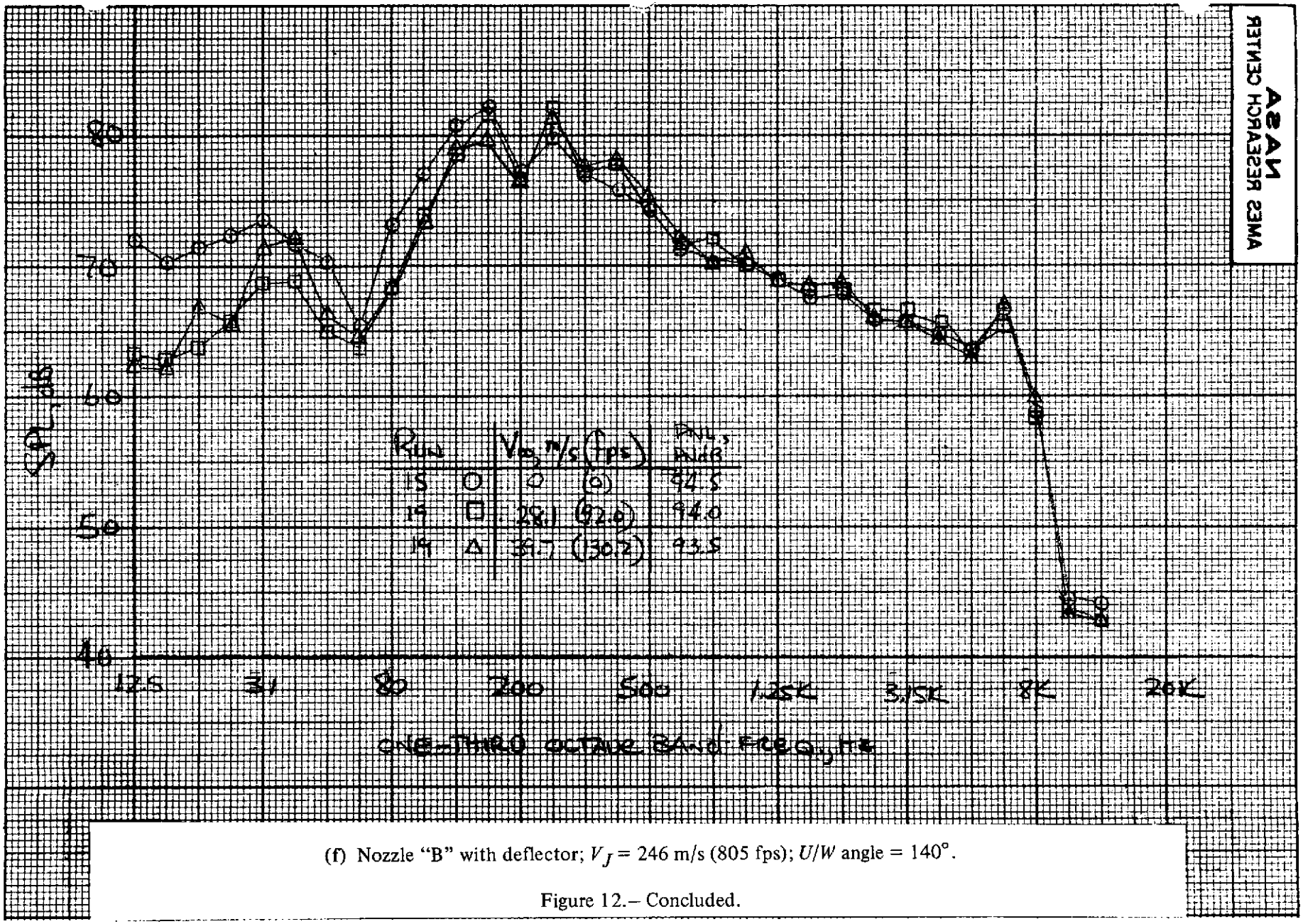

(f) Nozzle "B" with deflector; V_J = 246 m/s (805 fps); U/W angle = 140°.

Figure 12.– Concluded.

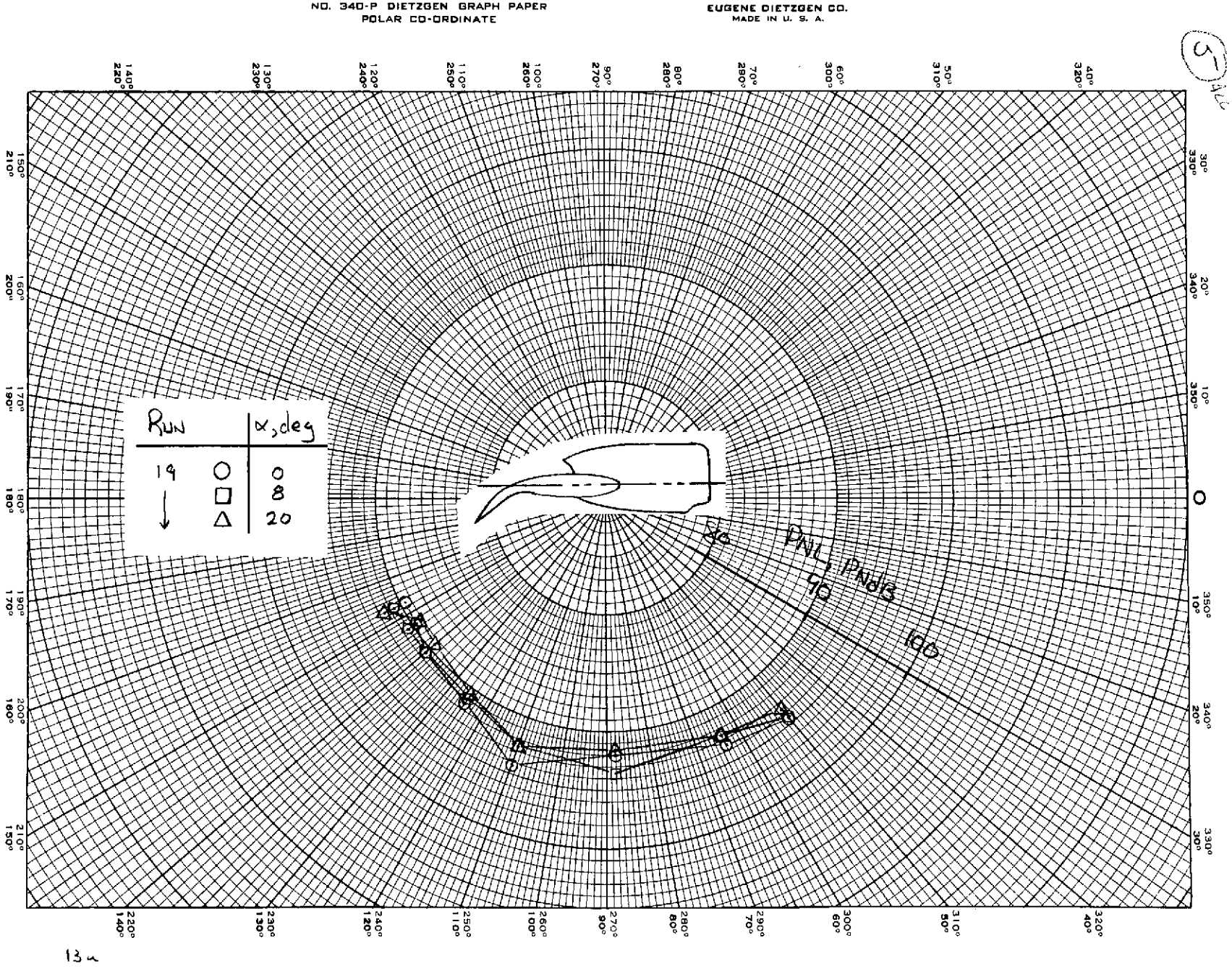

(a) Nozzle "B" with deflector; V_J = 144 m/s (475 fps); V_∞ = 19.8 m/s (65 fps); η_{co} = 11-48 percent.

Figure 13.– Variation of underwing *PNL* directivity with angle of attack.

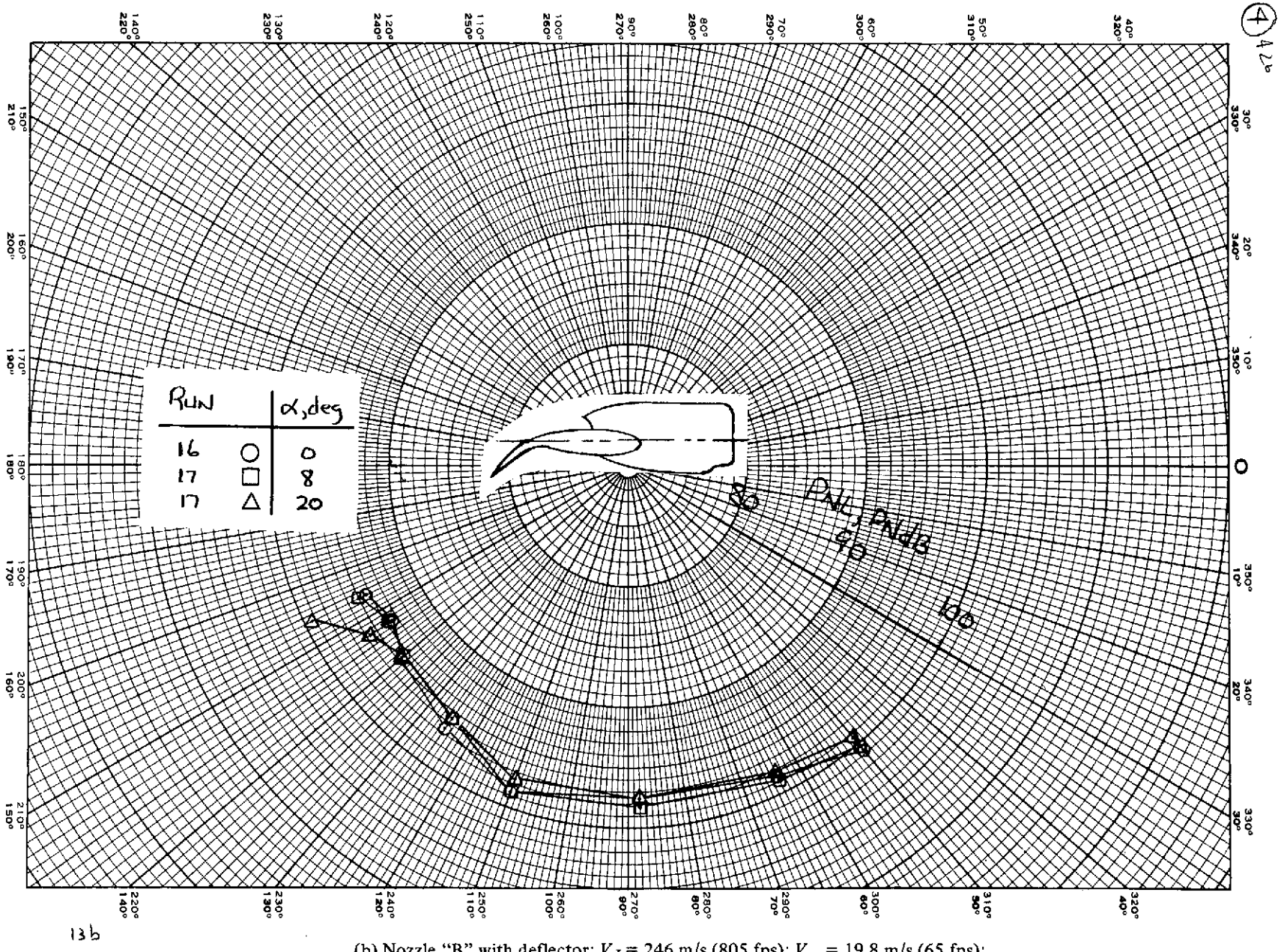

(b) Nozzle "B" with deflector; V_J = 246 m/s (805 fps); V_∞ = 19.8 m/s (65 fps); η_{CO} = 11-48 percent, δ_f = 75°.

Figure 13.– Continued.

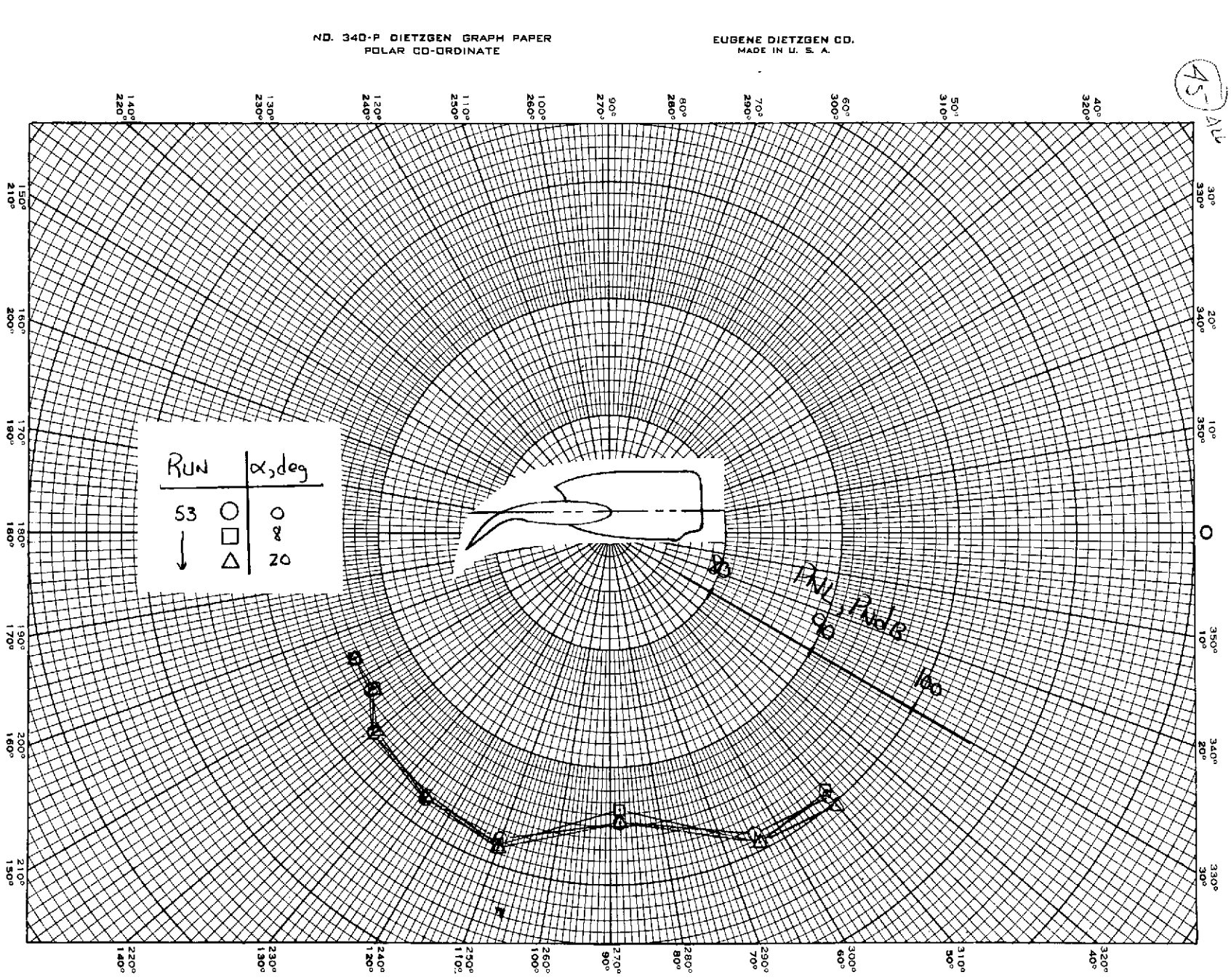

(c) Nozzle "B" with deflector; η_{CO} = 11-39 percent; V_J = 238 m/s (781 fps); V_∞ = 19.7 m/s (64.5 fps), $\delta_f = 30^\circ$.

Figure 13.– Continued.

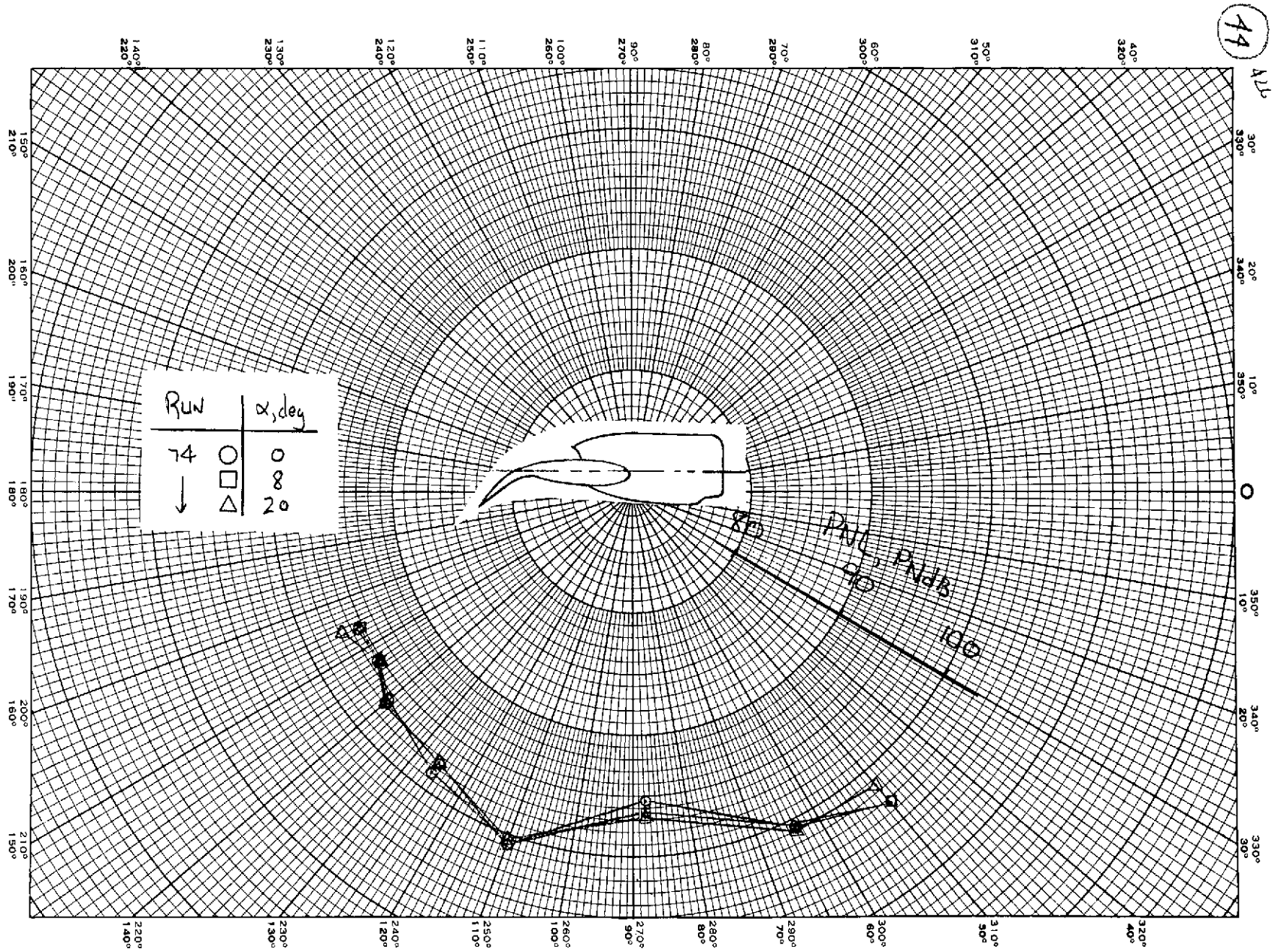

(d) Nozzle "D"; V_J = 254 m/s (835 fps); V_∞ = 17.2 m/s (56.5 fps); η = .11-.43, δ = 75°.

Figure 13.– Concluded.

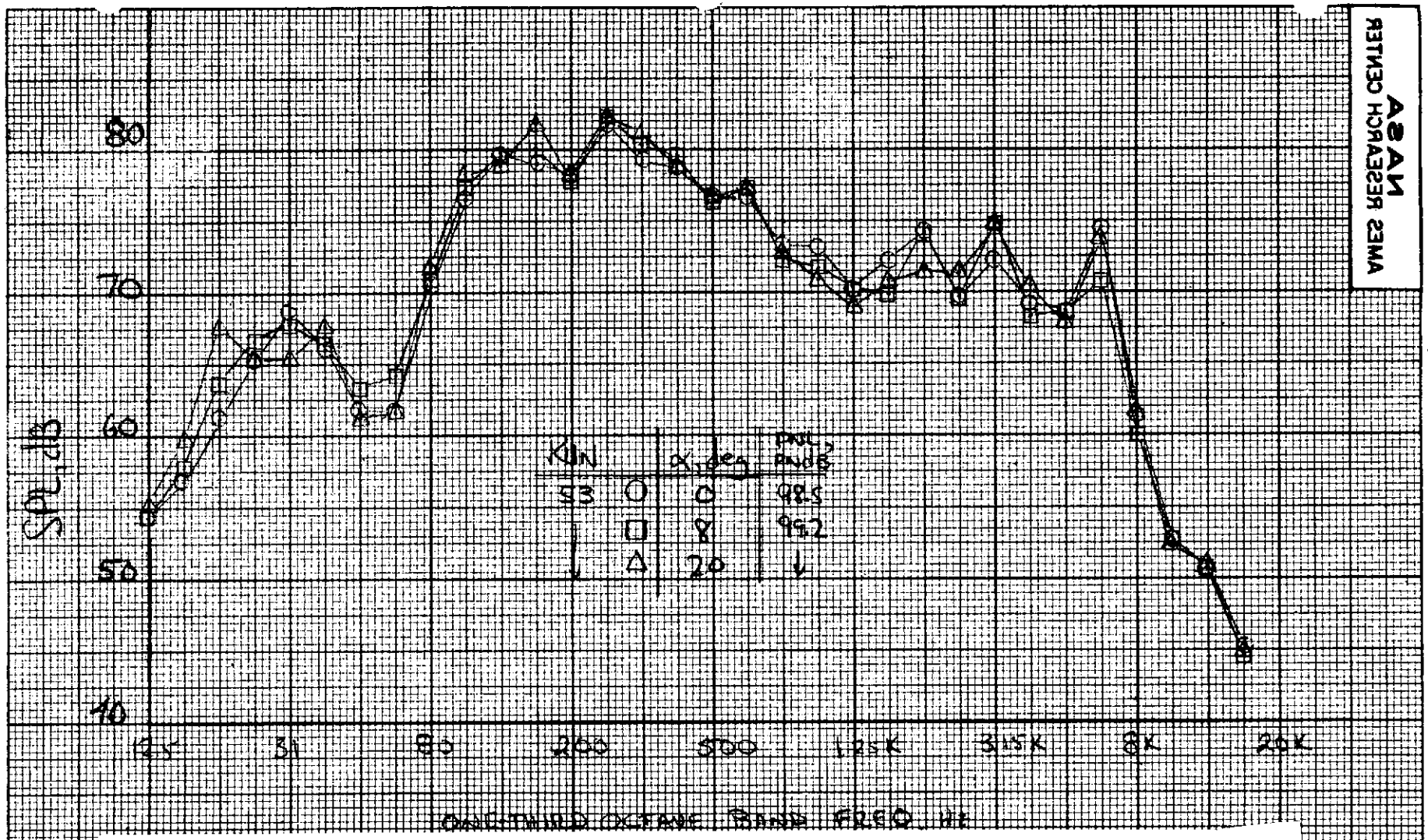

(a) U/W angle = 64°.

Figure 14.– Variation of the underwing frequency spectra with angle of attack. $\delta_f = 30°$; $V_J = 238$ m/s (781 fps); $V_\infty = 19.7$ m/s (64.5 fps); $\eta_{CO} = 11$-39 percent; nozzle "B" $\bar{w}$ deflector.

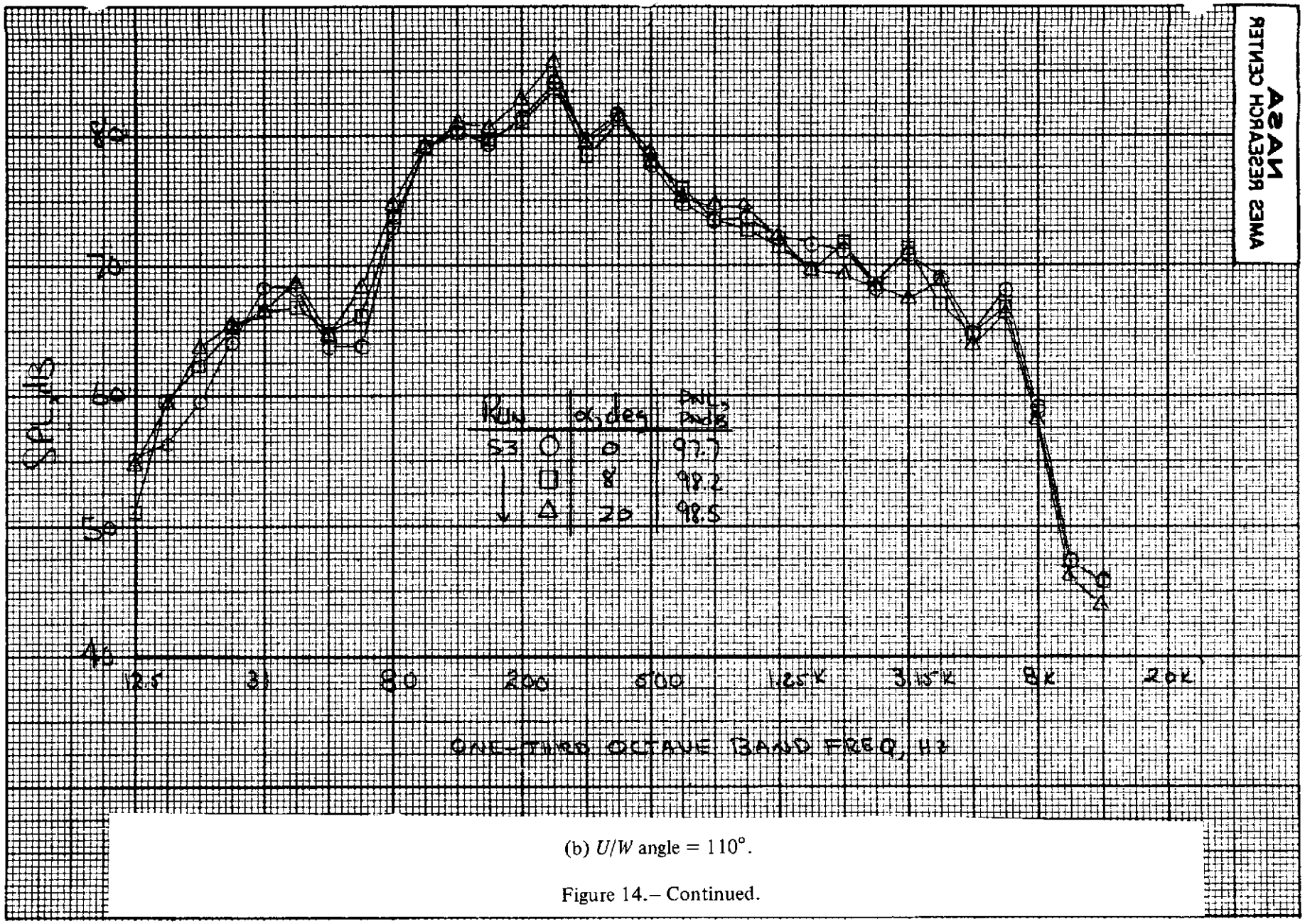

(b) U/W angle = 110°.

Figure 14.– Continued.

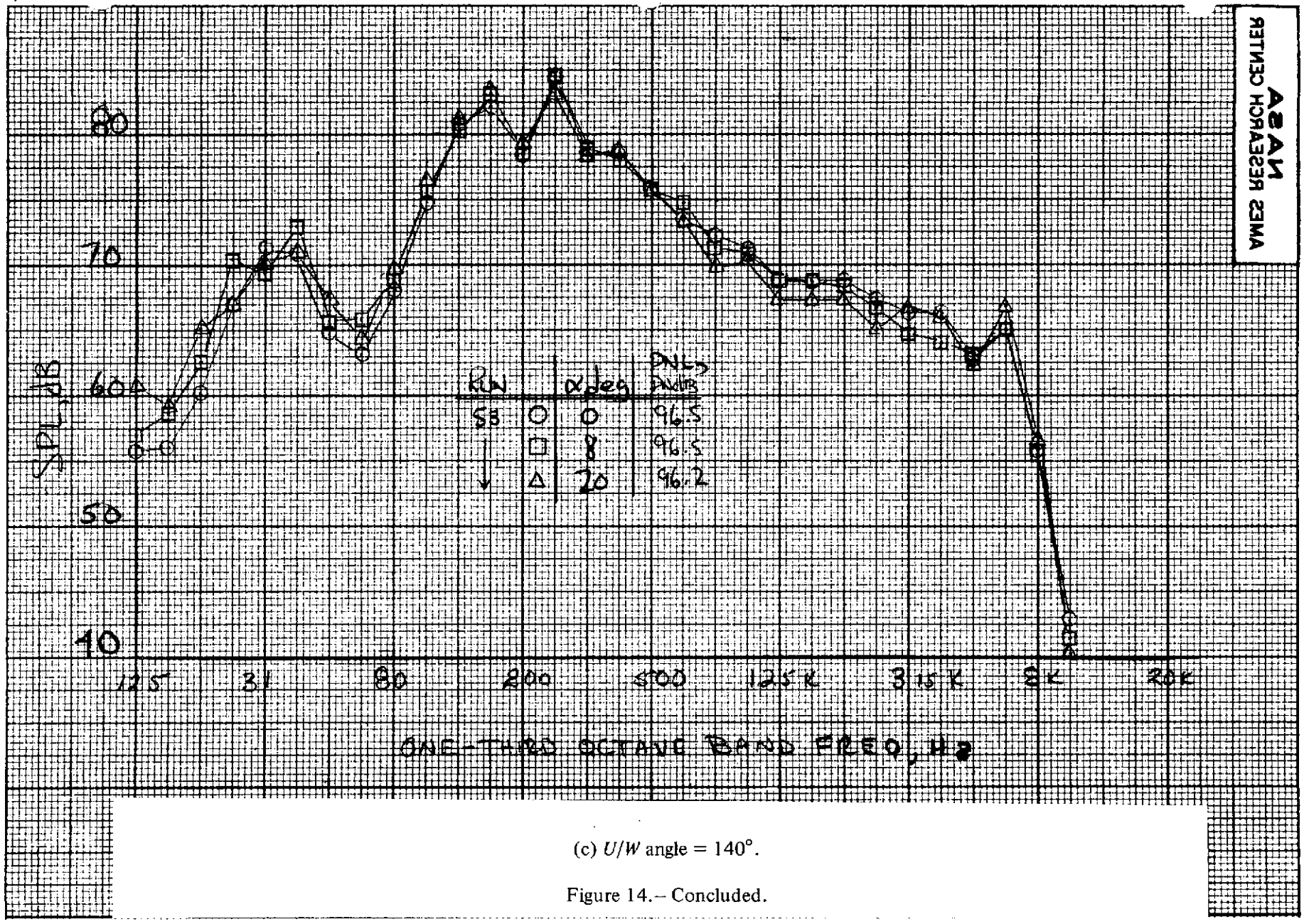

(c) U/W angle = 140°.

Figure 14.– Concluded.

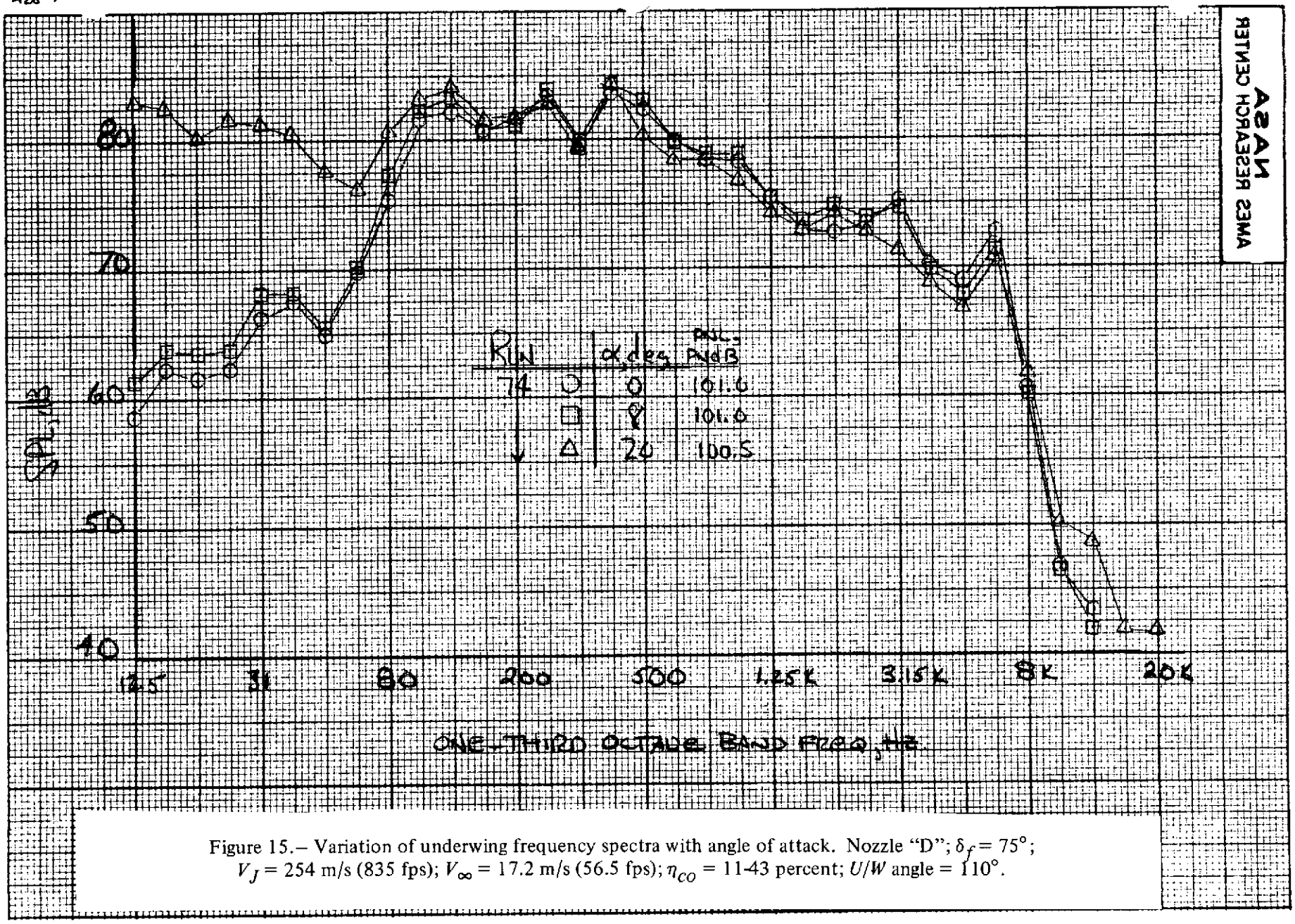

Figure 15.– Variation of underwing frequency spectra with angle of attack. Nozzle "D"; $\delta_f = 75°$; $V_J = 254$ m/s (835 fps); $V_\infty = 17.2$ m/s (56.5 fps); η_{CO} = 11-43 percent; U/W angle = 110°.

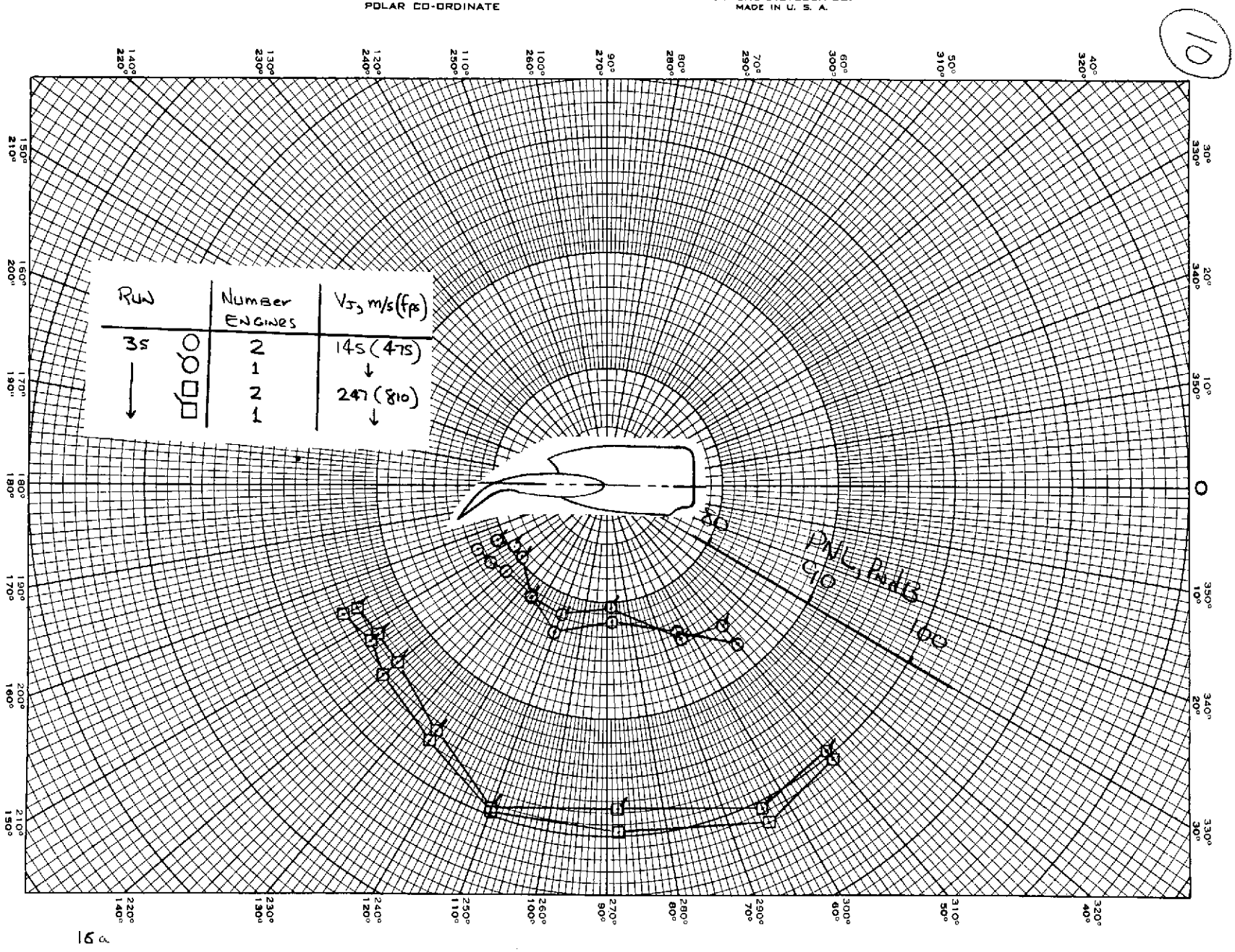

(a) PNL directivity.

Figure 16.– Effect of number of engines on the underwing acoustic characteristics. Nozzle "B" with deflector, $V_\infty = \alpha = 0$.

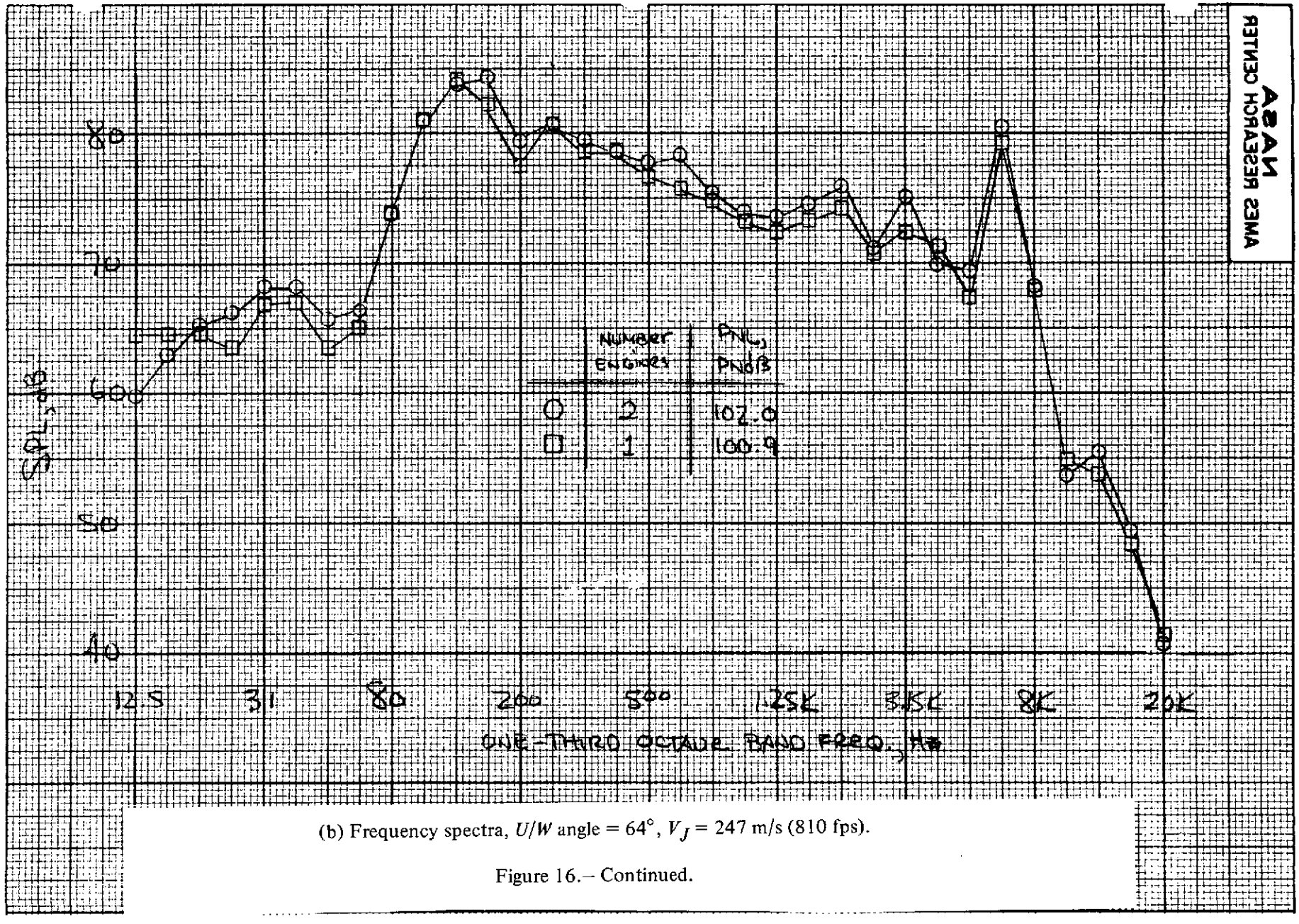

(b) Frequency spectra, U/W angle = 64°, V_J = 247 m/s (810 fps).

Figure 16.– Continued.

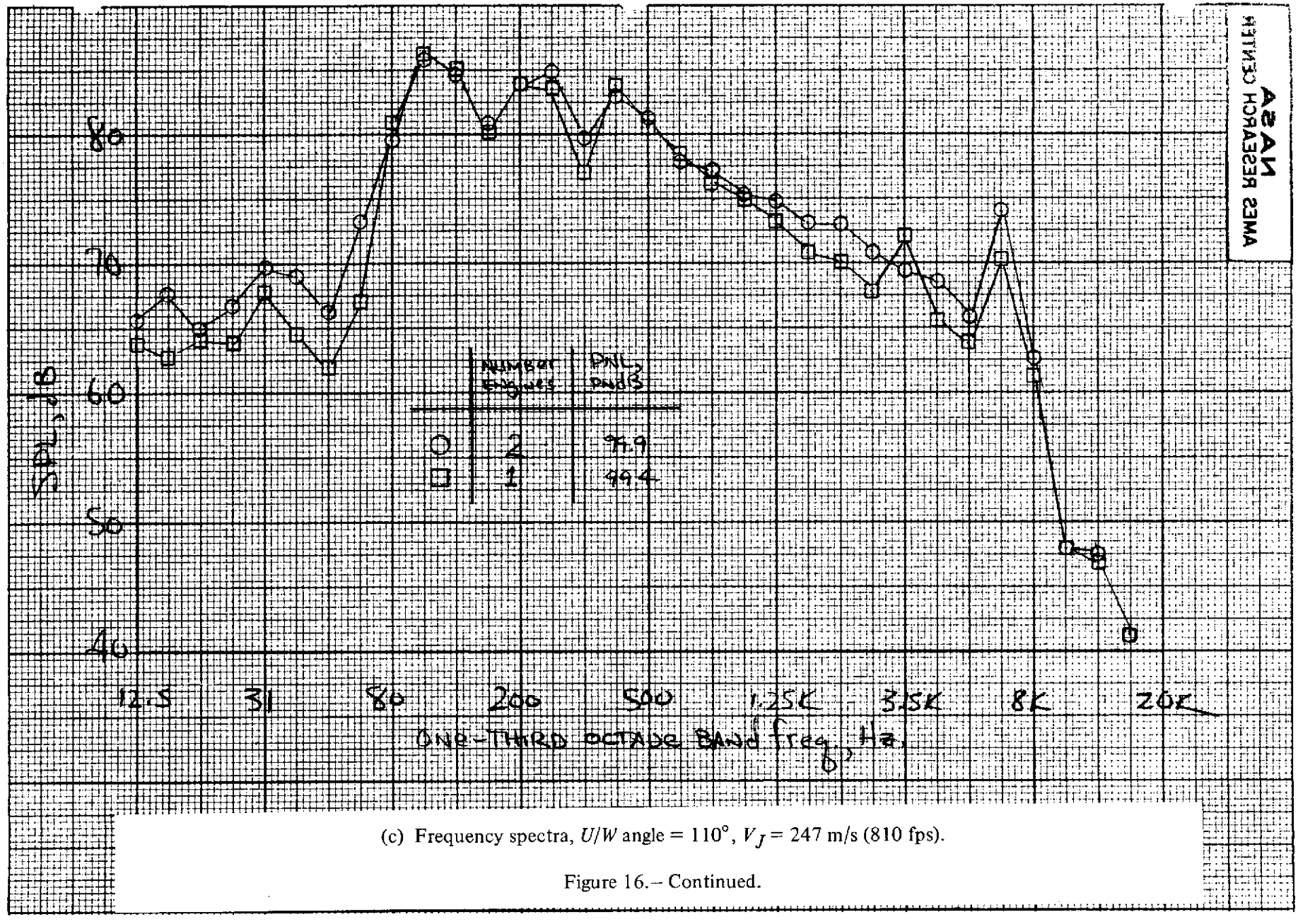

(c) Frequency spectra, U/W angle = 110°, V_J = 247 m/s (810 fps).

Figure 16.– Continued.

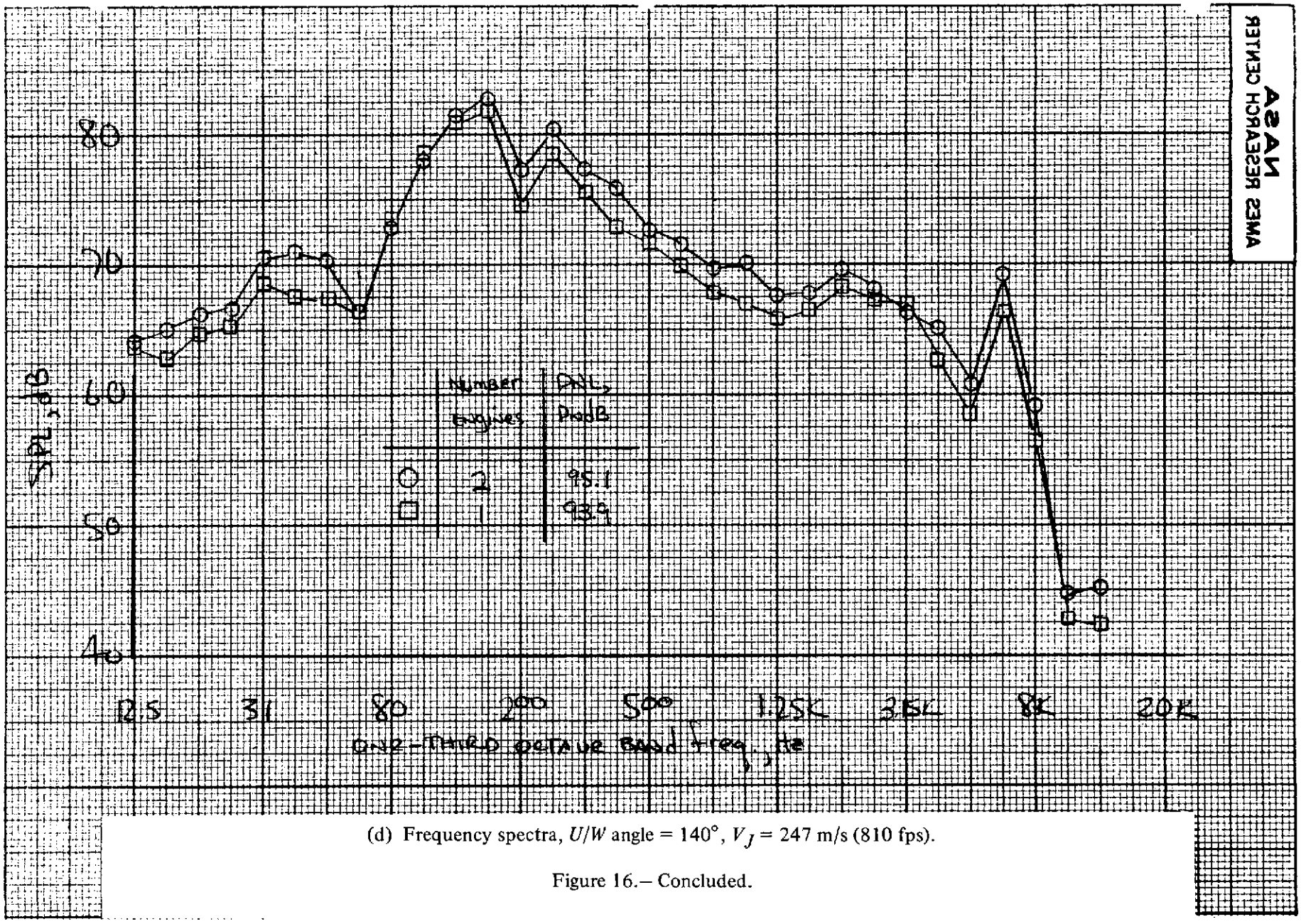

(d) Frequency spectra, U/W angle = 140°, V_J = 247 m/s (810 fps).

Figure 16.– Concluded.

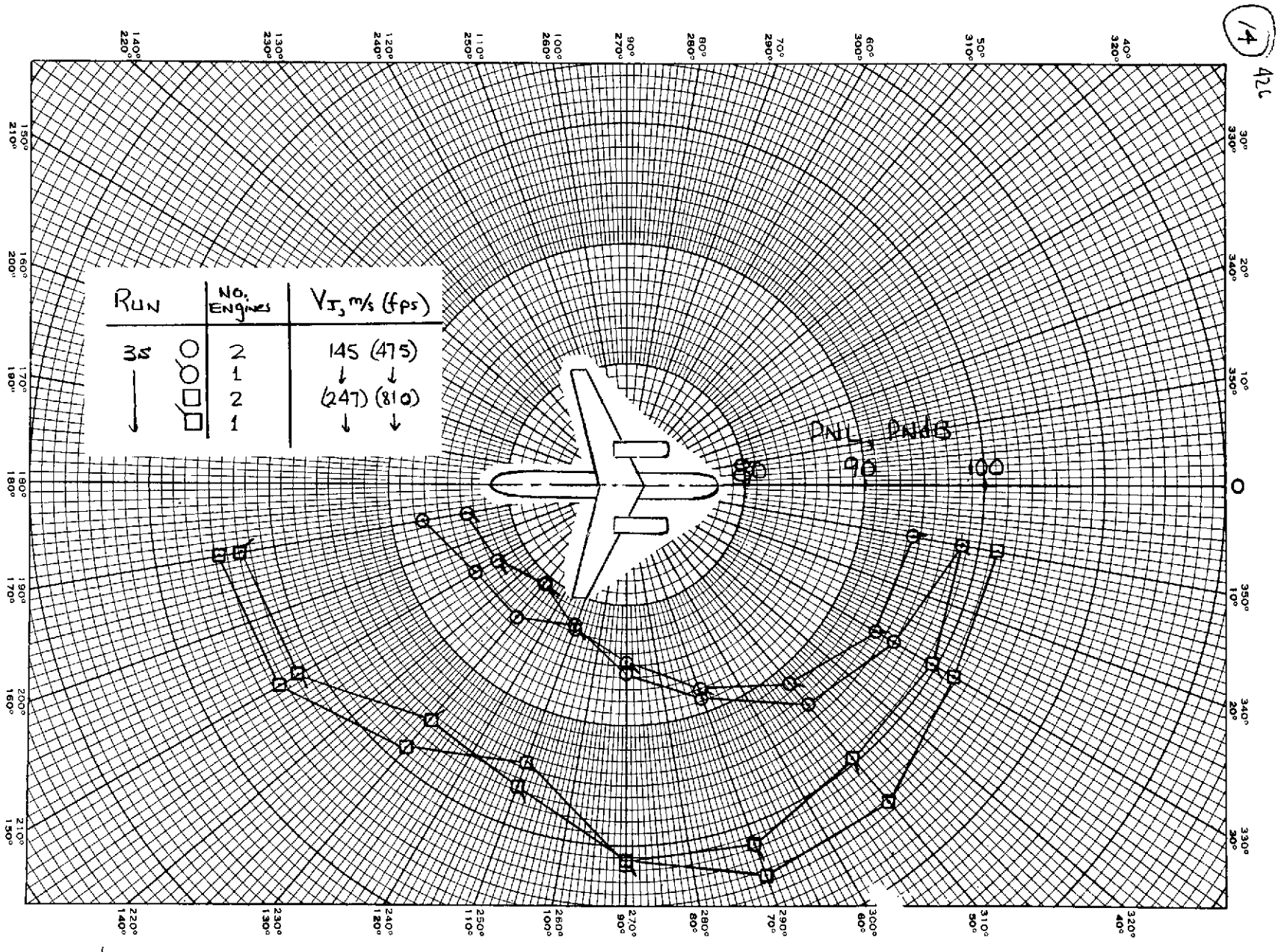

(a) PNL directivity.

Figure 17.– Effect of number of engines on sideline acoustic characteristics.
Nozzle "B" with deflector, $V_\infty = \alpha = 0$.

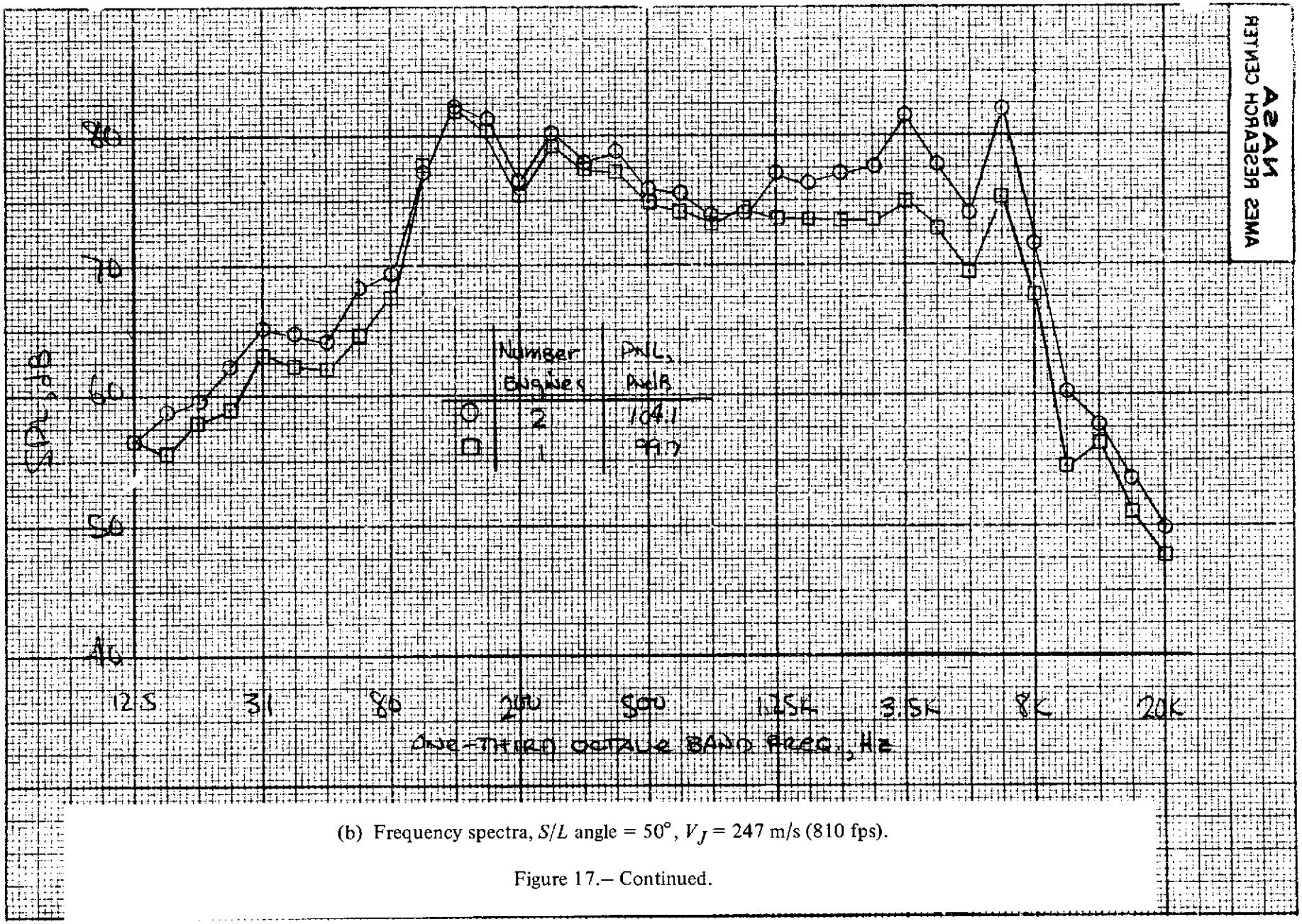

(b) Frequency spectra, S/L angle = 50°, V_J = 247 m/s (810 fps).

Figure 17.– Continued.

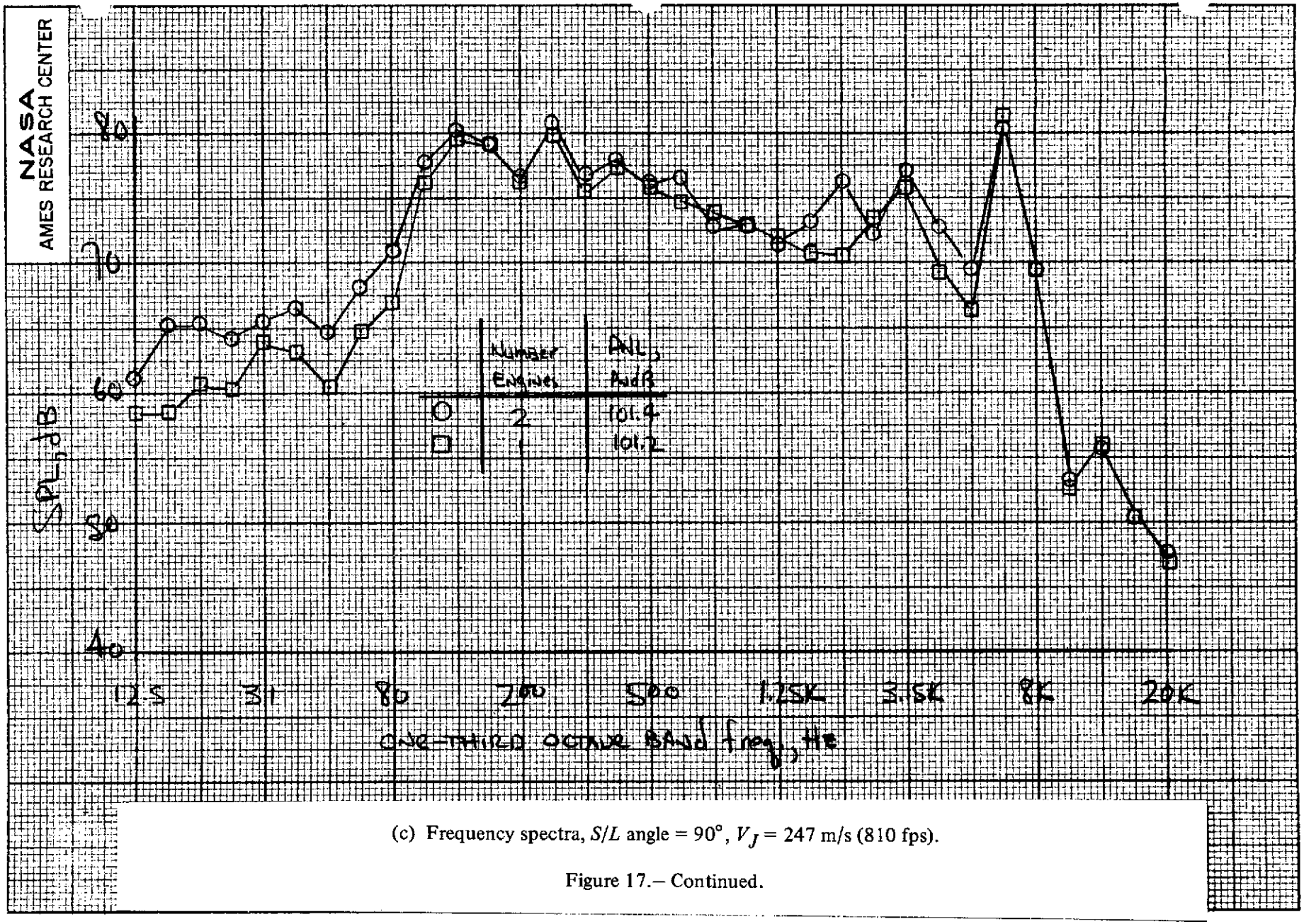

(c) Frequency spectra, S/L angle = 90°, V_J = 247 m/s (810 fps).

Figure 17.– Continued.

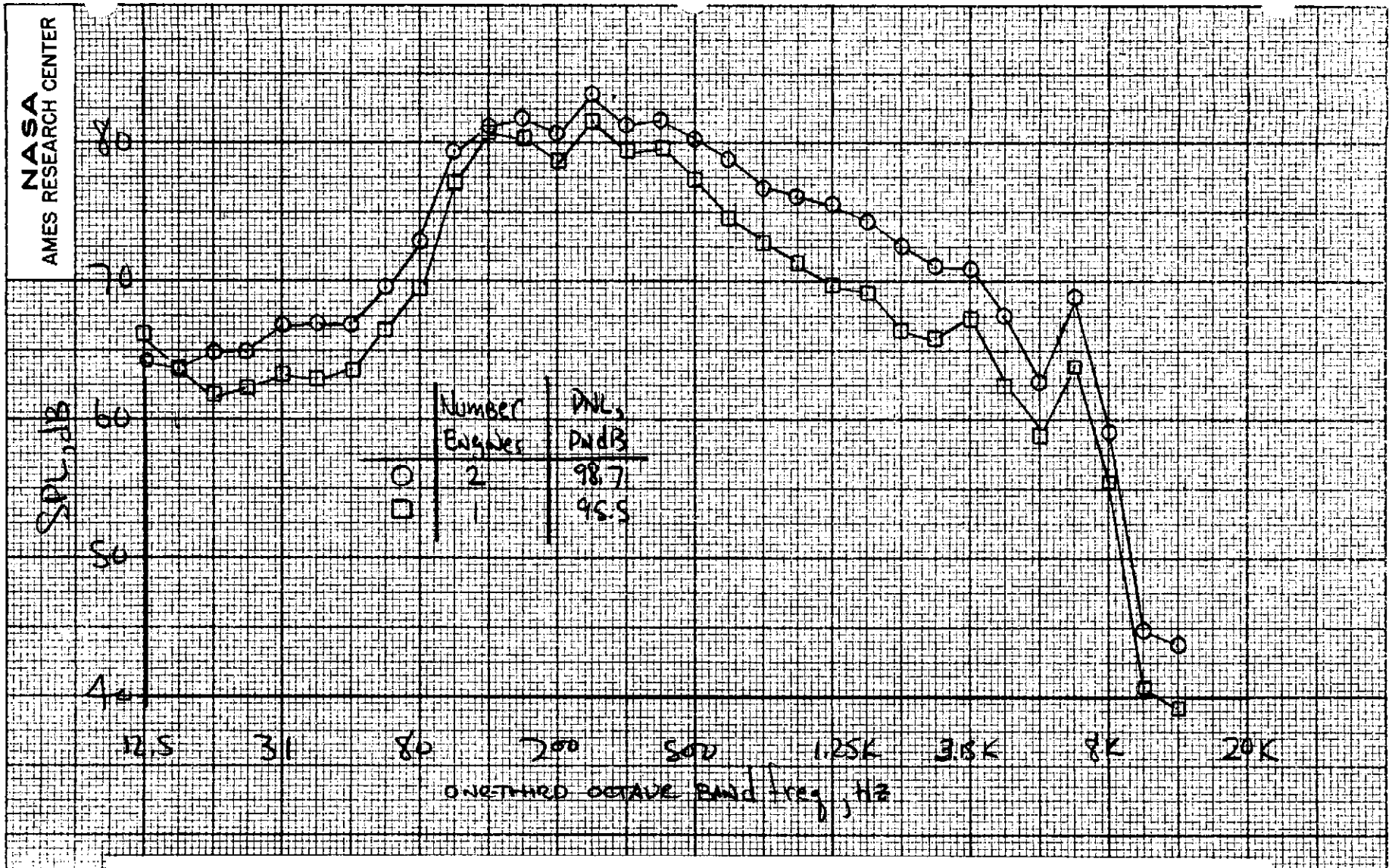

(d) Frequency spectra, S/L angle = 130°, V_J = 247 m/s (810 fps).

Figure 17.– Concluded.

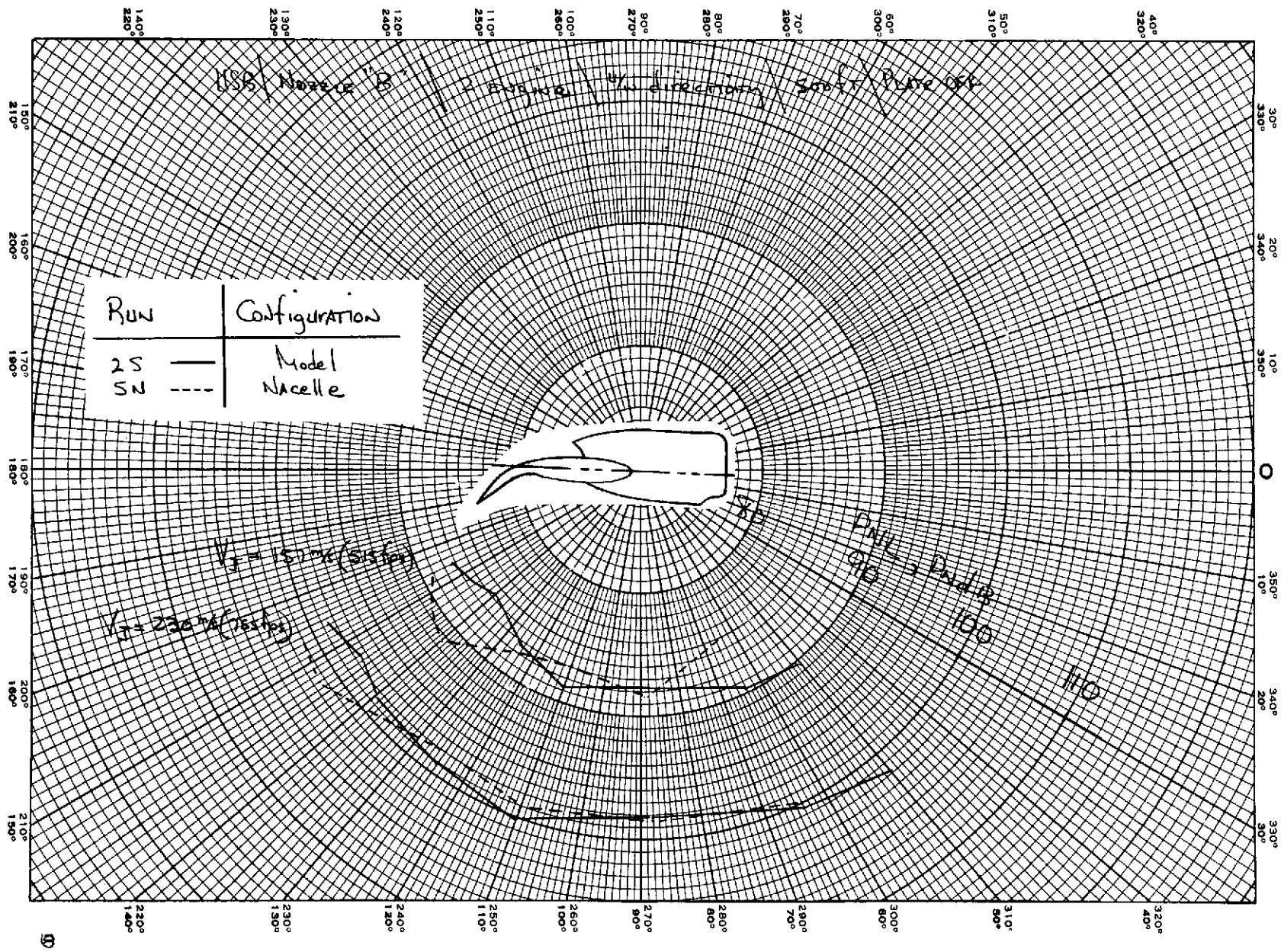

Figure 18.– Comparison of the nacelle and model underwing acoustic characteristics.
Nozzle "B", 2 engines, nozzle extension plate off nacelle, $V_\infty = \alpha = 0$.

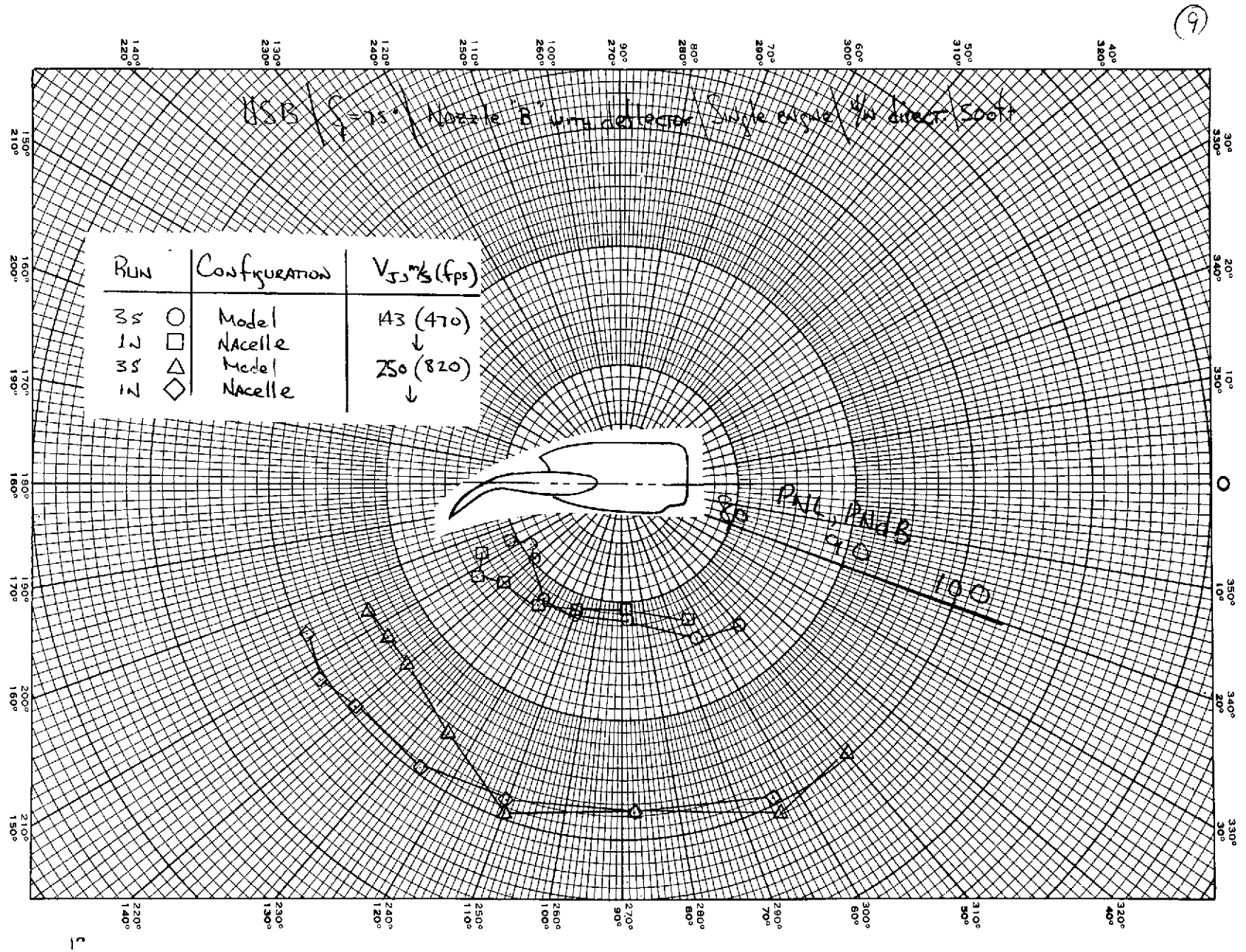

(a) *PNL* directivity.

Figure 19.– Comparison of the nacelle and model underwing acoustic characteristics.
Nozzle "B" with deflector, 1 engine, $V_\infty = \alpha = 0$, nacelle nozzle ext. plate on.

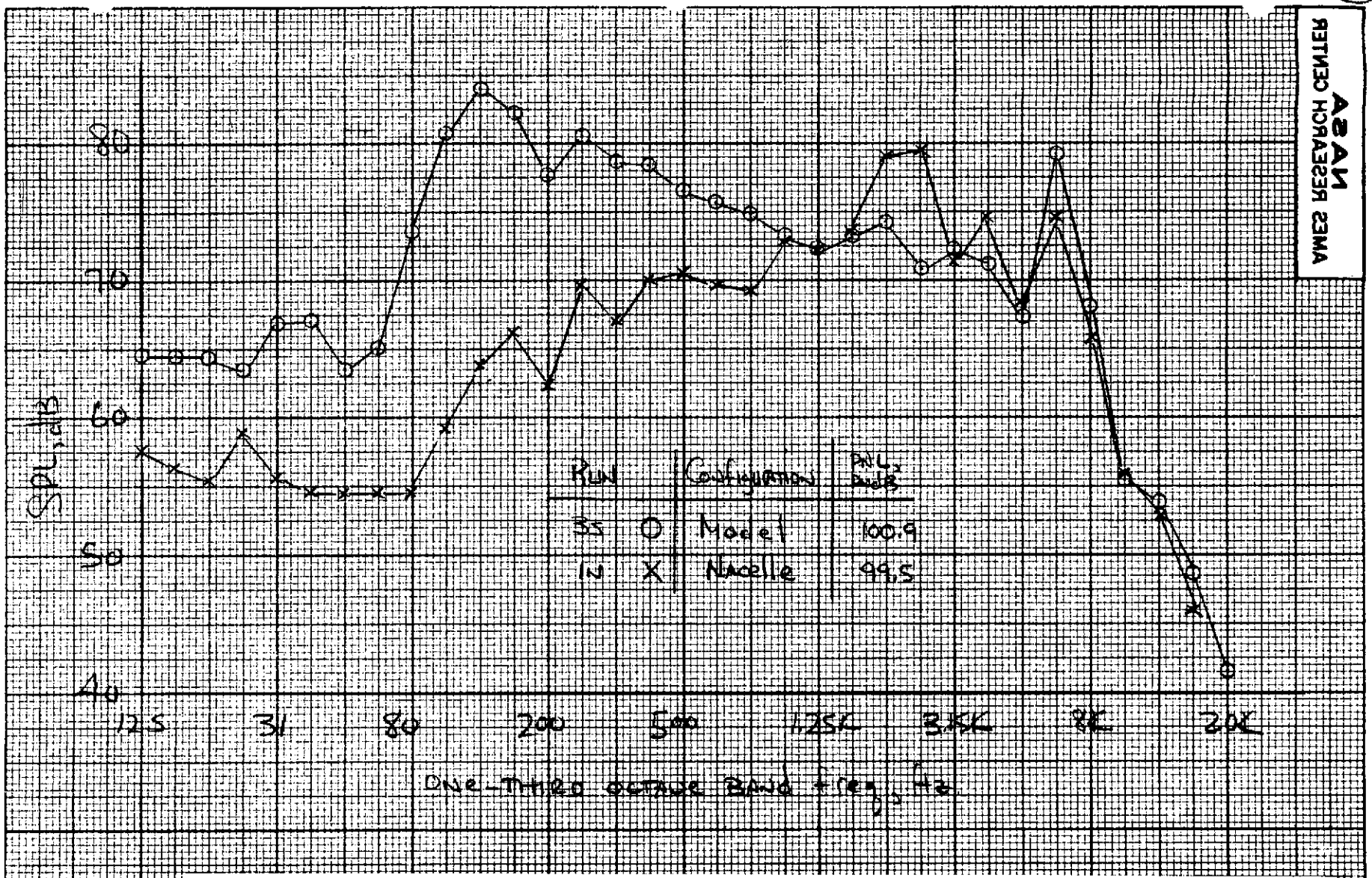

(b) Frequency spectra, U/W angle = 64°, V_J = 250 m/s (820 fps).

Figure 19.– Continued.

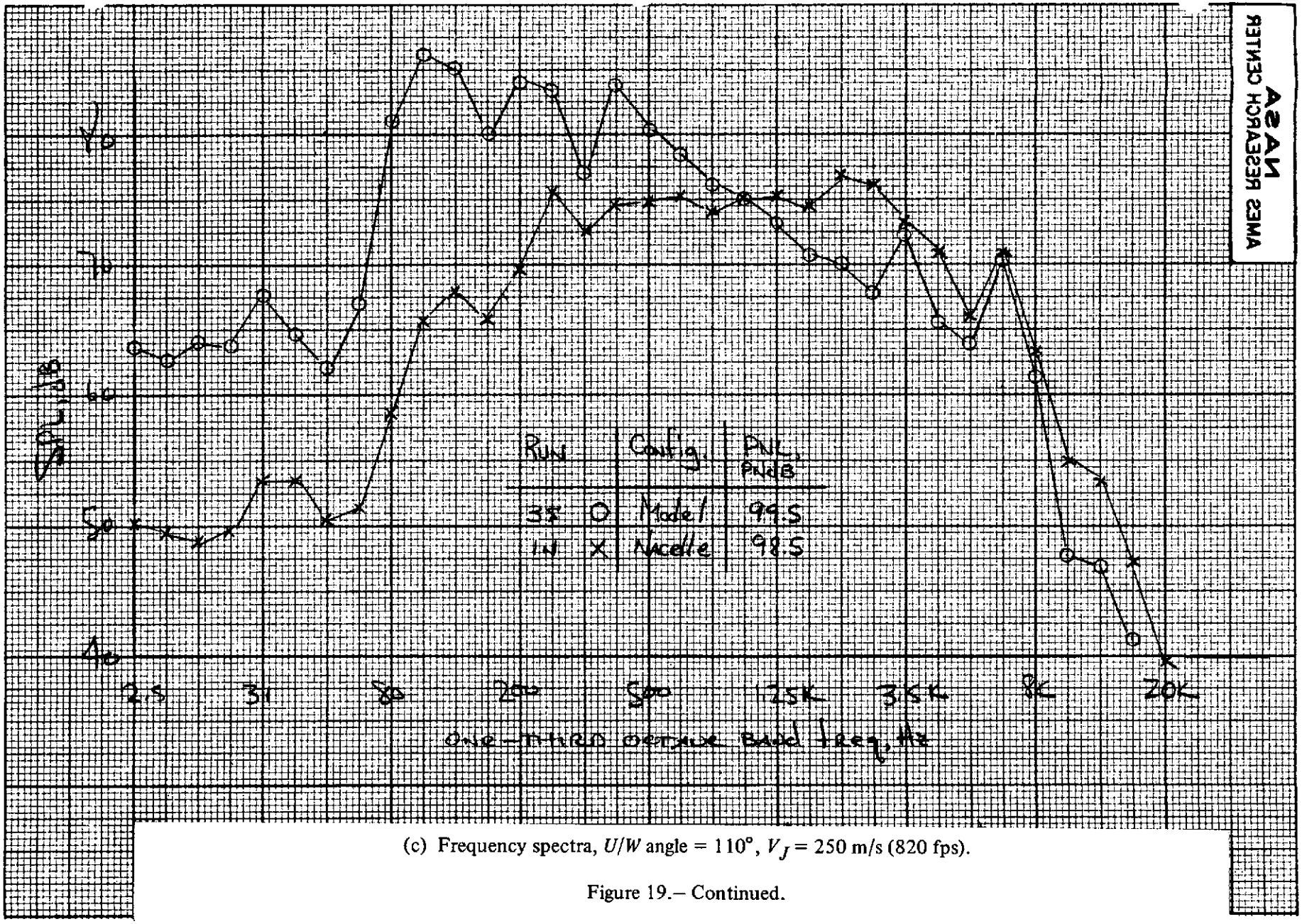

(c) Frequency spectra, U/W angle = 110°, V_J = 250 m/s (820 fps).

Figure 19.– Continued.

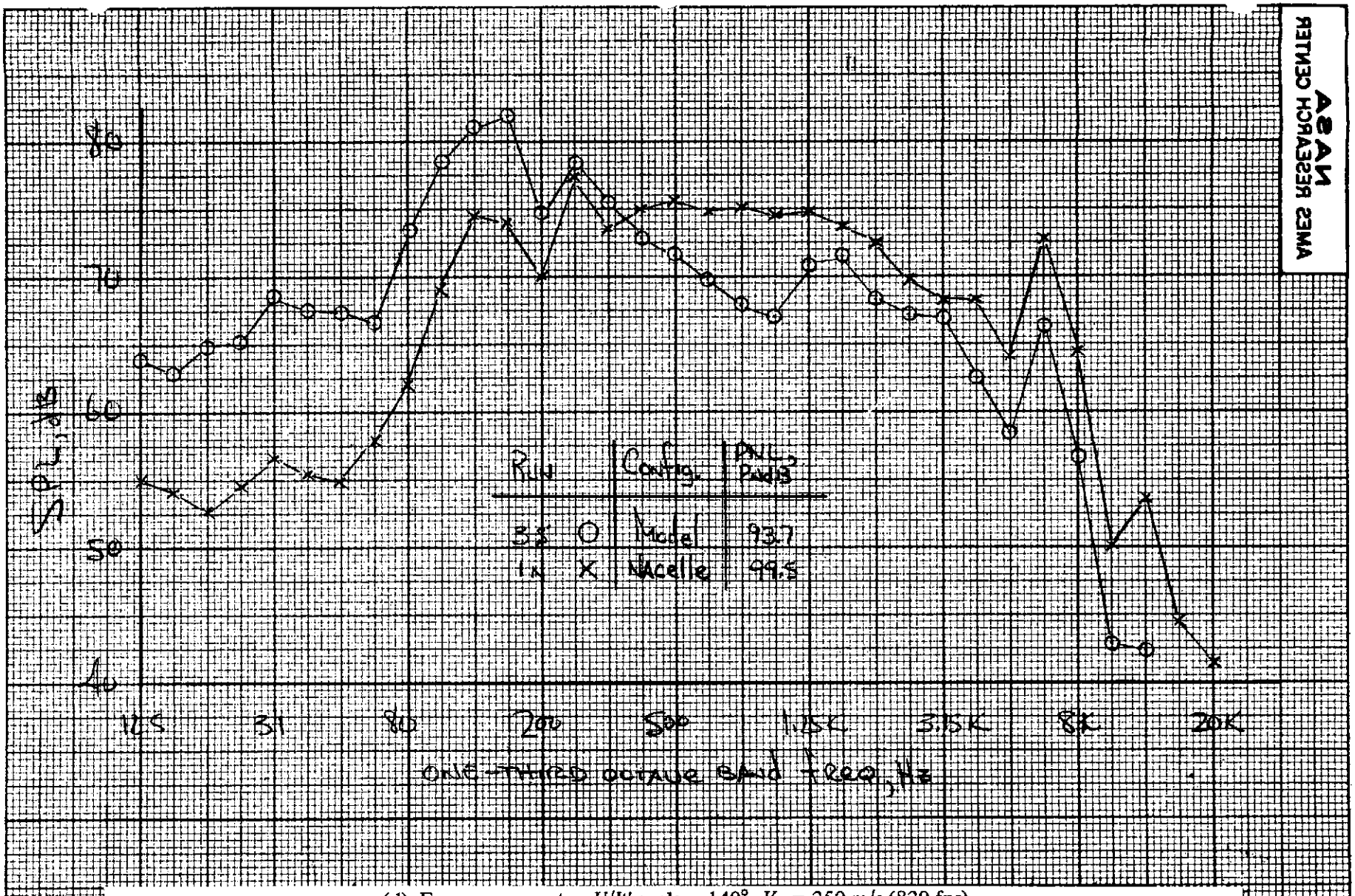

(d) Frequency spectra, U/W angle = 140°, V_J = 250 m/s (820 fps).

Figure 19.– Concluded.

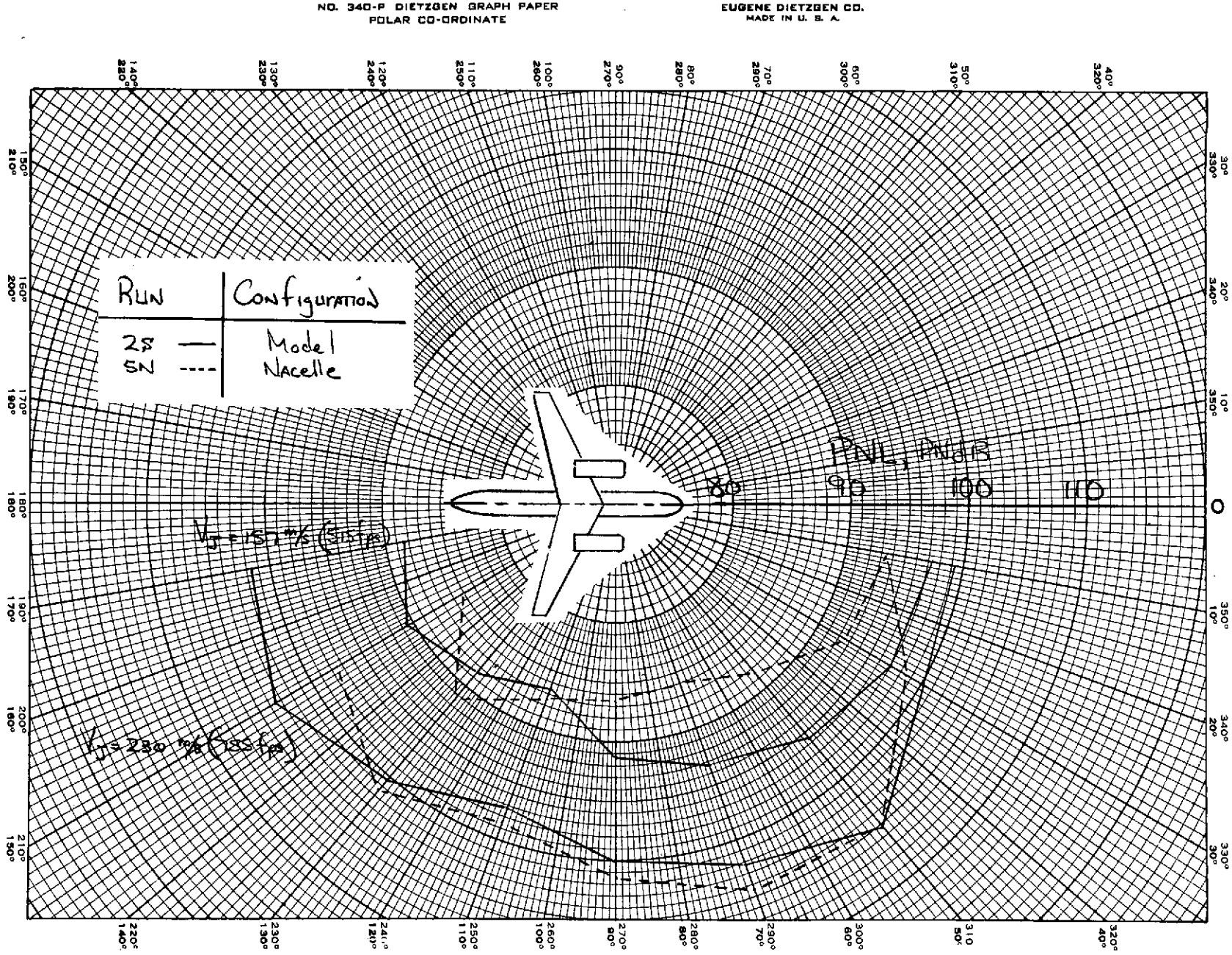

Figure 20.– Comparison of the nacelle and model sideline *PNL* directivity. Nozzle "B", 2 engines, $V_\infty = \alpha = 0$, nacelle extension plate off.

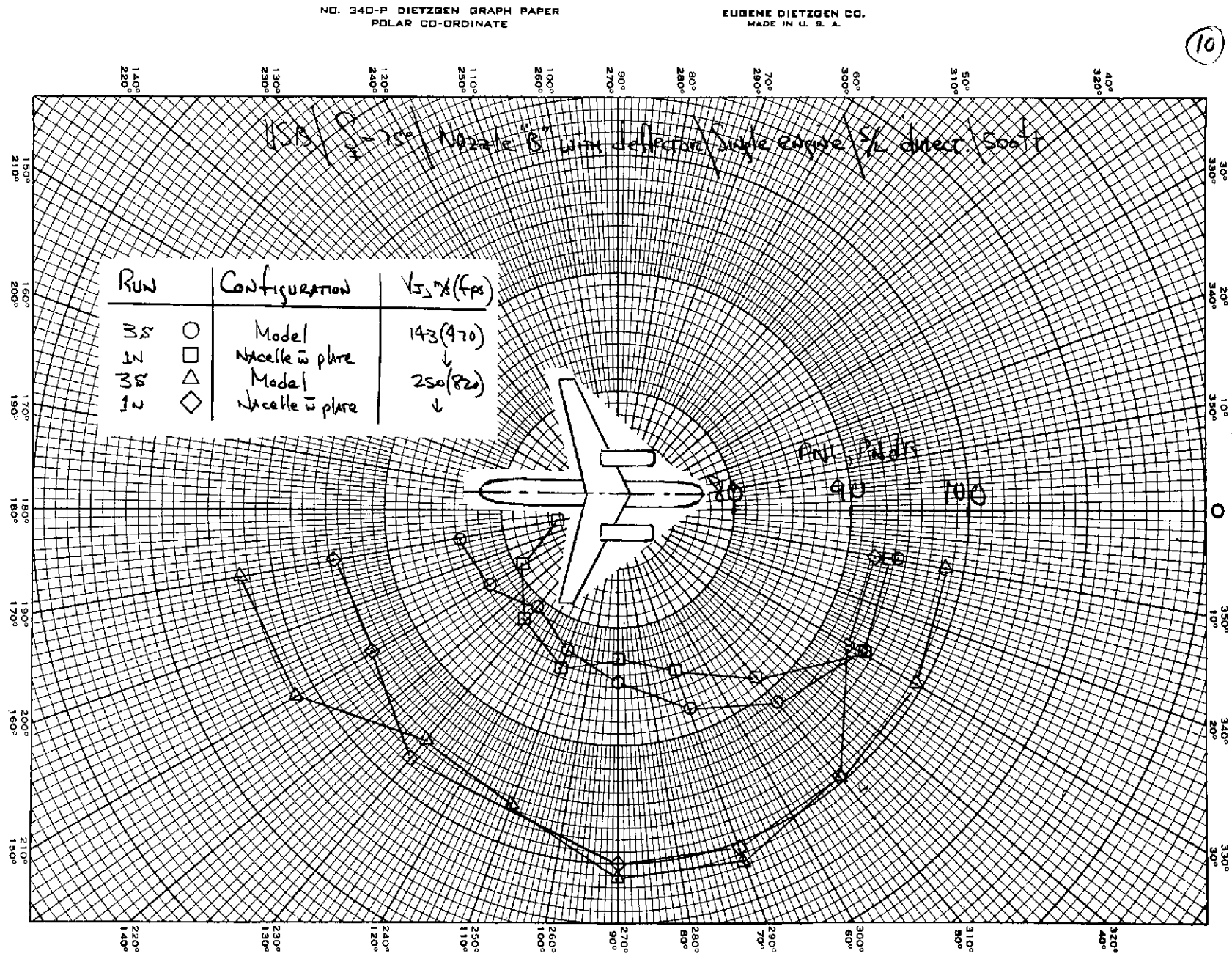

(a) PNL directivity

Figure 21.– Comparison of the nacelle and model sidelines acoustic characteristics. Nozzle "B" with deflector, 1 engine, $V_\infty = \alpha = 0$, nacelle extension plate on.

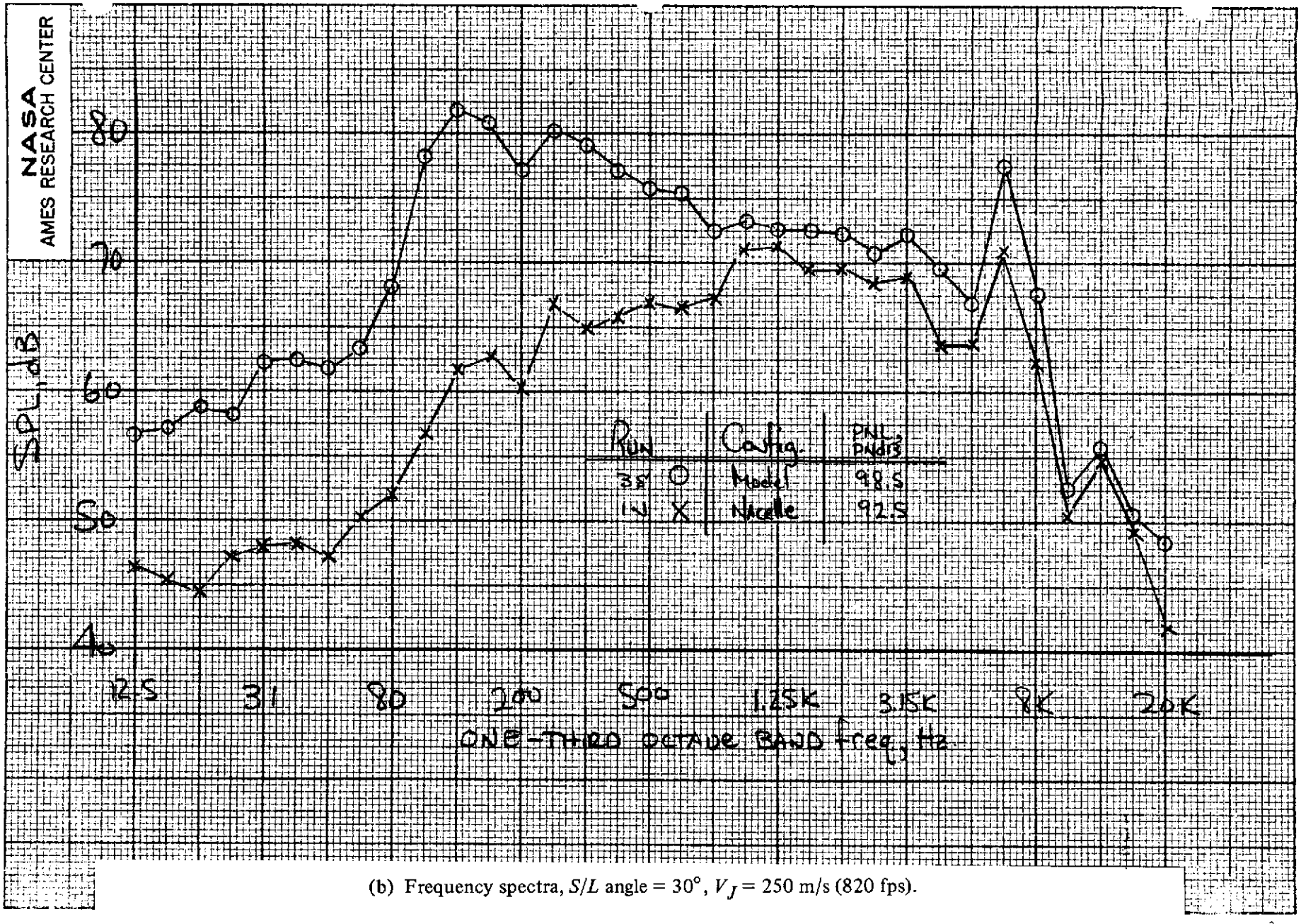

(b) Frequency spectra, S/L angle = 30°, V_J = 250 m/s (820 fps).

Figure 21.– Continued.

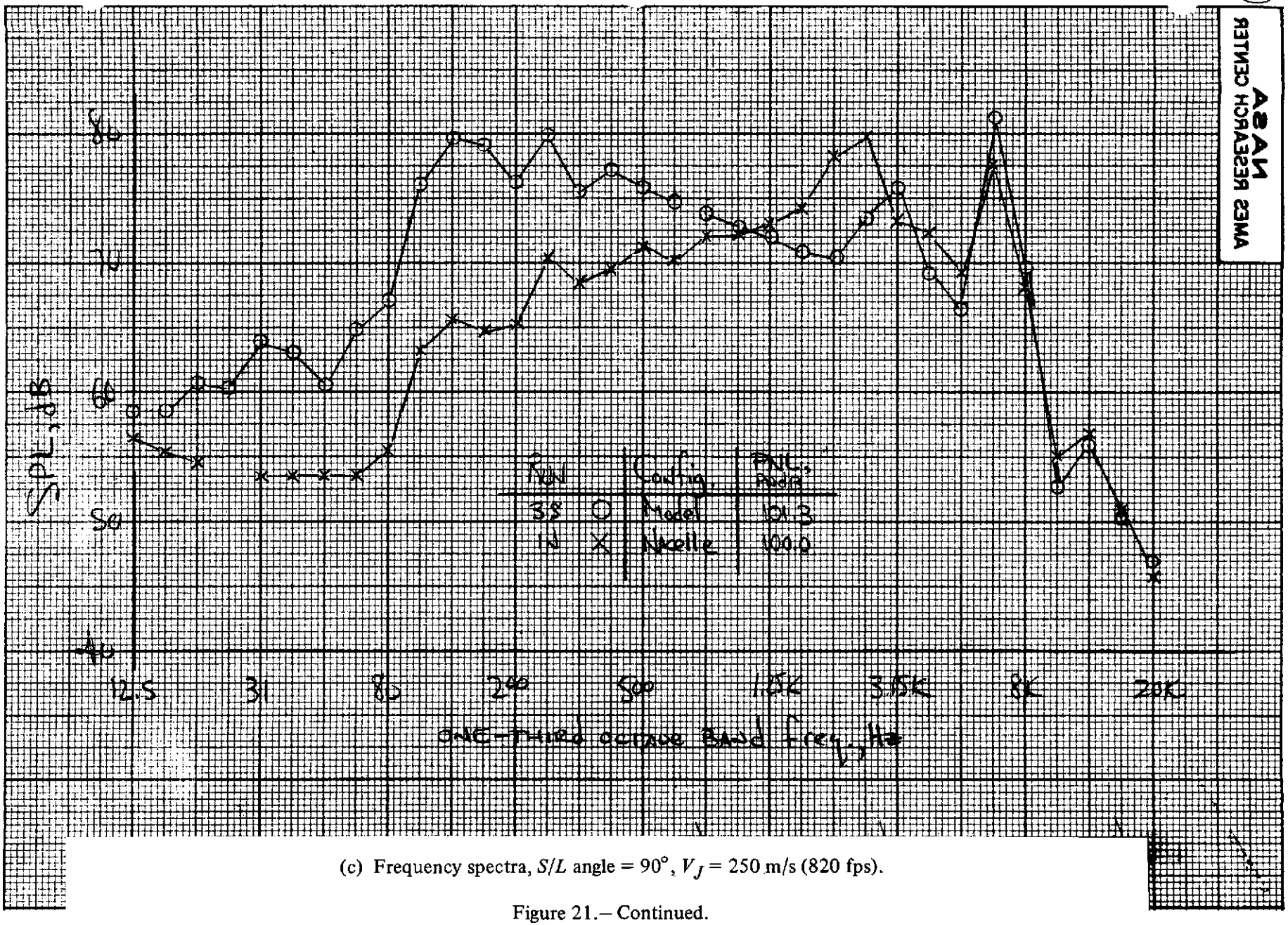

(c) Frequency spectra, S/L angle = 90°, V_J = 250 m/s (820 fps).

Figure 21.– Continued.

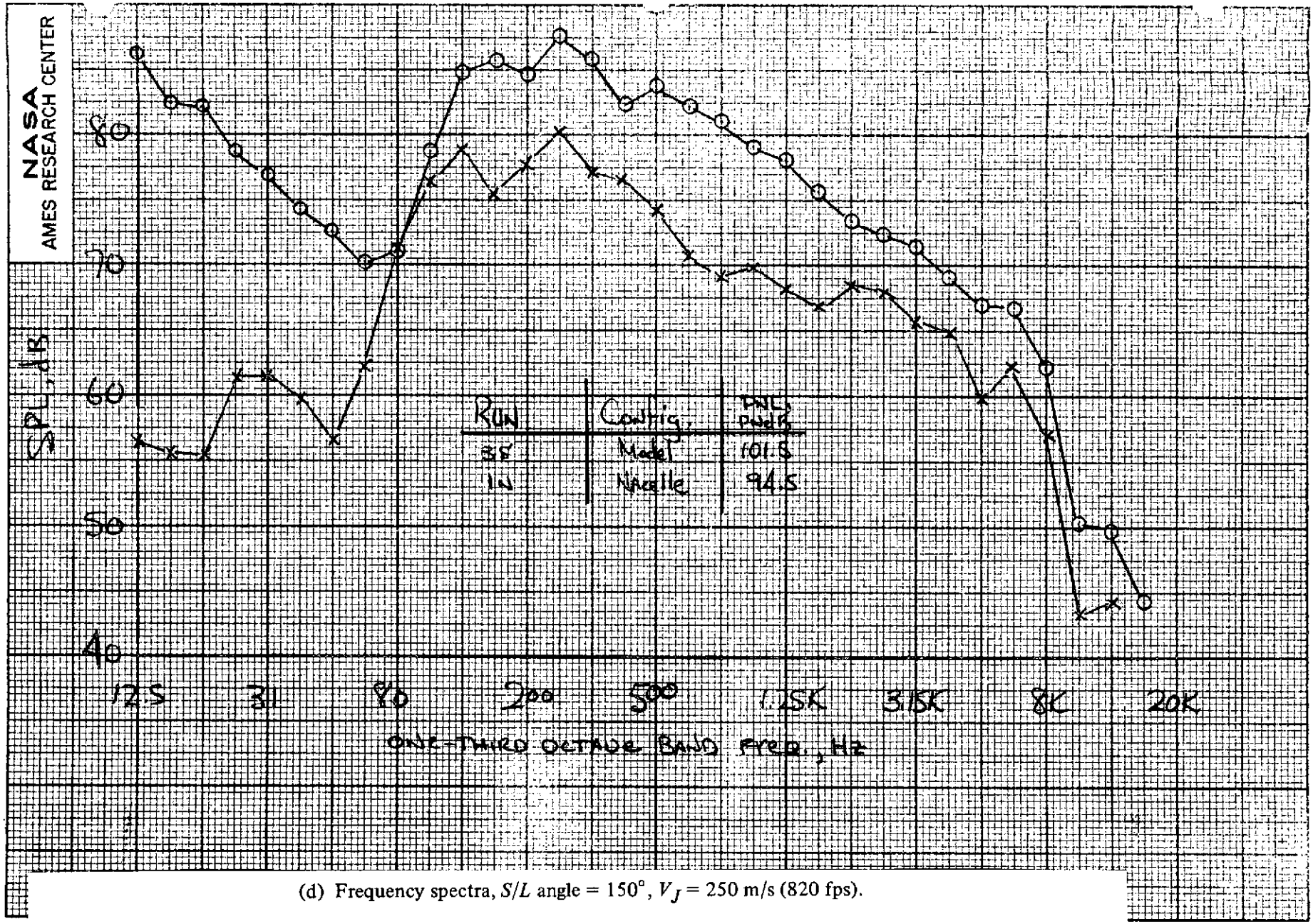

(d) Frequency spectra, S/L angle = 150°, V_J = 250 m/s (820 fps).

Figure 21.– Concluded.